The cranial morphology of *Tanystropheus hydroides* (Tanystropheidae, Archosauromorpha) as revealed by synchrotron microtomography (#50370)

First submission

Guidance from your Editor

Please submit by **24 Aug 2020** for the benefit of the authors (and your $200 publishing discount) .

Structure and Criteria
Please read the 'Structure and Criteria' page for general guidance.

Author notes
Have you read the author notes on the guidance page?

Raw data check
Review the raw data.

Image check
Check that figures and images have not been inappropriately manipulated.

Privacy reminder: If uploading an annotated PDF, remove identifiable information to remain anonymous.

Files
Download and review all files from the materials page.

29 Figure file(s)

Structure your review

The review form is divided into 5 sections. Please consider these when composing your review:

1. **BASIC REPORTING**
2. **EXPERIMENTAL DESIGN**
3. **VALIDITY OF THE FINDINGS**
4. General comments
5. Confidential notes to the editor

You can also annotate this PDF and upload it as part of your review

When ready submit online.

Editorial Criteria

Use these criteria points to structure your review. The full detailed editorial criteria is on your guidance page.

BASIC REPORTING

- Clear, unambiguous, professional English language used throughout.
- Intro & background to show context. Literature well referenced & relevant.
- Structure conforms to PeerJ standards, discipline norm, or improved for clarity.
- Figures are relevant, high quality, well labelled & described.
- Raw data supplied (see PeerJ policy).

EXPERIMENTAL DESIGN

- Original primary research within Scope of the journal.
- Research question well defined, relevant & meaningful. It is stated how the research fills an identified knowledge gap.
- Rigorous investigation performed to a high technical & ethical standard.
- Methods described with sufficient detail & information to replicate.

VALIDITY OF THE FINDINGS

- Impact and novelty not assessed. Negative/inconclusive results accepted. *Meaningful* replication encouraged where rationale & benefit to literature is clearly stated.
- All underlying data have been provided; they are robust, statistically sound, & controlled.
- Speculation is welcome, but should be identified as such.
- Conclusions are well stated, linked to original research question & limited to supporting results.

Standout reviewing tips

The best reviewers use these techniques

Tip	*Example*
Support criticisms with evidence from the text or from other sources	*Smith et al (J of Methodology, 2005, V3, pp 123) have shown that the analysis you use in Lines 241-250 is not the most appropriate for this situation. Please explain why you used this method.*
Give specific suggestions on how to improve the manuscript	*Your introduction needs more detail. I suggest that you improve the description at lines 57- 86 to provide more justification for your study (specifically, you should expand upon the knowledge gap being filled).*
Comment on language and grammar issues	*The English language should be improved to ensure that an international audience can clearly understand your text. Some examples where the language could be improved include lines 23, 77, 121, 128 – the current phrasing makes comprehension difficult.*
Organize by importance of the issues, and number your points	*1. Your most important issue* *2. The next most important item* *3. …* *4. The least important points*
Please provide constructive criticism, and avoid personal opinions	*I thank you for providing the raw data, however your supplemental files need more descriptive metadata identifiers to be useful to future readers. Although your results are compelling, the data analysis should be improved in the following ways: AA, BB, CC*
Comment on strengths (as well as weaknesses) of the manuscript	*I commend the authors for their extensive data set, compiled over many years of detailed fieldwork. In addition, the manuscript is clearly written in professional, unambiguous language. If there is a weakness, it is in the statistical analysis (as I have noted above) which should be improved upon before Acceptance.*

The cranial morphology of *Tanystropheus hydroides* (Tanystropheidae, Archosauromorpha) as revealed by synchrotron microtomography

Stephan N F Spiekman [Corresp., 1], **James M Neenan** [2], **Nicholas C Fraser** [3], **Vincent Fernandez** [4, 5], **Olivier Rieppel** [6], **Stefania Nosotti** [7], **Torsten M Scheyer** [1]

[1] Palaeontological Institute and Museum, University of Zurich, Zurich, Switzerland
[2] Oxford University Museum of Natural History, Oxford, United Kingdom
[3] National Museums Scotland, Edinburgh, United Kingdom
[4] The Natural History Museum, London, United Kingdom
[5] European Synchrotron Radiation Facility, Grenoble, France
[6] Field Museum of Natural History, Chicago, United States of America
[7] Museo Civico di Storia Naturale di Milano, Milan, Italy

Corresponding Author: Stephan N F Spiekman
Email address: stephanspiekman@gmail.com

The postcranial morphology of the extremely long-necked *Tanystropheus hydroides* is well-known, but observations of skull morphology were previously limited due to compression of the known specimens. Here we provide a detailed description of the skull of PIMUZ T 2790, including the endocast and endosseous labyrinth, based on synchrotron microtomographic data, and compare its morphology to that of other early Archosauromorpha. In many features, such as the wide and flattened snout and the configuration of the temporal and palatal regions, *Tanystropheus hydroides* differs strongly from other early archosauromorphs. The braincase possesses a combination of derived archosaur traits, such as the presence of a laterosphenoid and the ossification of the lateral wall of the braincase, but also differs from archosauriforms in the morphology of the ventral ramus of the opisthotic, the horizontal orientation of the parabasisphenoid, and the absence of a clearly defined crista prootica. *Tanystropheus hydroides* had a streptostylic skull and was a ram-feeder that likely caught its prey through a laterally directed snapping bite. Although the cranial morphology of other archosauromorph lineages is relatively well-represented, the skulls of most tanystropheid taxa remain poorly understood due to compressed and often fragmentary specimens. The recent descriptions of the skulls of *Macrocnemus bassanii* and now *Tanystropheus hydroides* reveal a large cranial disparity in the clade, reflecting wide ecological diversity, and highlighting the importance of Archosauromorpha to both terrestrial and aquatic ecosystems during the Triassic.

The cranial morphology of *Tanystropheus hydroides* (Tanystropheidae, Archosauromorpha) as revealed by synchrotron microtomography

Stephan N. F. Spiekman[1], James M. Neenan[2], Nicholas C. Fraser[3], Vincent Fernandez[4,5], Olivier Rieppel[6], Stefania Nosotti[7], Torsten M. Scheyer[1]

[1]University of Zurich, Palaeontological Institute and Museum, Karl-Schmid-Strasse 4, 8006 Zurich, Switzerland

[2]Oxford University Museum of Natural History, Parks Road, Oxford OX1 3PW, UK

[3]National Museums Scotland, Chambers St, Edinburgh EH1 1JF, UK

[4]European Synchrotron Radiation Facility, 71 Avenue des Martyrs, 38000 Grenoble, France

[5]The Natural History Museum, Cromwell Road, London SW7 5BD, UK

[6]Field Museum of Natural History, 1400 S Lake Shore Dr, Chicago, IL 60605, USA

[7]Museo Civico di Storia Naturale di Milano, Corso Venezia 55, 20121 Milan, Italy

Corresponding author:

Stephan Spiekman

Karl-Schmid-Strasse 4, 8006 Zurich, Switzerland

Email address: stephanspiekman@gmail.com

Abstract

The postcranial morphology of the extremely long-necked *Tanystropheus hydroides* is well-known, but observations of skull morphology were previously limited due to compression of the known specimens. Here we provide a detailed description of the skull of PIMUZ T 2790, including the endocast and endosseous labyrinth, based on synchrotron microtomographic data, and compare its morphology to that of other early Archosauromorpha. In many features, such as the wide and flattened snout and the configuration of the temporal and palatal regions, *Tanystropheus hydroides* differs strongly from other early archosauromorphs. The braincase possesses a combination of derived archosaur traits, such as the presence of a laterosphenoid and the ossification of the lateral wall of the braincase, but also differs from archosauriforms in the morphology of the ventral ramus of the opisthotic, the horizontal orientation of the parabasisphenoid, and the absence of a clearly defined crista prootica. *Tanystropheus hydroides* had a streptostylic skull and was a ram-feeder that likely caught its prey through a laterally

directed snapping bite. Although the cranial morphology of other archosauromorph lineages is relatively well-represented, the skulls of most tanystropheid taxa remain poorly understood due to compressed and often fragmentary specimens. The recent descriptions of the skulls of *Macrocnemus bassanii* and now *Tanystropheus hydroides* reveal a large cranial disparity in the clade, reflecting wide ecological diversity, and highlighting the importance of Archosauromorpha to both terrestrial and aquatic ecosystems during the Triassic.

Introduction

Archosauromorpha, the lineage that includes modern crocodylians and birds, first appeared in the Permian and subsequently radiated during the Triassic into one of the dominant vertebrate groups of the terrestrial realm (Ezcurra et al. 2014; Foth et al. 2016). Among the earliest members of the lineage are the non-archosauriform archosauromorphs, which consist of *Protorosaurus speneri*, *Prolacerta broomi*, the herbivorous Rhynchosauria and Allokotosauria, and the long-necked Tanystropheidae, among others (Ezcurra 2016). Tanystropheidae represents a particularly ecomorphologically diverse group that includes terrestrial (e.g. *Macrocnemus bassanii* and *Langobardisaurus pandolfii*), largely aquatic (*Tanytrachelos ahynis* and *Tanystropheus hydroides*), and possibly even fully marine (*Dinocephalosaurus orientalis*) taxa (Liu et al. 2017; Miedema et al. in press; Olsen 1979; Renesto & Dalla Vecchia 2000; Rieppel et al. 2008; Spiekman et al. in press). The clade had a likely worldwide distribution and occurred between the Early and Late Triassic (De Oliveira et al. 2018; De Oliveira et al. 2020; Formoso et al. 2019; Pritchard et al. 2015; Sennikov 2011; Spiekman & Scheyer 2019). Due to their unique morphology, diversity, distribution, and phylogenetic position, Tanystropheidae are important both in reconstructing early archosauromorph evolution and in understanding the complexity and composition of Triassic faunas.

Tanystropheidae are characterized by their elongate cervical vertebrae and accompanying cervical ribs, and individual taxa are often diagnosed based on characters of these and other postcranial elements. However, due to the generally poor and fragmentary preservation of specimens, our understanding of tanystropheids is limited, and information on skull morphology in particular is sparse. Nevertheless, tanystropheids likely exhibited widely diverse cranial morphologies, as can be deduced from their ecological disparity and the diversity of their dentitions, which range from small conical teeth in for instance *Macrocnemus bassanii* and *Amotosaurus rotfeldensis*, to the “fish-trap” type dentition of *Tanystropheus hydroides*, to the partially tricuspid dentition of *Tanystropheus longobardicus* and *Langobardisaurus pandolfii* (Fraser & Rieppel 2006; Li et al. 2017; Miedema et al. in press; Rieppel et al. 2008; Spiekman et al. in press). The dental morphology of the latter in particular is peculiar, as the premaxilla was likely edentulous and the posteriormost teeth of both the upper and lower jaw bore large and flat tooth plates used for crushing, thus representing a unique dental system among tetrapods (Renesto & Dalla Vecchia 2000).

In contrast to the poorly known skull morphology of tanystropheids, largely complete and generally three-dimensionally preserved skulls are known from other early archosauromorphs. Their morphology has revealed valuable insights into archosauromorph palaeobiology and phylogeny, and has shed light on the acquisition of typical archosaur characters such as the presence of recurved teeth, an antorbital

and mandibular fenestra, and the loss of the pineal foramen (Flynn et al. 2010; Pinheiro et al. 2019; Spiekman 2018).

Synchrotron radiation X-ray micro computed tomography (SRµCT) has recently revealed the cranial morphology of the tanystropheid taxa *Macrocnemus bassanii* and *Tanystropheus hydroides* in previously unachievable detail, providing much improved cranial reconstructions (Miedema et al. in press; Spiekman et al. in press). This has shown that the cranial morphology of the terrestrial *Macrocnemus bassanii* is remarkably similar to that of *Prolacerta broomi* and that *Macrocnemus bassanii* possessed many characters that are likely plesiomorphic to Archosauromorpha and Tanystropheidae (Miedema et al. in press). In contrast, *Tanystropheus hydroides* exhibits a highly derived cranial morphology that bears several adaptations indicating that it was an aquatic ambush predator (Spiekman et al. in press). Furthermore, its morphology, together with osteohistological data, revealed that *Tanystropheus hydroides* represents a separate species from the smaller specimens known from the same localities and referred to *Tanystropheus longobardicus*.

The aim of this study is to describe the skull and preserved cervical vertebrae of PIMUZ T 2790 in high detail based on the SRµCT data. This represents the most complete and detailed cranial description of any tanystropheid to date and expands our understanding of early archosauromorph cranial diversity and evolution.

Material and Methods

PIMUZ T 2790 consists of eight cervical vertebrae, including the atlas and axis, their associated cervical ribs, and a nearly complete, dorsoventrally compacted skull (Fig. 1). The length of the skull is 138 mm (from the tip of the premaxilla to the right retroarticular process; the posterior extent of the skull cannot be established in-situ) and the largest vertebra is 190 mm in length (all lengths are provided in table 3 of Wild 1973, PIMUZ T 2790 is specimen p therein). The specimen was figured in Wild (1973) but not described as it was considered too poorly preserved. The length of the cervical vertebrae of the specimen were also used for comparison in Nosotti (2007: figure 54). The specimen was discovered in 1952 at the Punkt 902 locality of the Besano Formation (formerly Grenzbitumenzone), which is of latest Anisian to earliest Ladinian age (Stockar 2010).

The specimen was SRµCT scanned at BM05 beamline of the European Synchrotron Radiation Facility (ESRF, Grenoble, France). The resulting data were segmented using Mimics Research v19.0 (https://biomedical.materialise.com/mimics; Materialise NV, Leuven, Belgium). The skull of PIMUZ T 2790 is dorsoventrally compressed and most elements have become disarticulated and overlap each other, hampering observation of their morphology and the overall configuration of the skull (Fig. 2). Using Blender 2.7 (https://blender.org; Stitching Blender Foundation, Amsterdam, the Netherlands), the elements were digitally positioned in their perceived in-vivo positions, thus ‘re-assembling’ the skull (Figs. 3-4). Blender 2.7 and Mimics Research v19.0 were also used to render images for publication. A more detailed overview of the data acquisition and processing can be found in the “Synchrotron micro Computer Tomography acquisition and image processing” section of the Material and Methods in Spiekman et al. (in press).

Results

Comparative morphological description.

Skull

Even though the skull of PIMUZ T 2790 is dorsoventrally compacted, most of the bones still preserve a three-dimensional morphology with only certain bones being somewhat deformed (Fig. 2). This is in stark contrast to the other known skulls of *Tanystropheus hydroides*, which are all largely or completely flattened. Most of the bones are preserved underneath the two large plate-like frontals, which have been displaced somewhat posteriorly from the mandible~~s~~ and premaxillae and maxillae and as such protected the bones underneath from breakage and distortion.

Premaxilla

Both premaxillae are complete and in articulation at the anterior end of the snout. Each bears six alveoli, as is also the case in *Tanystropheus longobardicus* (Spiekman & Scheyer 2019). The premaxilla is tall and maintains its height along most of its anteroposterior length but anteriorly gradually tapers to a point (Fig. 5). Instead, the nasals probably only connected to the premaxillae on their anterolateral margin (Fig. 4B). No clear prenarial process is present. Instead, there is a small posterior extension on the medial end of the bone, which does not bear an articulation surface for the nasal to form an internarial bar. The prenarial process of *Tanystropheus longobardicus* and *Macrocnemus* spp. is also incipient, and has been reduced completely in rhynchosaurs and the allokotosaurs *Azendohsaurus madagaskarensis* and *Pamelaria dolichotrachela* among other early archosauromorphs (Dilkes 1998; Flynn et al. 2010; Miedema et al. in press; Nosotti 2007). In contrast, the prenarial process is well-established and elongate in *Protorosaurus speneri*, *Prolacerta broomi*, *Dinocephalosaurus orientalis*, and *Pectodens zhenyuensis* (Gottmann-Quesada & Sander 2009; Li et al. 2017; Modesto & Sues 2004; Rieppel et al. 2008).

A postnarial process is also absent in *Tanystropheus hydroides* and the suture between the premaxilla and maxilla is consequently almost vertical and directly posterior to the last alveolus of the premaxilla (Fig. 5A-B). The posteriormost part of the premaxillary body is labiolingually flattened, indicating that this part would have overlapped the maxilla laterally. This represents the opposite morphology of that recently described for rhynchosaurs, in which the maxilla laterally overlaps the premaxilla distinctly (see supplementary figure 11 of Pritchard et al. 2018). The premaxilla of *Tanystropheus longobardicus* bears a pronounced posteriorly directed postnarial process that would have articulated on the dorsolateral surface of the anterior part of the maxilla (e.g., MSNM BES SC 1018, PIMUZ T 2484; Nosotti 2007). A similar postnarial process is also present in *Prolacerta broomi* and *Azendohsaurus madagaskarensis*, in which this process forms a simple articulation with the maxilla (Flynn et al. 2010; Spiekman 2018). The premaxilla of *Macrocnemus bassanii* also has an elongate postnarial process, but additionally bears a posteromedial process ~~of the premaxilla,~~ and these two processes form a complicated articulation with the maxilla (Miedema et al. in press). Since the medial surface of the premaxilla cannot be observed for any known specimen, it is unclear whether *Tanystropheus longobardicus* possessed a similar posteromedial process.

As in *Macrocnemus* spp., there is no lingual contribution of the premaxilla to the palate in *Tanystropheus hydroides* (Miedema et al. in press; Fig. 5D). No foramina are present on the premaxilla. In contrast, several small neurovascular foramina line the premaxilla of *Tanystropheus longobardicus* (MSNM BES SC 1018; Nosotti 2007).

Maxilla

The left maxilla is complete except for its anteriormost portion, which is ~~somewhat~~ broken. The anteriormost portion of the right maxilla is similarly broken and it additionally misses the posteriormost part of its posterior process. The left maxilla preserves 15 alveoli, whereas only 11 are present on the less complete right element. Even though the anterior portion of both maxillae are somewhat poorly preserved, it is clear that they do not taper. Instead, each has a tall, almost vertical anterior margin (Fig. 5). The anterior part of the dorsal margin is largely horizontal and would have articulated with the lateral margin of the nasal (Fig. 4B). Posteriorly, the dorsal margin of the maxilla rises to form an ascending process with a distinctly concave posterior margin. This morphology occurs widely among non-archosauriform archosauromorphs, with the notable exception of *Protorosaurus speneri* (Spiekman 2018). The dorsal margin of the posterior process of the maxilla is wide in both bones and bears a concave articulation facet, anteriorly for the lacrimal and perhaps the prefrontal, and posteriorly for the anterior process of the jugal (Fig. 5B-C). On its medial side the dorsal margin of the posterior process is thickened at approximately its mid-length, forming a facet for the lateral margin of the palatine, as well as possibly the distal end of the ectopterygoid (Fig. 5B). The posterior process of the left maxilla is long, being almost subequal in anteroposterior length to the rest of the maxilla. Anteriorly, both maxillae bear a large opening, through which dentary tooth 10 pierced. A similar opening can also be seen in *Tanystropheus hydroides* specimen PIMUZ T 2819 (see supplementary figure 1b of Spiekman et al. in press). No other foramina can be identified on the lateral surface of the maxilla.

Septomaxilla

A septomaxilla was previously tentatively assigned to *Tanystropheus hydroides* and *Tanystropheus longobardicus* (Wild 1973). However, no evidence for such an element could be found in the SRµCT data of PIMUZ T 2790, and none of the bones that would surround a septomaxilla (i.e. the premaxilla, vomer, and nasal), bear any articulation facets for such a bone. Nevertheless, it cannot be excluded that a small septomaxilla was present in *Tanystropheus hydroides* when taking into consideration the poor preservation of the vomer and the nasal in PIMUZ T 2790. Similarly, the presence of a septomaxilla cannot be determined confidently for *Tanystropheus longobardicus* (Nosotti 2007). Septomaxillae occur in several early archosauromorphs, including *Prolacerta broomi* and the early rhynchosaur *Mesosuchus browni* (Modesto & Sues 2004; SAM-PK-6536, pers. observ. SNFS).

Nasal

There are several flat and plate-like bone fragments present anterior to the frontals, which are preserved in a higher plane than the pterygoids and vomers. These fragments are therefore identified as parts of the nasals (Fig. 3C). They are clearly concave in the transverse plane. Only a short portion of the straight medial margin of the left nasal could be identified. No other margins are preserved. The

reconstruction of the nasal of *Tanystropheus hydroides* (Fig. 2B), which is based on inferences from PIMUZ T 2790, PIMUZ T 2819, and PIMUZ T 2787 and comparisons to *Tanystropheus longobardicus*, was discussed in Spiekman et al. (in press) and is expanded upon in the discussion section below.

Lacrimal

Directly posterior and medial to the ascending process of the left maxilla, a fragmented bone is preserved which is identified as the left lacrimal (Fig. 6A-B). Although its margins are incomplete it bears a large oval-shaped posterior opening, which is the foramen for the naso-lacrimal duct. Another bone with a similar association with the right maxilla is somewhat bigger than the left lacrimal. However, it is very poorly preserved and cannot be identified confidently.

The prefrontal had a broad anterior and dorsal contact with the frontal, nasal, and maxilla, as can be deduced from the SRµCT data of PIMUZ T 2790 and the better-preserved prefrontal of *Tanystropheus hydroides* specimen PIMUZ T 2819 (see supplementary figure 1A of Spiekman et al. in press). Therefore, the lacrimal was likely restricted to the ventral side of the prefrontal and contacted the maxilla on the ventral part of the posterior margin of the ascending process and along the posterior process of the latter. It possibly also reached the anterior process of the jugal. Based on the prefrontal of PIMUZ T 2819 it seems likely that the lacrimal formed part of the anteroventral margin of the orbit. The lacrimal of *Tanystropheus longobardicus* is best-preserved in MSNM BES SC 1018 and also shows a large posterior opening transmitting the naso-lacrimal duct, albeit comparatively much smaller than in *Tanystropheus hydroides* (Nosotti 2007).

Prefrontal

The right prefrontal is missing but a partial left prefrontal is preserved anterolaterally to the left frontal. It has a clear orbital rim formed by a distinctly raised ridge (Fig. 6C-D), which is similar to that observed in the right prefrontal of PIMUZ T 2819 and in other non-archosauriform archosauromorphs, including *Tanystropheus longobardicus* (e.g. MSNM BES SC 1018). The prefrontal would have formed the anterodorsal margin of the orbit. The remaining edges of the prefrontal are broken and poorly preserved. They are very likely incomplete, in part because the element was crushed over the surangular of the left ~~mandible~~. The prefrontal was orientated in the 're-assembled' skull based on the position of this bone in PIMUZ T 2819, which is in partial articulation (Wild 1973).

Frontal

Both frontals are preserved next to each other, posterior to the left ~~mandible~~. They are very broad elements, being almost equal in width and anteroposterior length (Fig. 7). They are at their widest posteriorly and become slightly but steadily narrower anteriorly. This is also the condition in *Tanystropheus longobardicus* (PIMUZ T 2484; figure 4 of Spiekman & Scheyer 2019) and represents a deviation of the morphology typically observed in early archosauromorphs, in which the frontals are constricted in the interorbital region. There is a clear sagittally orientated depression on the medial portion of the dorsal surface and the bone has a distinct convex curvature lateral to this depression (Fig. 7C). This curvature forms the rounded dorsal margin of the orbit. Both in *Tanystropheus hydroides* and

Tanystropheus longobardicus, the contribution of the frontal to the margin of the orbit is considerable (see figure 3 of Spiekman et al. in press), whereas it is generally only minor in other early archosauromorphs (e.g. *Macrocnemus bassanii* PIMUZ T 4822 and *Prolacerta broomi* BP/1/471). The frontals would have contacted the nasal anteriorly, the prefrontals anterolaterally, the parietal and postorbital posteriorly, and the postfrontal and likely part of the postorbital posterolaterally. They would have extended little beyond the level of the orbit, both posteriorly and anteriorly. The left frontal is complete, but the anterolateral part of the right frontal is broken. It was previously suggested that the frontals of the large specimens of *Tanystropheus* from Monte San Giorgio (now *Tanystropheus hydroides*) were possibly fused (Wild 1973). However, PIMUZ T 2790 clearly reveals that the frontals are unfused and that the suture between them was straight and simple, in contrast to the interdigitating suture seen *Tanystropheus longobardicus* (PIMUZ T 2484; figure 4A of Spiekman & Scheyer 2019). On the ventral surface of both frontals a faint sagittally orientated ridge is visible, which corresponds to the depression of the dorsal surface and likely represents the margin of a shallow gutter transmitting the olfactory tract (Fig. 7B). It is constricted at about the anteroposterior mid-length of both bones and reaches somewhat further laterally at its anterior end than at the posterior end. Although the ridge is quite faint, it is most pronounced posteriorly. There is no depression on either frontal ~~that accommodates~~ the olfactory bulb as has been observed for *Tanystropheus longobardicus* and *Macrocnemus bassanii* (Ezcurra 2016).

Parietal

The parietal is fused but broken into three pieces that became disarticulated. The main piece is located directly posterior to both frontals and the other two pieces, which represent the two posterolateral processes of the parietal, are located to the right and directly below the main body. The anterior part of the parietal is largely missing. A partial left anterolateral process is preserved, whereas the right process is completely absent. The bone has been reassembled in the digital reconstruction (Figs. 3 and 8). The anterolateral process is roughly equal in width to the posterolateral processes, indicating that it framed the anterior margin of the supratemporal fenestra completely. The distal portion of this process is dorsoventrally flattened and likely overlapped an adjacent bone, most likely the postorbital and possibly also the postfrontal. The anterior margin of the parietal contacted the frontal in a roughly straight transverse suture, as can be clearly seen in PIMUZ T 2819 (figure 4B of Spiekman & Scheyer 2019). The posterior portion of the pineal foramen is well-preserved and shows that it was large and with a marked rim. Posterior to the pineal foramen a low sagittal crest runs along the midline of the parietal. From this midline crest, the parietal slopes down steeply on both sides to form the surface area for the attachment of the jaw adductor musculature on the parietal. These surfaces, the supratemporal fossae, make up most of the dorsal side of the main body of the parietal. The posterolateral processes are dorsoventrally tall and almost entirely transversely orientated. Distally, the posterolateral processes slightly expand dorsoventrally. On the anterior surface of both posterolateral processes, a distinct articular surface for the medial process of the squamosals is present (Fig. 8D-E). The medial margin of this surface is orientated laterodorsally to medioventrally. It can be inferred from the tight fit between the parietal and squamosal that a supratemporal bone was certainly absent in *Tanystropheus hydroides*. The shape of the parietal of PIMUZ T 2790 corresponds with that seen in the well-preserved parietal

exposed in dorsal view in the *Tanystropheus hydroides* specimen PIMUZ T 2819 (see figure 4B of Spiekman & Scheyer 2019). From our new findings, it can be inferred that the anterolateral processes of the parietal of PIMUZ T 2790 are wider than interpreted for this specimen by Wild (1973). Instead, the bones identified there as the postfrontals represent parts of the anterolateral processes of the parietals, as was also reconstructed for this specimen in figure 3 of Jiang et al. (2011). The postfrontals were most likely not clearly exposed in dorsal view in *Tanystropheus hydroides*. The morphology of the parietal differs strongly from that of *Tanystropheus longobardicus*, which is best represented in PIMUZ T 2484 (see figure 4A of Spiekman & Scheyer 2019). In *Tanystropheus longobardicus* the parietal is unfused in the midline and lacks the pronounced anterolateral processes. No clear supratemporal fossae are present, and the main body of the parietal is relatively much wider compared to *Tanystropheus hydroides*.

The large and roughly dorsoventrally orientated supratemporal fossae of the parietal in combination with dorsoventrally tall posterolateral processes seen in *Tanystropheus hydroides* represent a similar morphology to that of the comparatively large-sized early archosauromorphs *Azendohsaurus madagaskarensis* and *Dinocephalosaurus orientalis* (IVPP-V13767; Flynn et al. 2010; Rieppel et al. 2008). It is also present to a lesser degree in *Protorosaurus speneri*, in which the supratemporal fossae are also quite large but largely dorsally facing, and which possesses narrower posterolateral processes (NMK S 180; Gottmann-Quesada & Sander 2009). However, the morphology of *Tanystropheus hydroides* differs distinctly from that seen in the parietal of smaller early archosauromorphs (e.g. *Macrocnemus bassanii*, *Prolacerta broomi*, *Jesairosaurus lehmani*, and *Tanystropheus longobardicus*; PIMUZ T 2484; Jalil 1997; Miedema et al. in press; Modesto & Sues 2004). In these taxa, the supratemporal fossae form less of a depression and are largely dorsally facing, and the posterolateral processes are much narrower. Both the supratemporal fossae and the posterolateral processes of the parietal are important muscle attachment sites for the jaw adductor musculature. However, these differences among early archosauromorphs appear to be more strongly correlated with size rather than phylogeny or feeding strategies, since closely related taxa exhibit strongly different morphologies (e.g. *Tanystropheus hydroides* and *Tanystropheus longobardicus*), whereas relatively large-sized taxa with a widely different diet (e.g. the piscivorous *Dinocephalosaurus orientalis* and the herbivorous *Azendohsaurus madagaskarensis*) show a similar morphology.

Postfrontal

A postfrontal could not be identified in PIMUZ T 2790. The width at the posterior end of the frontal might indicate that this element was comparatively small and mostly visible in lateral view (Figs. 3C and 4A-B). However, the lack of an identifiable postfrontal in any available specimen of *Tanystropheus hydroides* precludes any further interpretation without ambiguity. The postfrontal of *Tanystropheus longobardicus* is known from PIMUZ T 2484 (figure 4A of Spiekman & Scheyer 2019). This element is small and triangular and articulates posteromedially with the parietal and anteromedially with the frontal, slightly overlapping both bones dorsally (Nosotti 2007). The postfrontal framed the posterodorsal margin of the orbit, but its articulation with the postorbital is unclear.

Postorbital

The postorbital is a triradiate bone with two very elongate processes, and one shorter process (Fig. 9). Both postorbitals are preserved, each directly posterolateral to their respective frontals. The right element is the more complete of the two. The two long processes are the ventral and medial processes, of which the ventral process is slightly longer. Both processes are straight and form a slightly acute angle with each other, indicating a very abrupt and sharp transition between the lateral and dorsal surfaces of the postorbital region of the skull. This configuration differs strongly from the postorbital in all other known non-archosauriform-archosauromorphs, in which the ventral and medial or dorsal processes of the postorbital generally form a crescent shape. This sharp transition is further corroborated by the shape of the squamosal, as discussed below. As a result, the medial process was extensive, reaching almost to the midline of the skull. The medial process of the right postorbital is very thin but is incomplete posteriorly. This can be inferred from the medial process of the less complete left postorbital, which is considerably broader (Fig. 3C). The medial process has a vertically orientated and flat anterior surface that would have formed a long transverse suture with the posterior margins of the frontal and possibly the postfrontal (Fig. 9C). The ventral process tapers distally, where it bears a clear articulation surface for the ascending process of the jugal on its posterior surface (Fig. 9D, F). This facet is deeper and more conspicuous than that observed in *Prolacerta broomi* (BP/1/5066) and similar to that of *Macrocnemus bassanii* (Miedema et al. in press). Although it is partially broken, it seems likely that the ventral process gradually widened posterodorsally and would have been confluent with the posterior process, forming a dorsoventrally broad suture with the squamosal. The posterior process is largely laterally facing, with its dorsal margin forming part of the lateral margin of the supratemporal fenestra. The anterior part of the bone where the medial and ventral processes meet is somewhat thickened. The identification of the postorbital in several *Tanystropheus longobardicus* specimens (PIMUZ T 2791, in PIMUZ T 2484, and MSNM BES SC 265) was recently re-interpreted based on the shape of the postorbital in *Tanystropheus hydroides* (supplement of Spiekman et al. in press). The postorbital of *Tanystropheus longobardicus* is also preserved in MSNM BES SC 1018 and, like *Tanystropheus hydroides*, bears a long ventral process, with a groove on its posterior surface that received the ascending process of the jugal. The medial process of MSNM BES SC 1018 was probably also elongate, whereas the posterior process was comparatively much shorter, as in *Tanystropheus hydroides*. However, due to the lack of three-dimensionally preserved skulls, the exact shape of the postorbital and its articulation with the surrounding bones remains unclear for *Tanystropheus longobardicus*.

Jugal

The left jugal is missing but an apparently almost complete right jugal can be observed through external observation (i.e. without the use of SRµCT data) on the specimen lateral to the posterior part of the right mandible (Fig. 1B-C). However, parts of this element could not be recovered from the SRµCT data; the jugal has thus been partially reconstructed. The parts that were visible in the SRµCT data are the main body of the jugal, including the base of the anterior and ascending processes, and the complete posterior process, as well as the anterior half of the anterior process and the posterodorsal end of the ascending process (Fig. 10A-B). Filling in the missing parts of the jugal based on the well-preserved left jugal of PIMUZ T 2[illegible] resulted in a nearly identical reconstruction of the jugal as is visible in the

specimen externally (Fig. 10C-D). Its shape is virtually identical to that of *Tanystropheus longobardicus* (Nosotti 2007). The anterior process is quite long and curved and tapers to a sharp point anteriorly. It framed the entire ventral margin of the orbit based on the overall length of the process and the clear jugal facet present on the posterior process of the maxilla. The posterior process is directed posteriorly with a largely straight ventral margin and a curved dorsal margin, which meet at the tapered end of the process. Although the process is quite long, no facet is present, and it did not contact any bone posteriorly. The infratemporal bar was therefore incomplete, showing a similar morphology to other early archosauromorphs (e.g. *Macrocnemus bassanii* PIMUZ T 4822 and *Prolacerta broomi* BP/1/5375). The ascending process is somewhat posterodorsally orientated. The posterior ~~or ventral~~ margin of the ascending process formed the anterior margin of the infratemporal fenestra (Figs. 4A). Although the dorsal margin in PIMUZ T 2790 is absent, the complete jugal of PIMUZ T 2819 indicates that it was somewhat convex. This margin of the ascending process connected to the posteroventral margin of the postorbital along its entire length. At its base it fitted into the concave articulation facet on the ventral process of the postorbital. The construction of the postorbital region indicates that the dorsal tip of the ascending process of the jugal connected to the anteroventrally expanded anterior process of the squamosal (Fig. 3A and 4A). Together with the postorbital, these three bones formed a wide postorbital bar, and the infratemporal fenestra was consequently small.

Squamosal

Both squamosals are preserved. The right one is complete, whereas the left element is largely complete but missing the end of the medial process and its anterior process is badly broken. The right squamosal is located underneath the right frontal and directly anterior to the right posterolateral process of the parietal. The left squamosal is surrounded by the left postorbital and the left anterolateral process of the parietal posteriorly, the left quadrate ventrally and anteriorly, and the left frontal dorsally. The overall shape of the squamosal is that of a curved plate-like bone formed by an anterior and a medial process; a discrete ventral process is missing (Fig. 11). The anterior process is dorsoventrally tall, especially anteriorly, where it formed a broad suture with the postorbital and almost certainly contacted the ascending process of the jugal ventrally. On the lateral surface of the anterodorsal tip, a clear triangular-shaped facet received the posterior process of the postorbital. The shape of the facet indicates that ventral to it, the anterior margin of the squamosal was partially covered by the postorbital in lateral view. Although distinctly less tall than the anterior process, the medial process of the squamosal is also flat and dorsoventrally tall. The posterior side of its distal half bears a large facet for the posterolateral process of the parietal (Fig. 11D). In dorsal view, the angle formed between the anterior and medial process is approximately 90 degrees (Fig. 11E). On its posteroventral side the squamosal bears a peculiar articular facet. This facet would have accommodated the dorsal head of the quadrate. It forms a large, very deep, and roughly pyramidal concavity. Its medial and lateral margins are raised, the former of which in particular forms a distinct ridge. The location and shape of this facet differs distinctly from that of *Macrocnemus bassanii* and *Prolacerta broomi*. In these taxa this socket has a similar shape to that in a ball and socket joint, and it is formed on the ventral side of the posterior process of the squamosal (Miedema et al. in press; Modesto & Sues 2004). A posterior process of the squamosal is absent in *Tanystropheus hydroides*. Directly medial to the quadrate facet, a small concavity

is located on the posterior surface of the squamosal, which might represent an articulation facet of the distal end of the paroccipital process of the opisthotic (Fig. 11D). Directly anterior or lateral to the quadrate facet another anteroventrally orientated concavity is present, which is demarcated anteriorly by a low ridge on its ventral part.

Quadrate

The right quadrate is broken and only partially preserved to the right of the right frontal on the external surface of the specimen. The left quadrate, however, is very well-preserved and complete apart from the dorsolateral tip, which is broken off (Fig. 12). It is located underneath the left frontal, the left squamosal, and the quadrate ramus of the left pterygoid. The shaft is slightly sigmoidal in lateral view as the posterior margin is clearly concave on its dorsal portion and a straight to slightly convex on its ventral part (Fig. 12A). From the shaft, a very thin but wide pterygoid ramus is extended anteromedially. Its dorsal margin extends horizontally from the base of the dorsal head of the quadrate and forms a 90-degree angle with the medial margin. The medial margin is straight along its dorsal third before gradually but continuously decreasing in width ventrally until it terminates at the base of the ventromedial head of the quadrate. The surface of the pterygoid ramus bears a distinct fossa seen in posterior view, which results in an equally distinct convexity in anterior view. The morphology of the pterygoid ramus is similar in overall shape and orientation to that of the best-known quadrate of *Tanystropheus longobardicus*, preserved in PIMUZ T 2484 (Fig. 13). However, the ramus is considerably shorter comparatively in *Tanystropheus longobardicus*, and the presence of the fossa cannot be established due to the small size and compression of the specimen. The pterygoid ramus differs strongly from the short anteriorly directed ramus of *Macrocnemus bassanii* (Miedema et al. in press), but shows similarities to the pterygoid ramus of *Prolacerta broomi* (BP/I/5066) and possibly *Protorosaurus speneri* (NMK S 180; Gottmann-Quesada & Sander 2009). However, clear observation for the latter taxon is considerably hampered by the flattening of the specimen. The dorsal end of the shaft of the quadrate of PIMUZ T 2790 bears a very conspicuous posteroventrally directed hook (Fig. 12). Such a hook is only known for certain allokotosaurs (e.g. *Pomelaria dolichotrachela* and *Azendohsaurus madagaskarensis*) among early archosauromorphs (Flynn et al. 2010; Sen 2003; Spiekman et al. in press). The dorsal head of the quadrate is also posteroventrally expanded in *Tanystropheus longobardicus* but does not form a hook as conspicuous as described for the abovementioned taxa (Fig. 13). Anterolateral to this hook, the majority of a short tympanic crest is located, which is absent in *Protorosaurus speneri*, *Prolacerta broomi*, and *Macrocnemus bassanii* (Gottmann-Quesada & Sander 2009; Miedema et al. in press; BP/1/5066), but present in certain rhynchosaurs (e.g. *Mesosuchus browni*, Dilkes 1998) and allokotosaurs (e.g. *Azendohsaurus madagaskarensis*, Flynn et al. 2010). Ventral to the tympanic crest the quadrate is constricted before widening laterally towards the ventrolateral condyle. A quadrate foramen was previously identified for both *Tanystropheus longobardicus* and *Tanystropheus hydroides* (as the large morphotype of *Tanystropheus longobardicus* in Wild 1973). However, such a foramen is absent in PIMUZ T 2790. We were also not able to corroborate the presence of this foramen in the specimens in which it was considered to be present, PIMUZ T 2484 for *Tanystropheus longobardicus*, and PIMUZ T 2787 for *Tanystropheus hydroides*. This foramen was therefore absent in *Tanystropheus hydroides*, and likely also absent in *Tanystropheus longobardicus*. Both ventral condyles of the quadrate are rounded

and are separated by a concavity (Fig. 12D). The lateral condyle is wider than the medial condyle, whereas the medial condyle projects further ventrally than the lateral one, as is also the case in *Macrocnemus bassanii* and the allokotosaurs *Pamelaria dolichotrachela* and *Azendohsaurus madagaskarensis* (Flynn et al. 2010; Miedema et al. in press; Sen 2003). The medial condyle would have articulated with the glenoid fossa of the articular. The skull reconstruction reveals that the quadrate was orientated somewhat posteroventrally to anterodorsally, as well as lateroventrally to mediodorsally (Figs. 3-4). This angled orientation of the quadrate is also known and considerably more pronounced in *Proterosuchus fergusi* (Ezcurra & Butler 2015). The dorsolateral surface of the lateral condyle bears a faint, somewhat rectangular-shaped facet (Fig. 12A). Here, the ventral footplate of the quadratojugal would have attached to the quadrate (Fig. 14).

Quadratojugal

Two small, curved and rod-shaped elements are identified as the quadratojugals, which were previously considered to be absent in both *Tanystropheus hydroides* and *Tanystropheus longobardicus* (Nosotti 2007; Wild 1973). The left quadratojugal is located directly anterior to the left prefrontal and dorsal to the left surangular, whereas the right quadratojugal is located anterolaterally to the poorly preserved right quadrate and lateral to the posterior part of the right mandible. The quadratojugal is a flattened, rod-like bone with a helical curvature (Fig. 14). The ventral end is thin and would have articulated on the dorsolateral surface of the lateroventral condyle of the quadrate. The dorsal end articulated with the squamosal and possibly the laterodorsal part of the quadrate. Because of the curvature of the bone, the articular surface of the dorsal end almost faces in the direct opposite direction of the ventral articulation. There is no anterior process of the quadratojugal and it therefore did not connect to the jugal (Fig. 3A-B). This corresponds largely to the configuration seen in many early archosauromorphs (e.g. *Macrocnemus bassanii*, *Mesosuchus browni*, and *Prolacerta broomi*; (Dilkes 1998; Miedema et al. in press; Modesto & Sues 2004), in which the quadratojugal is also curved and has a similar position relative to the quadrate. However, the quadratojugal of these taxa appear to lack the helical or twisting curvature present in *Tanystropheus hydroides*. The morphology of the quadratojugal of allokotosaurs differs distinctly from that of other early archosauromorphs, including *Tanystropheus hydroides*. In *Azendohsaurus madagaskarensis* and *Teraterpeton hrynewichorum* the quadratojugal is roughly straight (Flynn et al. 2010; Sues 2003), whereas in *Trilophosaurus buettneri* the infratemporal fenestra is completely missing and the quadratojugal possibly had a triangular shape (Spielmann et al. 2008).

Vomer

Both vomers are fragmentary and are surrounded by the mandibles, premaxillae, and maxillae. The tooth bearing outer margins of both bones are intact, but most of their medial surfaces are lost, probably because they were exposed on the surface of the specimen during excavation and preparation (Fig. 15). There are 15 alveoli preserved on the right vomer and 14 on the left. The vomers were very thin and only thickened around the tooth bearing lateral margin. They were wide and enclosed the roof of the mouth anteriorly and laterally and restricted the internal choanae to relatively narrow openings (Fig. 3D). The morphology of the vomers corresponds to that of the well-preserved vomers of PIMUZ T 2787. The vomers of *Dinocephalosaurus orientalis* are likely equally broad as those of *Tanystropheus*

hydroides, but were probably edentulous (Rieppel et al. 2008). The vomers of other early archosauromorphs, including *Tanystropheus longobardicus*, are generally much narrower and bear one or more rows of small teeth (Dilkes 1998; Flynn et al. 2010; Miedema et al. in press; Modesto & Sues 2004; Spiekman et al. in press). Therefore, the vomeral morphology of *Tanystropheus hydroides* appears to be unique among early archosaurmorphs, and the large recurved teeth along the lateral margin of the bone likely represent a feeding adaptation.

Palatine

A plate-like bone is preserved directly anteroventral to the left frontal and dorsal to the transverse flange of the left pterygoid. It is incomplete, with the straight medial margin being the only complete margin of the element. Based on its position in the specimen and overall shape, which is in correspondence with the palatines of PIMUZ T 2787 (see figure 4G of Spiekman & Scheyer 2019), it is tentatively identified as the left palatine. No right palatine could be identified. The element is edentulous, thin, roughly flat, and anteroposteriorly longer than transversely wide.

Ectopterygoid

The left ectopterygoid could not be identified, but directly to the right of the parabasisphenoid and anterior to the right quadrate, an element is preserved that is tentatively identified as a complete right ectopterygoid (Fig. 16). This element is distinctly different from the ectopterygoid seen in other archosauromorphs (e.g. *Azendohsaurus madagaskarensis*, *Mesosuchus browni*, and *Macrocnemus bassanii*, Dilkes 1998; Flynn et al. 2010; Miedema et al. in press). Nevertheless, the element is identified as an ectopterygoid due to its relative position in the skull and its shape and size, which allow it to articulate with the pterygoid and maxilla in the ‘re-assembled’ skull model (Figs. 3D and 4C). The element is a dorsoventrally flattened bone with a plate-like shaft. Its medial end is flattened and curved ventrally (Fig. 16D). No clear articulation facet with the pterygoid is present and the ectopterygoid would have overlapped considerably with the pterygoid ventrally. It would thus have formed a loose and possibly movable connection to the pterygoid just anterior to its transverse flange at the posterior part of the palatal ramus. The anterior or medial margin of the ectopterygoid shaft is gently concave and somewhat thickened, whereas the posterior or lateral margin is straight and thin. On the lateral end of the dorsal surface of the shaft a triangular concavity is located anteriorly (Fig. 16A). If our interpretation is correct, this facet would have received the posterior part of the palatine. The lateral margin of the ectopterygoid is formed by a small flat surface that would have articulated with the medial side of the posterior process of the maxilla (Fig. 16E). Anterior or lateral to this, the ectopterygoid is projected slightly further anteriorly to form a ventrally deflected process of unknown function.

Pterygoid

Both pterygoids are preserved and are located below and anterior to the frontals. Both are largely complete, with only the anterior third of the bones being broken and partially missing. Both pterygoids are completely edentulous. In this, and in their overall shape, the pterygoids conform to the morphology of the pterygoids in PIMUZ T 2787 (see figure 4D of Spiekman & Scheyer 2019). The right pterygoid is slightly more complete than the left (Fig. 3D). Even though its anterior part is broken, it is clear that the

palatal ramus (=anterior process) of the pterygoid of PIMUZ T 2790 is wide along its entire length. In this feature and the complete absence of the pterygoid teeth, *Tanystropheus hydroides* differs from all other early archosauromorphs for which the pterygoid is known, including *Tanystropheus longobardicus*, but with the possible exception of *Dinocephalosaurus orientalis* (Rieppel et al. 2008; Spiekman et al. in press). The shape and size of the palatal rami suggests that the pterygoids contacted each other anteriorly. The pterygoid is concave in the transverse plane, with a concavity in the centre of the bone and a somewhat dorsally inclined lateral portion (Fig. 17E-F). The pterygoid is similarly concave in the sagittal plane, with the pterygoid being the lowest at the level of the transverse process and the palatal and quadrate rami being slightly inclined dorsally (Fig. 17C-D). The lateral surface of the transverse flange is distinctly rugose and dorsoventrally thickened (Fig. 17D). This surface is orientated posteroventrally to anterodorsally. The angle between the anterior and lateral margins of the transverse flange is roughly right-angled, whereas that between the posterior and lateral margins is acute. At the base of the quadrate ramus, the articulation facet for the basipterygoid process of the parabasisphenoid can be clearly made out on the medial surface (Fig. 17C). It is framed by a dorsally directed upper lip and a medially directed lower lip. Directly anterior to this facet a concavity is present, which might have facilitated the articulation of the ventral foot plate of the epipterygoid. However, a clear articulation surface cannot be discerned. The quadrate ramus has a posterolateral orientation and is somewhat dorsally inclined. From the main ramus project two thin flanges, a dorsomedially orientated dorsal flange and a ventromedially orientated arcuate flange (sensu Ford & Benson 2018). The dorsal flange is larger and reaches further posteriorly along the ramus (Fig. 17C-D). The dorsal flange is straight whereas the arcuate flange is curved ventrally and even slightly laterally at its distal end (Fig. 17E). The dorsomedial orientation of the dorsal flange seems to indicate it did not directly contact the pterygoid wing of the quadrate. Anterior to the quadrate ramus, the arcuate flange transitions into a low ridge that is anterolaterally orientated and almost reaches the transverse flange (Fig. 17B).

Epipterygoid

Both epipterygoids are preserved. The left element is located in between the left anterolateral process of the parietal and the left postorbital. The right is preserved directly posterior to the ascending process of the right jugal. Both are complete, except for the middle part of the shaft of the left element, which is broken. The epipterygoid is a lateromedially flattened, columnar bone that has a gradual anteroposterior expansion towards its dorsal end and a more abrupt expansion on its ventral end (Fig. 18). The expansion on the dorsal end is larger than on the ventral end. The ventral end is rounded with a ventrolaterally facing flat surface that likely connected to the pterygoid directly anterior to the facet for the basipterygoid process on this bone. The shape of the epipterygoid differs from that described for *Macrocnemus bassanii*, in which the shaft bears a distinct posterior expansion, the shaft has an oval rather than flattened cross-section, and in which the epipterygoid is not expanded dorsally (Miedema et al. in press).

Basioccipital

The basioccipital is located below the anterior part of the right frontal and anterior to the two fused braincase elements. This element, which forms the posteroventral part of the braincase (Fig. 19), is

largely complete and distinctly deformed from left to right in posterior view (Fig. 20). Nevertheless, the original morphology of the bone can still be inferred. The occipital condyle contribution of the basioccipital is ventrally concave at its base. The dorsal surface of the occipital condyle contribution bears two large dorsolaterally directed, concave facets for the articulation of the condylar contributions of the exoccipitals. As can be seen from the morphology of the exoccipitals, they contributed substantially to the occipital condyle and they possibly even excluded the basioccipital from contributing to the floor of the foramen magnum (Fig. 20C), which was possibly also the case for *Tanystropheus longobardicus* (PIMUZ T 2484). The combined shape of the exoccipitals and the basioccipital gave the condyle a hemispherical shape (Fig. 19E). Anterior to the occipital condyle on the ventral surface, two ridges run from the occipital neck ventrolaterally towards the basal tubera of the basioccipital (Fig. 20A). The surface between these ridges is concave. The surfaces lateral to these ridges are also concave and face posterolaterally. The basal tubera of the basioccipital are rounded and more medially located than the basal tubera of the parabasisphenoid. A transverse ridge that is slightly depressed in its centre connects the basal tubera. Such a ridge is absent in *Macrocnemus bassanii* and *Prolacerta broomi* but common in allokotosaurs and non-archosaurian archosauriforms (Evans 1987; Ezcurra 2016; Flynn et al. 2010; Sen 2003). In contrast to *Euparkeria capensis* (Sobral et al. 2016), posterior to this ridge, the contribution of the basioccipital to the median pharyngeal recess appears to be minimal. On the anterior surface of the basioccipital indentations are present that are similar to those recently described for *Macrocnemus bassanii* (Fig. 20B; Miedema et al. in press). However, the compression of the bone has distorted these structures, preventing a detailed description of their shape.

Parabasisphenoid

The para –and basisphenoid are fully fused into a single element, the parabasisphenoid, which forms the anteroventral portion of the braincase (Fig. 19). It is preserved anterior to the right frontal and the right quadrate. It is virtually complete and somewhat deformed from right to left in anterior view. The cultriform process is long and straight and tapers to a sharp point anteriorly (Fig. 21). It is somewhat dorsoventrally constricted at its base as in *Prolacerta broomi* and *Euparkeria capensis* (Evans 1986; Sobral et al. 2016), among other archosauromorphs, but from this constriction the cultriform process gains in height anteriorly until approximately one-third of its anteroposterior length (Fig. 21C-D). From there, it slowly decreases in dorsoventral height towards its anterior terminus. It bears a concave trough on its dorsal surface forming a V-shaped cross section (Fig. 21B). The basipterygoid processes are prominent but short and are facing anterolaterally (Fig. 21A). Distinct, but thin, parasphenoid crests run along the ventral surface of the main body posterolaterally towards the basal tubera. No foramina were found on the ventral surface of the main body, but these could have been present but simply not visible in the SRµCT data, since they are generally present in early archosauromorphs (Ezcurra 2016). The parasphenoid crests are connected by a deeply concave bony plate, the median pharyngeal recess (sensu Nesbitt 2011). This character was originally identified in archosauriforms, but was recently determined to be present in the non-archosauriform archosauromorphs *Bentonyx sidensis* and *Azendohsaurus madagaskarensis* (Ezcurra 2016). There was no intertuberal plate as in *Prolacerta broomi* and *Azendohsaurus madagaskarensis* (Evans 1986; Flynn et al. 2010). The entire parabasisphenoid has a horizontal orientation, similar to most early diapsids and non-archosauriform archosauromorphs, but in

contrast to *Azendohsaurus madagaskarensis* and most early archosauriforms, in which the posterior portion of the parabasisphenoid is orientated anteroventrally (Flynn et al. 2010; Gower & Sennikov 1996). The basal tubera of the parabasisphenoid are thin and open posteriorly (Fig. 21E). The contribution of the parabasisphenoid to the basal tubera is wider by comparison than that of the basioccipital contribution so that there may have been an open space in this region, the so-called pseudolagenar recess as described for several archosauriforms (Gower & Sennikov 1996). However, because the elements are not preserved in articulation, this cannot be stated with any certainty. There is no evidence for pneumatic foramina, as were recently discovered in *Mesosuchus browni* (Sobral & Müller 2019). Of the dorsal portion of the parabasisphenoid, only the right side is largely preserved. A clinoid process with an anteriorly concave margin is located dorsal to the right basipterygoid process (Fig. 21C-D). Posterior to the clinoid process, the lateral margin remains tall at first, before gently sloping down ventrally towards the basal tubera. This, in combination with the morphology of the prootic, indicates that the contact between these two bones was continuous posterior to the clinoid process. Anteromedial to the clinoid process, a shallow concavity represents the pituitary fossa (=hypophyseal fossa; Fig. 21B). No foramina can be observed on the dorsal surface of the parabasisphenoid, but as for the ventral surface, their absence cannot be assumed. Posterior to the right clinoid process the dorsal surface of the parabasisphenoid is interrupted abruptly by the vertical slope of the dorsum sellae.

Fused Braincase

The exoccipital, opisthotic, supraoccipital, prootic, and laterosphenoid were all preserved in full articulation. No sutures between these bones were discernible from the SRµCT data indicating that these bones were likely fused. The individual elements were instead distinguished based on their morphology. The fused braincase is split into two pieces along the midline. Both pieces are still closely associated and are located anterior to the parietal and right squamosal, posterior to the two pterygoids and ventral to the right frontal. The left piece is distorted, with the dorsal surface facing laterally, the exoccipital having been tilted slightly dorsally, and the prootic medially. The right piece is virtually undistorted, and therefore the description of the elements below is based on this side (Fig. 22).

Exoccipital

Ventrally the exoccipital bears a large flat ventromedially orientated surface, the occipital foot, that articulated on the dorsolateral surface of the basioccipital (Fig. 22). Although the foot extended far medially and posteriorly, it is unclear the extent to which both exoccipitals may have touched each other ventrally. The ventrolateral and lateral margin of the foramen magnum was certainly formed by the exoccipitals. However, due to the lack of observable sutures, the dorsal extent of the exoccipitals cannot be determined. Anterior to the exoccipital foot, but not visible in occipital view, a small, ventrolaterally orientated foramen is present; the opening for the hypoglossal nerve (CN XII, Fig. 22E). Anterior to this, a larger oval-shaped opening, the metotic foramen, is present, which forms the passageway for the glossopharyngeal nerve, vagus nerve, and accessory nerve (CN IX, CN X, and CN XI, respectively). The metotic foramen is framed by the exoccipital posteriorly and the ventral ramus of the opisthotic anteriorly in archosauromorphs and other diapsids (Evans 1986; Gardner et al. 2010; Gower 1997; Sobral & Müller 2019; Sobral et al. 2016), and thus demarcates the anteroventral extent of the

exoccipital. The exoccipital and opisthotic fully enclose the metotic foramen, which is thus not framed by the basioccipital.

Opisthotic

The paroccipital process of the opisthotic projects laterally and slightly posteriorly (Fig. 22). The posterodorsal surface of the process is flattened, whereas the anteroventral surface bears a large ridge running along its dorsal margin which terminates close to the distal end of the process. This ridge forms the dorsal margin of a stapedial groove and corresponds to the ventral ridge or keel described for the paroccipital processes of PIMUZ T 2819 (Fig. 22B, D-E; Wild 1973). The paroccipital process is virtually straight and maintains its width distally. Likely, the distal end of the paroccipital process was received in a concavity on the squamosal. In *Tanystropheus longobardicus*, the paroccipital process is much shorter and dorsoventrally expands at its dorsal end (see figure 4A of Spiekman & Scheyer 2019). The opisthotic connects to the exoccipital ventrally, the supraoccipital dorsomedially, and the prootic anteriorly, but none of these sutures are visible in the SRµCT data. Ventrally the ventral ramus of the opisthotic, which is clearly visible in lateral view, frames the anterior margin of the metotic foramen anteriorly and the posterior margin of the fenestra ovalis, through which the stapes was connected to the inner ear (Fig. 22E). The fenestra ovalis is irregularly shaped, but, in contrast to *Prolacerta broomi* and *Youngina capensis* (Evans 1986; Gardner et al. 2010), its margin is well-ossified. The fenestra ovalis was previously considered to be enclosed by both the opisthotic and prootic in *Tanystropheus hydroides*, based on the elements preserved in PIMUZ T 2819 (Wild 1973). However, a comparison of this specimen with the braincase of PIMUZ T 2790 presented here, reveals that this interpretation is incorrect. Instead, the ventralmost foramen visible in PIMUZ T 2819 represents the metotic foramen and the opening dorsal to this is the fenestra ovalis, with the two being separated by the ventral ramus of the opisthotic. The space between the opisthotic-exoccipital complex and the prootic is the result of the slight deformation that likely occurred during compression of the specimen, rather than the fenestra ovalis. The ventral ramus is narrow at its base, widens ventrally, and expands posteriorly where it contacts the anteroventral part of the exoccipital below the metotic foramen. The ventral ramus is incomplete anteroventrally in the right opisthotic as can be deduced from the complete ventral ramus of the left element. Following the morphology in the latter, the ventral ramus is anteroposteriorly expanded at its distal end but does not form a rounded, bulbous process. It thus differs from *Macrocnemus bassanii*, in which the ventral ramus is not expanded, and from *Prolacerta broomi*, in which the ventral ramus has a large bulbous head (Evans 1986; Miedema et al. in press). As for most of the details of the braincase, the morphology of the ventral ramus of the opisthotic is currently unknown for *Tanystropheus longobardicus*. Because the suture between the opisthotic and supraoccipital cannot be observed, the nature of the articulation between these bones is unclear.

Prootic

The prootic contacts the opisthotic posteroventrally, the supraoccipital posterodorsally, the parabasisphenoid ventrally, the laterosphenoid anteriorly, and likely the parietal anterodorsally. The anteroventral portion of the prootic is tilted somewhat laterodorsally to medioventrally in the right element, which might be the result of slight deformation (Fig. 22). However, all the different structures

present on the prootic appear intact. Although a clear suture cannot be established, the posterior outline of the prootic can be delineated because its margin is somewhat raised compared to the opisthotic, whereas the margin of the supraoccipital is somewhat raised above the prootic along their connection. This shows that a narrow tapering process of the prootic contributed to the anterior side of the paroccipital process along the anterior ridge (Fig. 22B, D-E). This contribution tapers to a point almost halfway along the distal extent of the process. Posteroventrally, the prootic connects with the ventral ramus of the opisthotic to enclose the fenestra ovalis. The crista prootica, which is a ridge running posterodorsally to anteroventrally along the lateral surface of the prootic in archosauromorphs, cannot confidently identified. In contrast, a sharply anterodorsally curving ridge, the crista alaris (sensu Sobral & Müller 2019), can be clearly discerned (Fig. 22E). The foramen for the exit of the facial nerve (CN VII) is apparently not preserved on either prootic. The large and oval-shaped opening for the trigeminal nerve (CN V) is completely enclosed by the prootic and anteriorly by the laterosphenoid. The portion of the prootic ventral to CN V is the rectangular-shaped anterior inferior process, of which the anterior margin would have connected to the clinoid process of the parabasisphenoid. The connection between the prootic and parabasisphenoid likely continued posteriorly to the clinoid process, closing off the lateral wall of the braincase. This character and the considerable contribution of the prootic to the anterior side of the paroccipital process represent derived characters in *Tanystropheus hydroides* that are also present in early archosauriforms but absent in *Prolacerta broomi*, *Macrocnemus bassanii*, and *Youngina capensis* (Evans 1986; Evans 1987; Gardner et al. 2010; Gower & Sennikov 1996; Miedema et al. in press).

Laterosphenoid

The presence of a laterosphenoid is widespread among archosauriforms and has also been identified for *Azendohsaurus madagaskarensis* (Clark et al. 1993; Flynn et al. 2010; Gower & Sennikov 1996). However it is absent in other non-archosauriform archosauromorphs such as *Macrocnemus bassanii* and *Prolacerta broomi*, as well as in non-saurian diapsids such as *Youngina capensis* (Evans 1986; Gardner et al. 2010; Miedema et al. in press). The presence of a laterosphenoid in *Tanystropheus hydroides* represents the phylogenetically earliest occurrence of this element in the archosauromorph lineage. It is located immediately anterior to the prootic and identified as the bone anteriorly and dorsally enclosing CN V (Fig. 22). As in *Azendohsaurus madagaskarensis*, the laterosphenoid is small and not anteriorly expanded as in archosauriforms. The dorsal part of the anterior margin of the bone bears a distinct notch, which might have transmitted branches of the trigeminal nerve (Sobral et al. 2012). The suture between the laterosphenoid and the prootic cannot be observed and therefore the exact outline of the bone is unclear.

Supraoccipital

The supraoccipital is located dorsal to the exoccipital, dorsomedial to the opisthotic, and posterodorsal to the prootic (Fig. 22A, C). The supraoccipital is incomplete and broken into two uneven parts. Therefore, it appears that the break did not occur along a suture and that the supraoccipital was most likely fused. This is supported by the only other known supraoccipital of *Tanystropheus hydroides*, present in PIMUZ T 2787 and visible in anterior view, which is fused (Wild 1973). Little remains of the

supraoccipital on the left side of the braincase and it is heavily distorted. The right half is virtually undistorted and complete except for a portion of the medial side. Dorsally the supraoccipital would have connected to the parietal, although no clear facet is present. The supraoccipital is large and plate-like in shape and appears more sloped than in most early archosauromorphs, in which the orientation is more vertical. However, it is unclear whether this represents the original orientation or if it is the result of distortion. The posterodorsal surface of the supraoccipital is largely flat but slightly concave, although it is also unclear whether this is due to deformation. A low sagittal crest along the midline of the supraoccipital was described for PIMUZ T 2787 based on an X-ray (Wild 1973). Presumably, this was also the case for PIMUZ T 2790, but this cannot be corroborated because the medial portion of the supraoccipital is not preserved. A small convexity also runs along the midline of the supraoccipital in the closely related taxa *Tanystropheus longobardicus* (PIMUZ T 2484; figure 4A of Spiekman & Scheyer 2019) and *Macrocnemus bassanii* (Miedema et al. in press). Laterally the supraoccipital thickens distinctly on its anteroventral surface, where the supraoccipital contributes to the otic capsule (Fig. 22F).

Stapes

A small rod-like bone preserved between the left frontal dorsally, and the dorsal end of the left quadrate ventrally might represent the left stapes. Its tentative identification is based on its overall shape and size, and because the structure fits neatly within the stapedial groove of the paroccipital process (Fig. 23). It is a thin element, which would correspond to the stapes of other archosauromorphs, but contrasts with the much more robust stapes of non-saurian diapsids such as *Youngina capensis* (Ezcurra 2016; Gardner et al. 2010). The element is apparently incomplete and one of its ends is forked. These two prongs could represent part of the margin of the stapedial foramen. The stapes was previously tentatively identified for *Tanystropheus longobardicus* in PIMUZ T 2485, PIMUZ T 2482, and MSNM BES SC 1018 (Nosotti 2007; Wild 1973). The morphology of these elements roughly corresponds to the tentative stapes described here, but a stapedial foramen cannot be established in any of these specimens.

Endocast

The excellent preservation of the right side of the braincase allows for the reconstruction of its endocast, which includes parts of the cerebellum, pons, medulla oblongata, cranial nerves, and the endosseous labyrinth (Fig. 24). The flocculus is remarkably large and extends laterally between the anterior semicircular canal and the vestibule of the endosseous labyrinth. Large flocculi are also present in the early archosauromorphs *Mesosuchus browni* and *Euparkeria capensis*, whereas it is only poorly developed in *Proterosuchus fergusi* (Brown et al. 2019; Sobral & Müller 2019; Sobral et al. 2016). Posterior to the flocculus, the cerebellum is constricted before expanding again posteriorly towards the medulla oblongata. As described for the braincase elements, three bundles of cranial nerves could be reconstructed. The passage for the facial nerve (CN VII) was not identified. Anterior to the endosseous labyrinth and ventral to the flocculus, the trigeminal nerve (CN V) diverges from the pons. The bundle of the glossopharyngeal nerve, vagus nerve, and accessory nerve (CN IX, CN X, and CN XI) is located directly posterior to the cochlea of the endosseous labyrinth. Posterior to this, a smaller canal would have carried the hypoglossal nerve (CN XII). A small canal in the exoccipital connects the bundle of the CN IX,

X, and XI to CN XII. However, it is unclear whether this represents an original feature or is the result of deterioration or deformation of the bone.

Endosseous labyrinth

Like all other archosauromorphs, the endosseous labyrinth is enclosed by the opisthotic, prootic, and the supraoccipital (Sobral & Müller 2016). However, the degree to which each element encloses each part of the labyrinth is unclear because no sutures between these elements are discernible. All semicircular canals and the common crus are gracile (Fig. 24). The anterior semicircular canal (ASC) is incomplete. Because it must have curved around the large flocculus, the shape of the ASC can be inferred from the flocculus and the preserved part of the ASC directly dorsal to the common crus (see also figure 1D of Spiekman et al. in press). The ASC was quite tall and elongate and would have been larger than the posterior semicircular canal (PSC). The greater length of the ASC compared to the PSC has been suggested to be a derived crocodylomorph feature, and in non-archosaurian archosauromorphs these canals are approximately similar in size (Brown et al. 2019; Pierce et al. 2017). However, the ASC is also considerably longer than the PSC in the recently described endosseous labyrinth of the early rhynchosaur *Mesosuchus browni* (Sobral & Müller 2019). The PSC is less arched than the ASC and exhibits sinusoidal curvature. The lateral semicircular canal (LSC) is similar in length to the PSC and does not exhibit a continuous curvature, instead bending inwards at its approximate mid-point. In the 're-assembled' skull of PIMUZ T 2790, the LSC is orientated at approximately the same angle as the horizontal plane of the skull as estimated from the tooth row of the maxilla (angle = ~2°). However, this measurement might deviate slightly, as it is dependent on the orientation of the braincase in relation to the rest of the skull, which can only be approximated in the 're-assembled' skull. The endosseous cochlear duct is well defined and posteroventrally orientated. It is relatively elongate, similar to that of *Youngina capensis*, and considerably longer than in *Mesosuchus browni* and *Proterosuchus fergusi* (Brown et al. 2019; Gardner et al. 2010; Sobral & Müller 2019). The extent of the cochlea of *Euparkeria capensis* is unclear (Sobral et al. 2016).

Cranial openings

External naris

The lack of any distinct prenarial process of the premaxilla indicates that the external nares were likely confluent. However, the lack of anything but a very fragmentary nasal makes any additional inferences with regards to the external naris based on PIMUZ T 2790 impossible. The nasals and external naris have been reconstructed for *Tanystropheus hydroides* based on inferences from PIMUZ T 2787 and PIMUZ T 2819 (Fig. 4B; see also the discussion on the nasal below and Spiekman et al. in press and supplementary figures 1A and 2B therein). This reveals that the external naris was framed only by the premaxillae and nasals and that it was confluent and faced dorsally.

Orbit

The outline of the posterodorsal margin of the orbit is unclear due to the lack of information on the shape of the postfrontal and its articulation with the surrounding bones. Nevertheless, the orbit appears

to be subcircular and slightly longer anteroposteriorly than tall dorsoventrally (Figs. 3A-B and 4A). The dorsal margin of the orbit is largely formed by the curved lateral margin of the wide frontal. In most archosauromorphs, the contribution of the frontal to the dorsal margin of the orbit is limited and this margin is instead formed by the prefrontal anteriorly and the postfrontal posteriorly (Ezcurra 2016). The anterior margin of the orbit is framed by the prefrontal dorsally and the lacrimal ventrally. The curved anterior process of the jugal forms the entire ventral margin of the orbit. The ventral process of the postorbital largely covers the jugal anteriorly and thus forms most of the posterior margin of the orbit. The overall arrangement of the bones framing the orbit results in a largely laterally and slightly anteriorly directed orbit.

Temporal fenestra

The three-dimensional preservation of PIMUZ T 2790 allows for a clear rendition of the temporal fenestrae of *Tanystropheus hydroides*. The supratemporal fenestra is considerably wider than it is long (Figs. 3C and 4B). At least the medial half of the anterodorsal margin was formed by the anterolateral process of the parietal, with the margin of the lateral half being either formed by the parietal or the medial process of the postorbital. Although the shape of the postfrontal is unknown for *Tanystropheus hydroides*, it seems unlikely that the postfrontal contributed to the margin of the supratemporal fenestra based on the articulation of the postorbital and parietal. The medial margin of the supratemporal fenestra was very short and formed by the lateral portion of the parietal. The supratemporal fossa of the parietal is strongly sloped ventrally and very tall, presenting a large surface area for the attachment of jaw adductor musculature (Fig. 8A, D-E). Posteriorly, the margin of the supratemporal fenestra is formed by an equal contribution of the dorsoventrally tall posterolateral process of the parietal medially and the similarly shaped medial process of the squamosal laterally (Fig. 3C). The lateral margin is formed by the posterior process of the postorbital anteriorly, and the anterior process of the squamosal posteriorly.

The infratemporal fenestra is relatively small in *Tanystropheus hydroides* among archosauromorphs because of the dorsoventrally tall postorbital bar and generally short length of the temporal region of the skull (Figs. 3A-B and 4A). The dorsal margin of the infratemporal fenestra has an oblique anteroventral to posterodorsal orientation, which is largely formed by the squamosal and anteriorly by the jugal. Because the ascending process of the jugal reaches the squamosal, the postorbital is excluded from the margin of the infratemporal fenestra. The squamosal does not possess a separate ventral process and the posterior margin of the infratemporal fenestra was formed by the anterolateral margin of the quadrate and the quadratojugal. The horizontally orientated posterior process of the jugal formed the ventral margin of the fenestra but did not connect to any bone posteriorly and therefore the infratemporal fenestra was open ventrally.

Choana

The palatal region is only partly preserved in PIMUZ T 2790 (Fig. 3D), but the morphology of the palatal elements can additionally be inferred from the well-preserved elements of PIMUZ T 2787 (see figure 4D, G of Spiekman & Scheyer 2019). The combined information from these two specimens allows for a

complete reconstruction of the palate, which reveals the size and shape of the ventral openings of the skull (Fig. 4C). The choana is long but narrow and framed by a row of large teeth on both the lateral and medial side. It is enclosed laterally by the maxilla, anteriorly by the premaxilla, medially by the vomer, and posteriorly by the palatine.

Suborbital fenestra

Because our identification of the ectopterygoid is tentative, we are not able to confidently interpret the shape of the suborbital fenestra. It was likely framed by the palatine, ectopterygoid, pterygoid, and maxilla (Figs. 3D and 4C). A clear facet on the medial side of the ventral surface of the palatine indicates how this bone articulated with the palatal ramus of the pterygoid and suggests that a small vacuity might have also been present anteriorly between both elements and the vomer.

Posttemporal fenestra

The preservation of the posterolateral process of the parietal and the braincase elements including the paroccipital process of the opisthotic allows for the detailed reconstruction of the occipital region of *Tanystropheus hydroides* (see figure 2C of Spiekman et al. in press). This reveals the presence of a triangular posttemporal fenestra with a curved ventral margin. It is framed by the posterolateral process of the parietal dorsally, the supraoccipital medially, and the paroccipital process of the opisthotic ventrally.

Mandible

Both mandibles have been preserved and are mostly complete. In the right mandible, the dentary is detached from the more posterior elements and overall, the preservation of the left mandible is better than that of the right. Therefore, its reconstruction is largely based on the left mandible (Fig. 25), supplemented by information from the right mandible and other *Tanystropheus hydroides* specimens.

Dentary

Both dentaries have been displaced very little and are located beneath their corresponding premaxilla and maxilla. The dentary makes up roughly two-thirds of the surface of the mandible in lateral view. It is a long, labiolingually thin bone. The mandibular symphysis is exclusively formed by the dentaries and both mandibles were strongly connected by an interdigitating suture, as is indicated by the complex pattern of ridges and grooves on the medial surface on the anterior end of the dentary (Fig. 25B-C). Here, the dentary is also conspicuously expanded ventrally, forming a distinct keel that decreases in height posteriorly and terminates in between the level of the third and fourth alveolus. The presence of this keel is autapomorphic for *Tanystropheus hydroides* among non-archosauriform archosauromorphs. No foramina could be identified on either of the dentaries of PIMUZ T 2790. However, up to nine foramina were previously identified in specimens that are now referred to *Tanystropheus hydroides* in PIMUZ T 2819 and PIMUZ T 2793, and at least one of these was considered to open into the Meckelian groove medially (Wild 1973). The broken surfaces of the dentaries in these specimens hamper clear observation of these foramina, but it is possible that at least a few small foramina were indeed present.

Foramina on the anterior part of the dentary are unambiguously present in *Tanystropheus longobardicus* (Nosotti 2007). In total, 18 alveoli can be identified in the left dentary and 17 in the less complete right one. The three anteriormost are the largest. The tooth margin appears to be straight to slightly convex posteriorly, with a slight concavity in between the three large anterior alveoli and the remaining alveoli. On the medial surface, the Meckelian canal is dorsoventrally high posteriorly, taking up more than half of the medial surface of the dentary (Fig. 25C). Anteriorly the canal narrows, especially around the level of the eighth alveolus. Further anteriorly, approximately at the level of the third alveolus, the canal expands again and finally terminates near the symphysis. The posterior margin of both dentaries is incomplete, and therefore the sutures of this bone with the surangular and angular cannot be established. However, the dentary of the largest known specimen of *Tanystropheus hydroides*, PIMUZ T 2793, is intact, and bears tapering posterodorsal and posterocentral processes (sensu Ezcurra 2016; see figures 18-19 of (Wild 1973)). PIMUZ T 2790 clearly shows that the dentary overlapped the surangular and angular laterally, as had also previously been observed by Wild 1973. In contrast, in *Tanystropheus longobardicus* the surangular is considered to overlap the dentary laterally, based on specimens MSNM BES SC 265, MSNM BES SC 1018, and PIMUZ T 3901 (Nosotti 2007).

Splenial

Both splenials are preserved medial to their corresponding dentary and are incomplete posteriorly. The splenial has an elongate plate-like shape and does not curve around the dentary ventrally as in *Macrocnemus bassanii* or *Tanystropheus longobardicus* (Miedema et al. in press; Nosotti 2007), and was thus not visible in lateral view (Fig. 25A, E). The anteromedial curvature of the splenial follows that of the dentary. Based on their corresponding curvature, the splenial likely extended anteriorly to approximately the level of the third alveolus of the dentary. The bone is dorsoventrally tall, covering the dentary almost completely in medial view (Fig. 25B). In contrast, the splenial of *Tanystropheus longobardicus* is much shorter dorsoventrally and does not reach as far anteriorly (MSNM BES SC 1018; Nosotti 2007). The posterior extent of the splenial is unclear, although based on the right element, it possibly reached the adductor fossa.

Angular

The right angular is located posteromedial to the posterior extent of the left dentary. It is slightly disarticulated from the surangular. The right angular, although less complete than the left, appears to still be in its natural articulation with the surangular and dentary. It is broken in two pieces due to a large break in the ventral margin of the left mandible directly behind the posterior extent of the dentary. In lateral view the angular clearly extended further anteriorly than the surangular on the left mandible (Fig. 25A). Although the angular wraps around the surangular ventrally, the angular is only slightly exposed medially and is restricted to the ventral border of the mandible on this side (Fig. 25B-C). Although its preservation is somewhat poor, the right angular shows most of the lateral exposure of the element. Its dorsal margin was orientated anteroventrally to posterodorsally and is largely straight to slightly concave. Based on the preservation in the left mandible, its dorsal border was likely connected to the lateral margin of the surangular shelf. The exact posterior extent is unclear, but it appears to have terminated anterior to the glenoid fossa at the posterior end of the surangular shelf. However, it is

possible that the angular reached further posteriorly on its ventral side. In this regard, the contribution of the angular to the lateral surface of the mandible is much larger than that in *Macrocnemus bassanii*, and its dorsal margin is less curved than in other early archosauromorphs such as *Prolacerta broomi* and *Azendohsaurus madagaskarensis* (Flynn et al. 2010; Miedema et al. in press; Spiekman 2018).

Surangular

The left surangular is located dorsal to the left angular and directly posterior to the left dentary (Fig. 25A). The right surangular is located dorsal to the right angular and posteromedially to the right dentary. It was not possible to separate the surangular from the articular and prearticular in the right mandible (Fig. 3A), whereas in the left mandible, where these elements are largely in their natural articulation, they can clearly be distinguished (Fig. 3B). The left surangular is complete apart from its ventral margin, which is poorly preserved. The right surangular appears complete except for its anterior portion, which is somewhat broken. The anterior end of the surangular, together with the dentary, clearly indicates that there was no external mandibular fenestra as in *Teyujagua paradoxa* and archosauriforms (Fig. 25A; Pinheiro et al. 2019). The surangular was covered anteriorly by the dentary in lateral view and the splenial in medial view (Fig. 25A-B). Ventrally a clear articulation surface on the surangular indicates the outline of where the angular covered the surangular laterally. The dorsal margin of the surangular is straight anteriorly, but further posteriorly bears an anteroposteriorly long but low convexity. On this convexity, a very small process protrudes dorsally, which represents a small coronoid process. A separate coronoid bone could not be distinguished. However, it is possible that it tightly articulates with the surangular and that the suture between these two elements could not be discerned in the SRµCT data on either side. Therefore, the absence of a coronoid for *Tanystropheus hydroides* cannot be confirmed. It is similarly unclear whether the coronoid represented a separate element in *Tanystropheus longobardicus* (Nosotti 2007). On both surangulars, a large posteriorly opening foramen is present directly anterior to the glenoid fossa (Fig. 25F). This foramen represents the posterior surangular foramen sensu Ezcurra 2016 and is present in various archosauromorphs, such as *Prolacerta broomi*, *Azendohsaurus madagaskarensis*, and *Eohyosaurus wolvaardti* (Butler et al. 2015; Flynn et al. 2010; Spiekman 2018), but apparently absent in *Macrocnemus* spp. (Jaquier et al. 2017). No other foramina could be identified on the lateral surface of either surangular. In lateral view an inconspicuous surangular shelf can be discerned. It is horizontal posteriorly, but directed anteroventrally further anteriorly, where it disappears posterior to the level of the coronoid process. Below the dorsal convexity of the surangular, a large and deep concavity is present on the medial surface (Fig. 25B-C). This represents the lateral wall of the adductor fossa, which is quite large in *Tanystropheus hydroides*, and would have formed the attachment site on the mandible for the adductor musculature. A posteriorly directed process extends from the posteromedial side of the surangular, which would have reached the anterior extent of the medial surface of the prearticular to form the medial wall of the adductor chamber.

Prearticular

Both prearticulars are preserved, although it was not possible to isolate the right element from its surrounding bones in the SRµCT data. The right prearticular is located medial to the surangular. The left

prearticular is still in its natural articulation, covering the articular ventrally along the entire length of the latter (Fig. 25E). The anterior portion of the prearticular is covered by the angular ventrally and laterally. The anteriormost part of the left prearticular is missing because of the same break that affects the left angular (Fig. 25B-C, E). Based on the prearticular from the right mandible, in which the anterior extent of the bone can be made out, the prearticular extends anteriorly to approximately the anterior margin of the adductor fossa. The prearticular is a thin, elongate bone that mediolaterally widens distinctly at the level of the glenoid fossa on the articular (Fig. 25E). It is largely flat and somewhat concave posteriorly with a deep groove that receives the articular dorsally. Further anteriorly, the bone becomes dorsoventrally tall and lateromedially thin, and fits tightly into the curved angular ventrally and the surangular medially, whilst forming most of the ventral margin of the adductor fossa. The prearticular extends roughly equally far posterior as the articular and thus contributes distinctly to the retroarticular process as in *Macrocnemus bassanii* (Miedema et al. in press). Posterior to the posteriormost extent of the angular, the prearticular is clearly visible in lateral view (Fig. 25A).

Articular

As with the other posterior bones of the mandible, the articular is present in the right mandible but cannot be separated from the surrounding elements. The left articular is complete and in articulation, fitting tightly on the dorsal surface of the prearticular (Fig. 25). The articular has a very short, blunt projection anterior to the glenoid fossa, which fits anterodorsally and laterally against the posterior part of the surangular and anteroventrally onto the prearticular. The ventral surface bears an anteroposteriorly directed keel that articulates tightly with the concave groove on the dorsal surface of the prearticular. The glenoid fossa, which forms the articulation with the ventromedial head of the quadrate, is framed by a raised margin (Fig. 25F-G). This margin is raised into a thin vertical ridge on its posterior side. The lateral part of the margin is also raised to form a ridge, particularly on its posterior part. The posterolateral margin in between the posterior and lateral margins is distinctly lower than its neighbouring ridges. The medial margin of the glenoid fossa is strongly displaced ventrally and only somewhat raised posteriorly. The rest of the medial margin, as well as the anterior margin, is not raised. The dorsal surface of the glenoid fossa is formed by a concavity that is orientated posterolaterally to anteromedially (Fig. 25F). Additionally, the fossa slopes laterodorsally to medioventrally. Posterior to the glenoid fossa a retroarticular process is developed on the lateral side of the articular. It forms approximately one-third of the anteroposterior length of the articular and is thus comparatively much larger than in *Macrocnemus bassanii* and *Dinocephalosaurus orientalis* (IVPP-V13767; Miedema et al. in press; Rieppel et al. 2008), and similar to that of early rhynchosaurs such as *Howesia browni*, *Eohyosaurus wolvaardti*, and *Mesosuchus browni* (Butler et al. 2015; Dilkes 1995; Dilkes 1998). It is mediolaterally constricted at its base and widens posteriorly (Fig. 25G). Its posterolateral margin is only very slightly upturned. The posterior end of the retroarticular process is slightly rounded, but less distinctly so than in *Macrocnemus bassanii* (Miedema et al. in press).

Dentition

The dentition on both upper and lower jaws is heterodont and characterized by very large, recurved fangs on the premaxilla and anterior part of the dentary and sharp, conical teeth of varying sizes on the

maxilla and the remainder of the dentary (Figs. 3 and 26). Although not visible in the SRµCT data, external observation of the specimen reveals that there are distinct striations running along all the marginal teeth. The teeth are not serrated. In these characteristics, the teeth of *Tanystropheus hydroides*, as well as those of *Dinocephalosaurus orientalis*, are very similar to certain sauropterygians and indicate a piscivorous diet acquired through a similar feeding mechanism (Rieppel 2002). All marginal teeth are distinctly labiolingually compressed. They exhibit a subthecodont tooth implementation (sensu Fraser & Shelton 1988), marked by a strong and tall labial ridge and a strongly reduced lingual margin. The latter is particularly visible in the premaxilla and the maxilla (Fig. 5B, D). As mentioned above, the premaxilla bears six teeth, the maxilla 15, and the dentary likely 18, of which the anterior three teeth are enlarged fangs (Fig. 26). In some cases a replacement tooth is present lingual to the erupted tooth, indicating ~~there~~ continuous tooth replacement. Because the size of each tooth is partially dependent of their growth stage, and because many teeth are missing in PIMUZ T 2790, it is hard to establish the relative size of the teeth throughout the marginal dentition. Nevertheless, the three fangs on each side of the mandible appear to be somewhat larger than the fangs on the premaxilla, and they interlock with each other to form a “fish-trap” structure (sensu Rieppel 2002). Based on the size of the alveoli, the first five teeth of the premaxilla were large fangs, with the sixth tooth being somewhat reduced in size (Fig. 26). Posterior to this, the anteriormost maxillary tooth is very small. From here, the size of the maxillary teeth increases gradually until the sixth maxillary tooth. Maxillary teeth six through eight are the largest ones. From the eighth tooth, the size of the teeth gradually decreases posteriorly, with the final, the 15th, maxillary tooth only protruding slightly ventral to the maxilla in lateral view (Figs. 5A and 26). This last tooth is located at the tapering end of the posterior process of the maxilla. In the dentary, the size pattern is quite different. It starts with the three large anterior fangs, followed by three strongly reduced alveoli that are barely visible (Fig. 25D and 26). Posterior to this, at the level of the last premaxillary tooth, the first of the larger conical teeth is located. As with the maxillary teeth, this tooth is still comparatively small and the size of the subsequent three teeth increases posteriorly. The large 10th dentary tooth pierces through the surface of the maxilla. Dentary teeth also pierce upper jaw bones in certain crocodylians and temnospondyls (e.g. Cidade et al. 2017; Schoch 1999). After the 10th tooth, the alveoli gradually reduce in size posteriorly (Fig. 26). The posteriormost alveolus on the dentary is located at the same level as the third-to-last (13th) alveolus of the maxilla. The conical dentition of the skull posterior to the fangs overlapped their counterparts on the mandible, rather than interlocking with them (Fig. 3A).

The vomerine teeth are smaller than most marginal teeth but still comparatively large for palatal teeth among archosauromorphs (Fig. 3D). They are recurved, being orientated ventrolabially at their base and ventrally at their distal end (Fig. 15B). They are homodont in shape and gradually decrease in size posteriorly. They are not serrated, but since the teeth can only be observed in the SRµCT data it cannot be assessed whether they were striated. The tooth implantation is subthecodont, with the anterior alveoli having a distinctly higher labial margin compared to the lingual one. Further posteriorly this distinction decreases until, at approximately the 7th alveolus counted from anterior on the right vomer, both margins are roughly equally well-developed. As mentioned above, the more complete right vomer bears 15 teeth positions (Fig. 26). This is likely the total number of teeth on the vomer, although it cannot be fully excluded that one or two additional tooth positions have been lost. As for the marginal

dentition, vomerine tooth replacement was continuous and small replacement teeth are in some cases preserved lingual to an erupted tooth in the alveolus.

Postcranial skeleton

In addition to the skull, PIMUZ T 2790 preserves cervical vertebrae one through eight (Fig. 1A). Of these, the atlas-axis complex and anterior part of the third cervical were scanned together with the skull. This allows for the first detailed description of the atlas-axis complex of *Tanystropheus hydroides*, as well as a description of the internal anatomy of the three anteriormost cervical vertebrae (Fig. 27).

Atlas-axis complex

The atlas-axis complex is preserved but disarticulated in PIMUZ T 2790, and consists of the atlas pleurocentrum, atlas intercentrum, two atlantal neural arches, axis intercentrum, and axis. The atlas pleurocentrum and intercentrum are preserved in between the axis ventrally and right postorbital dorsally. The right atlantal neural arch is located above the left quadrate and below the left frontal and squamosal, whereas the left atlantal neural arch is preserved underneath the right squamosal and the anterior end of the axis. Anterior to the atlas pleurocentrum and intercentrum, the axis intercentrum is preserved between the right posterolateral process of the parietal dorsally and the anterior part of the neural spine of the axis ventrally.

No proatlases could be identified. Proatlases are small elements that are present dorsal to the atlantal neural arches in various diapsids and, among non-archosauriform archosauromorphs, have been identified in *Macrocnemus bassanii*, *Trilophosaurus buettneri*, and *Azendohsaurus madagaskarensis* (Miedema et al. in press; Nesbitt et al. 2015; Spielmann et al. 2008). Because these elements are small and easily disarticulated, it is possible that they were present in *Tanystropheus hydroides* but not preserved or identified in PIMUZ T 2790.

The atlantal neural arch is a tripartite element with a complex structure (Fig. 27). Its posterior process is elongate and formed the articulation with the small prezygapophysis of the axis. Anteriorly the neural arch has a dorsomedial and a ventromedial projected process. The dorsomedial process is a flattened wing-like structure, whereas the ventromedial process expands somewhat distally and ends in a flattened foot-like structure, which would have articulated with the atlas pleurocentrum (Fig. 27D). Together, the two anterior processes of the atlantal neural arch would have framed the neural canal anterior to the axis.

The atlas intercentrum is the smallest element of the complex and is crescent-shaped. It would have been located anteroventral to the atlas pleurocentrum and anterodorsal to the axis intercentrum (Fig. 27).

In the allokotosaurs *Trilophosaurus buettneri* and *Azendohsaurus madagaskarensis* the atlas pleurocentrum is partially or fully fused to the axis intercentrum, forming an odontoid complex (Nesbitt et al. 2015; Spielmann et al. 2008). However, as in *Macrocnemus bassanii* and *Mesosuchus browni*, these elements are present as separate elements in *Tanystropheus hydroides* (Fig. 27; Dilkes 1998; Miedema

et al. in press). The atlas pleurocentrum has an oval cross-section and a flat posterior surface that articulated with the anterior surface of the centrum of the axis pleurocentrum. The anterior margin is distinctly convex and forms the odontoid process that would have articulated with the basioccipital directly below the occipital condyle, thus aligning the neural canal of the axis with the foramen magnum of the skull (Fig. 27E). The dorsal surface of the atlas pleurocentrum forms the floor of the neural canal and is flattened, whereas in *Macrocnemus bassanii* and *Azendohsaurus madagaskarensis* it is distinctly excavated (Miedema et al. in press; Nesbitt et al. 2015).

The axis intercentrum has a similar shape to the atlas intercentrum but is considerably larger. It would have articulated with the axis posteriorly, the atlas intercentrum anteriorly, and the atlas pleurocentrum dorsally (Fig. 27). The anterior margin of the axis intercentrum is flattened as in *Azendohsaurus madagaskarensis*, but in contrast to *Macrocnemus bassanii*, in which it is rounded (Miedema et al. in press; Nesbitt et al. 2015).

At its anterior end the neural spine of the axis is slightly raised, but it is otherwise similar to that of the postaxial cervical vertebrae and very poorly developed (Fig. 27). Short anterolaterally projecting processes on the anterior end of the neural arch of the axis represent the poorly developed prezygapophyses, which would have received the atlantal neural arches dorsally (Fig. 27C-D). The postzygapophyses are typical to those of the post-axial cervical vertebrae, being well-developed and with distinct epipophyses, which extend posterior to the postzygapophyses (Wild 1973). Between the postzygapophyses, a wide and elongate postzygapophyseal trough with a roughly straight posterior margin is preserved, similar to that described for the postaxial cervical vertebrae of *Tanystropheus conspicuus* from the Upper Muschelkalk and *Tanystropheus haasi* from Maktesh Ramon in Israel, now considered nomina dubia (sensu Spiekman & Scheyer 2019). Such a trough has also been described for a dorsal vertebra now assigned to *Tanystropheus hydroides* (MSNM BES 215; Nosotti 2007). In contrast to the postaxial cervical vertebrae, the pleurocentrum of the axis bears a distinct ventral keel (Fig. 27B). The neural canal of the axis is straight and does not run substantially through the pleurocentrum, in contrast to the morphology in postaxial cervical (Fig. 28; Edinger 1924; Wild 1973).

No ribs are preserved in articulation with the atlas-axis complex. Four partial cervical ribs can be seen on the slab externally next to the third cervical vertebra (Fig. 1A). Three additional sections of cervical ribs are preserved underneath the skull and have been revealed by the SRµCT data (Fig. 2B). One rib segment is orientated almost perpendicular to the skull and has broken in three pieces over the right lower jaw and right pterygoid. Another rib fragment is orientated parallel and underneath the right jugal and is also broken over the right lower jaw. Finally, the smallest fragment is orientated parallel to the main axis of the skull and preserved underneath the right pterygoid. However, because these elements are broken and disarticulated, it is unclear whether they represent parts from the same or separate ribs, and therefore it cannot be established how many ribs in total were present in the anterior part of the neck. Thus, although it is almost certain that the axis bore ribs, it is unknown whether there were ribs associated with the atlas.

Postaxial cervical vertebrae

The anterior third of the first postaxial cervical vertebra was included in the SRµCT data and reveals an anatomy congruent with that of large-sized *Tanystropheus* specimens (Fig. 29; Spiekman & Scheyer 2019). It is somewhat compressed transversely. The anterior articular surface of the centrum is flat to slightly concave and is taller than it is wide. The ventral surface of the centrum is flattened. The left prezygapophysis is absent but the right one is completely preserved and extends slightly anterior to the centrum. On the right side of the centrum, the two small articulation facets for the tuberculum and capitulum of the cervical rib are preserved near to each other. The neural spine is short but clearly present anteriorly, and gradually reduces in height posteriorly. It is virtually absent at the posterior end of the section of the vertebra present in the SRµCT data. The inner anatomy visible in the slice data shows that the neural canal clearly passes through the pleurocentrum, as has previously been described for postaxial cervical vertebrae for *Tanystropheus* spp. and the axis for *Macrocnemus bassanii* (Fig. 29; Edinger 1924; Miedema et al. in press; Wild 1973).

The remaining postaxial cervical vertebrae are also transversely compressed. Furthermore, large parts of the cervical vertebrae are reconstructed, obscuring the observation of many anatomical details externally, particularly at their anterior and posterior ends. Their overall morphology and relative lengths (specimen p in table 3 of Wild 1973) corresponds to that of other *Tanystropheus hydroides* specimens.

Discussion

Configuration of the nasals

Although no complete nasal is known for *Tanystropheus hydroides*, partial nasals can be observed in specimens PIMUZ T 2787 (supplementary figure 2B of Spiekman et al. in press) and PIMUZ T 2819 (supplementary figure 1A of Spiekman et al. in press). The fragmentary nasals of the latter show a similar clear concavity on ~~the dorsal surface of the nasals~~ as described here in PIMUZ T 2790 (see also figure 3 of Jiang et al. 2011). The reconstruction of the nasals of *Tanystropheus hydroides* (Fig. 4B) has been inferred from these specimens and through comparison with *Tanystropheus longobardicus*. Complete but disarticulated nasals are preserved in *Tanystropheus longobardicus* specimen PIMUZ T 2484. The elements lack the clear concavity on the dorsal surface of the nasal seen in PIMUZ T 2790 and PIMUZ T 2819 of *Tanystropheus hydroides*, but it is uncertain whether this represents a true morphological feature because the elements of PIMUZ T 2484, including the nasals, are strongly compressed. Both nasals of PIMUZ T 2484 form a single, tapering process anteriorly (supplementary figure 2D of Spiekman et al. in press). The posterior margin of the nasals and the anterior margins of the corresponding frontals in this specimen allow the articulation between these elements to be inferred confidently (supplementary figure 2D-E of Spiekman et al. in press). Their configuration implies that the anterior process of the nasal in *Tanystropheus longobardicus* was located on the anterolateral side of the element and therefore did not form an internarial bar, but instead contacted the dorsal margin of the maxilla and premaxilla. The lack of an anteromedial process on the nasal and a well-developed prenarial process on the premaxilla suggests the complete absence of an internarial bar and the presence of a single, confluent external naris in *Tanystropheus longobardicus* (see figure 3E of Spiekman et al. in press). The partially visible nasal in PIMUZ T 2787 of *Tanystropheus hydroides* is preserved

directly anterior to the left frontal and it therefore most likely represents the left nasal. However, since the nasal almost certainly was somewhat displaced posteriorly, it cannot be excluded that it represents the right nasal that was also laterally displaced. As in *Tanystropheus longobardicus* only a single clear process projects anteriorly on the nasal and a well-developed prenarial process of the premaxilla is also absent in *Tanystropheus hydroides*. Since the identification of the nasal of PIMUZ T 2787 as the left nasal is most parsimonious, which would imply the anterior process projects anterolaterally, and because this corresponds to the configuration present in the congeneric species *Tanystropheus longobardicus*, we consider it most likely that this anterior process was located on the anterolateral side of the nasal in *Tanystropheus hydroides*, and that consequently, the external naris was also confluent in this species (Fig. 4B). This interpretation is further supported by the lack of a prenarial process of the premaxilla in *Tanystropheus hydroides*

***The mandible of* Tanystropheus longobardicus**

The reconstruction of the lower jaw of *Tanystropheus hydroides*, based on the well-preserved left mandible of PIMUZ T 2790, allows for the reinterpretation of the posterior part of the mandible of *Tanystropheus longobardicus*. This was previously reconstructed based on the well-preserved, but strongly compressed and cracked mandibles of MSNM BES SC 1018 (see figures 13 and 53B of Nosotti 2007). In this specimen the splenial was interpreted as reaching far posteriorly, approximately to the level of the glenoid fossa in medial view. However, the posterior part of what was interpreted as the splenial has the same morphology as the angular in PIMUZ T 2790 (Fig. 25). Both form the ventral margin of the mandible ventral to the adductor fossa, and both bear the same distinct concave dorsal surface, which receives the ventral margin of the element dorsal to it in a deep groove. Therefore, this structure is reinterpreted as part of the angular and correspondingly, the splenial of *Tanystropheus longobardicus* likely did not reach much further posteriorly than the anterior margin of the adductor fossa. Similarly, the bone previously identified as the angular in medial view in MSNM BES SC 1018 corresponds in position and morphology to the prearticular of PIMUZ T 2790, and we therefore re-identify it as the angular in medial view. The portion of the mandible previously identified as the prearticular of MSNM BES SC 1018 also represents part of the prearticular, which was likely considered as a separate element due to cracks widely present in the specimen.

The sutures on the lateral side of the mandible of *Tanystropheus longobardicus* are hard to establish in all available specimens. They were previously reconstructed largely based on the left mandible of PIMUZ T 2484, which is broken into two pieces (Nosotti 2007; Wild 1973). However, the reconstructions of this specimen by Wild (1973) and Nosotti (2007) differ in some respects (see figure 49A-B of Nosotti 2007). The suture between the angular and surangular was reconstructed as being positioned more dorsally by Nosotti (2007) than by Wild (1973). A foramen observed in PIMUZ T 2484 could correspond to the surangular foramen that we identified in PIMUZ T 2790 (Fig. 25F). In the reconstruction presented by Wild (1973), this foramen is also placed on the surangular, whereas in the arrangement by Nosotti (2007) this foramen is located on the angular. No foramen is known on the angular in early archosauromorphs, but the presence of a foramen is much more common on the lateral surface of the surangular (Ezcurra 2016). Furthermore, the distribution of the sutures in the reconstruction by Wild (1973), both for the angular and the surangular, and for the dentary with both these elements,

corresponds more closely with that of *Tanystropheus hydroides* than that hypothesized by Nosotti (2007), and it is therefore preferred here. However, the interpretation of the sutures of the lateral side of the mandible in *Tanystropheus longobardicus* remains somewhat equivocal.

Palaeobiology and aquatic adaptations

Although historically the lifestyle of *Tanystropheus* has been the subject of contentious debate, new data increasingly support a mainly aquatic lifestyle for *Tanystropheus hydroides*. An amphibious or semi-aquatic habit was inferred from a bone density analysis of an isolated femur assigned to *Tanystropheus conspicuus* (Jaquier & Scheyer 2017). *Tanystropheus conspicuus* is considered a nomen dubium, but is undoubtedly very closely related, if not synonymous, with *Tanystropheus hydroides* (Spiekman & Scheyer 2019). The skull of *Tanystropheus hydroides* additionally supports an at least semi-aquatic lifestyle for this taxon, as indicated by the external nares being placed on the top of the snout and by the marginal teeth, which conform to the "fish-trap" dentition also present in certain sauropterygians (Spiekman et al. in press).

The postcranial anatomy of *Tanystropheus hydroides* lacks clear adaptations for aquatic propulsion (Nosotti 2007; Renesto 2005; Wild 1973) and its extremely long neck would have significantly increased drag (Massare 1988; Troelsen et al. 2019). Therefore, rather than actively pursuing its prey, which consisted of fast-moving fish and cephalopods, as can be inferred from stomach contents (Wild 1973), *Tanystropheus hydroides* must have been an ambush predator (Spiekman et al. in press). The presence of a small head on the end of a very elongate neck would have likely allowed *Tanystropheus hydroides* to approach its prey with a lower chance of detection.

The endocranial anatomy observed in the SRµCT data of PIMUZ T 2790 provide additional information relevant for palaeobiological inferences, some of which have also been discussed in Spiekman et al. (in press). The flocculus is a cerebral lobe that regulates both head and eye stabilization during movement (Voogd & Wylie 2004). Therefore, it is possible that the presence of a large flocculus is related to the complex head and eye stabilization that *Tanystropheus hydroides* might have required because of its extremely elongated neck. However, a correlation between floccular size and head manoeuvrability for vertebrates is not supported (Ferreira-Cardoso et al. 2017). Furthermore, the orientation of the LSC of the endosseous labyrinth has been used as a proxy for head posture, although its reliability has been questioned (Brown et al. 2019; Hullar 2006; Marugán-Lobón et al. 2013; Neenan & Scheyer 2012). Nevertheless, the virtually horizontal orientation of the LSC in PIMUZ T 2790 could suggest a horizontal head posture for *Tanystropheus hydroides*. The elongate cochlea of *Tanystropheus hydroides* indicates advanced auditory capabilities, as the length of the cochlear duct is a relatively reliable proxy for inferring auditory capabilities in reptiles and birds (Walsh et al. 2009). As was also discussed in Spiekman et al. (in press), the geometry of the semicircular canals is correlated to certain aquatic adaptations. Most evidently, the semicircular canals of deep-diving pelagic reptiles are generally short and robust in comparison to terrestrial and nearshore aquatic taxa (Evers et al. 2019; Neenan et al. 2017; Neenan & Scheyer 2012; Schwab et al. 2020). The comparatively elongate and gracile semicircular canals and common crus of PIMUZ T 2790 therefore clearly indicate that it was not a deep-diving pelagic animal,

which is also supported by a taphonomical analysis of *Tanystropheus* specimens from the Besano Formation of Monte San Giorgio (Beardmore & Furrer 2017).

***Feeding mode of* Tanystropheus hydroides**

Streptostyly

Streptostyly is a form of cranial kinesis in which the quadrate has the ability to swing approximately anteroposteriorly with the rotational axis being formed by the joint between the dorsal head of the quadrate and the squamosal and/or supratemporal (Metzger 2002). In PIMUZ T 2790, the quadrate facet on the posteroventral surface of the squamosal bears a deep pyramidal excavation which was likely covered by a cartilaginous cap (Fig. 11), whereas the dorsal surface of the dorsal head of the quadrate is anteroposteriorly elongated and terminates posteriorly in a conspicuous hook (Fig. 12). This would have allowed the dorsal head of the quadrate to rotate within the concave facet on the squamosal in a loose articulation, thus forming a streptostylic configuration in *Tanystropheus hydroides* (Spiekman et al. in press). In addition to a movable quadrate-squamosal articulation, streptostyly also requires a sliding contact between the pterygoid flange of the quadrate and the quadrate ramus of the pterygoid, to allow the quadrate to move independently of the pterygoid. This movement is facilitated by a concavity present on the distal portion of the pterygoid flange of the quadrate in PIMUZ T 2790 (Fig. 12).

Streptostyly has independently evolved numerous times among sauropsids and although it influences jaw adduction, it does not appear to have a universal function (Metzger 2002). Mosasaurs, a diverse group of predatory aquatic squamates, also had streptostylic skulls. In this group, streptostyly likely functioned similarly to varanids, and facilitated ratchet feeding (i.e. locking prey in the jaw through extensive palatal dentition) and hard biting (Lingham-Soliar 1995). The absence of teeth on the palatine and pterygoid indicates that *Tanystropheus hydroides* did not employ an extensive form of ratchet feeding. One possibility is that streptostyly optimized the moment arm of the jaw adductor musculature, either the M. adductor mandibulae externus or M. pterygoideus, thus providing a mechanical advantage (i.e. the muscle requires less exertion to achieve the same bite force, Rieppel 1978; Smith 1980). However, statistical modeling is required to test whether streptostyly would indeed improve the mechanical efficiency of the cranial biomechanics of *Tanystropheus hydroides*.

Hyobranchial apparatus

Suction feeding in vertebrates can be inferred from skeletal adaptations of the hyobranchial apparatus. The contraction of muscles (e.g., the M. coracohyoideus and M. sternohyoideus connecting the hyobranchial apparatus to the pectoral girdle retracts this apparatus, which creates a negative pressure within the buccal cavity (Motani et al. 2013). The apparatus of a suction feeder generally exhibits several adaptations to handle the considerable stress it experiences during a retraction that is strong enough to create a sufficiently negative pressure. These adaptations typically include the presence of an ossified hyoid corpus and robusticity of the hyobranchial rods that connect to the corpus.

No elements of the hyobranchial apparatus are preserved in PIMUZ T 2790. However, ceratobranchial I is known from *Tanystropheus hydroides* specimens PIMUZ T 2819 and SNSB-BSPG 1953 XV 2. This slightly curved bone is comparatively thin (measurements provided on page 44 of Wild 1973). No other hyobranchial elements are known and therefore there is no evidence of an ossified hyoid corpus in *Tanystropheus hydroides*. Furthermore, the "fish-trap" dentition seems to preclude the possibility of suction feeding in *Tanystropheus hydroides*, since the elongate fangs would interfere with the prey item entering the buccal cavity.

Hyobranchial elements were previously also identified in *Tanystropheus longobardicus* specimens PIMUZ T 2791, PIMUZ T 2484 (both in Wild 1973), and MSNM BES SC 265 (Nosotti 2007). We were not able to corroborate the identification of these elements due to poor preservation (PIMUZ T 2791 and MSNM BES SC 265) or disarticulation, which does not allow a thin ceratobranchial I to be clearly differentiated from surrounding gastralia and rib fragments (PIMUZ T 2484). However, a pair of hyobranchial rods, possibly ceratobranchial I, are clearly preserved in *Tanystropheus longobardicus* specimen PIMUZ T 3901, directly posterior to the left lower jaw (see figure 2B of Spiekman & Scheyer 2019). These elements have a rod-like shape and are slightly curved. They are relatively gracile (total length: 10.8 mm; maximum width: 0.9 mm). As in *Tanystropheus hydroides*, an ossified hyoid corpus was likely not present in *Tanystropheus longobardicus*. The apparent absence of an ossified hyoid corpus and the lack of robust hyobranchial rods therefore indicate that both species of *Tanystropheus* were not suction feeders.

Salt glands

A tetrapod spending large amounts of time in a marine environment needs to excrete excess salt from its body. This is achieved by salt glands. Salt glands are generally located within the nasal or orbital cavities (an overview is provided in Babonis & Brischoux 2012). No evidence for a salt gland can be found in the orbital cavity of *Tanystropheus hydroides*, but the large space of confluent external nares could have facilitated such a gland. This is also the case in Triassic sauropterygians such as *Nothosaurus marchicus* (Voeten et al. 2018). However, due to the poor preservation of the nasals, no skeletal correlates for a salt gland have been found in the SRµCT data of PIMUZ T 2790. The generally poor preservation of the nasals in all known *Tanystropheus* specimens, both of *Tanystropheus hydroides* and *Tanystropheus longobardicus*, limits the observation of this trait and therefore nothing can be said unambiguously about the presence of salt glands in *Tanystropheus* currently.

Conclusions

The detailed morphological study of the SRµCT data presented here provides much additional information on the skull and anterior cervical region of *Tanystropheus hydroides*, and highlights that the configuration of the skull is entirely unique among archosauromorphs and adapted for a lifestyle as an aquatic ambush hunter. The external naris is confluent and positioned on the dorsal surface of the snout. As in *Tanystropheus longobardicus*, but in contrast to other archosauromorphs, the frontals are wide across the interorbital region and form most of the dorsal margin of the orbit. The postorbital region is characterized by dorsally directed supratemporal fenestrae, laterally facing supratemporal

fossae of the parietals, a dorsoventrally tall squamosal, and dorsally hooked quadrate. The braincase is characterized by several derived archosaur traits, such as the presence of a laterosphenoid, and the ossification of the lateral wall of the braincase by a connection between the prootics and parabasisphenoid. However, the braincase differs from more derived archosauriforms in the morphology of the ventral ramus of the opisthotic, the horizontal orientation of the parabasisphenoid, and the lack of a clearly defined crista prootica. There is no indication of pneumatization in the braincase of *Tanystropheus hydroides*. The flocculus was pronounced and possibly required for processing complicated head and eye stabilization as a result of the extremely elongated neck. The cochlear duct of the endosseous labyrinth is well-developed, indicating advanced auditory capabilities in *Tanystropheus hydroides*. The configuration of the palate is distinct from other archosauromorphs, including *Tanystropheus longobardicus*, but possibly resembles in some respects the poorly known palatal region of the marine archosauromorph *Dinocephalosaurus orientalis*. The marginal dentition is also comparable to that of *Dinocephalosaurus orientalis* and forms a clear indication of a piscivorous diet. The skull of *Tanystropheus hydroides* was very likely streptostylic, as is indicated by the specialized articulation between the quadrate and squamosal, and the sliding contact between the quadrate and pterygoid, which allowed the quadrate to be retracted posteriorly. The dentition, as well as the morphology of the hyoid apparatus, indicates that *Tanystropheus hydroides* was clearly not a suction feeder but likely employed a laterally directed snapping bite like certain sauropterygians. The lower jaw of *Tanystropheus hydroides* allows for the reinterpretation of the mandible of *Tanystropheus longobardicus*, specifically with regards to the splenial, surangular, angular, and prearticular.

The SRµCT data of PIMUZ T 2790 previously revealed the taxonomic and ecomorphological distinction between *Tanystropheus hydroides* and *Tanystropheus longobardicus* from the Besano Formation of Monte San Giorgio, thus indicating niche partitioning within the genus (Spiekman et al. in press). Furthermore, the remarkable divergence in cranial morphology between these two *Tanystropheus* species and other tanystropheid taxa such as *Macrocnemus bassanii* as revealed in this study provides a clear indication of the ecomorphological diversity of Tanystropheidae, which was previously only marginally understood.

Institutional abbreviations

BP – Evolutionary Studies Institute (previously Bernard Price Institute for Palaeontological Research), University of Witwatersrand, Johannesburg, South Africa

BSPG – Bayerische Staatssammlung für Paläontologie und Geologie, Munich, Germany

IVPP - Institute of Vertebrate Paleontology and Paleoanthropology, Beijing, China

MSNM - Museo di Storia Naturale, Milan, Italy

NMK – Naturkundemuseums im Ottoneum der Stadt Kassel, Kassel, Germany

PIMUZ - Paläontologisches Institut und Museum der Universität Zürich, Zurich, Switzerland

SAM – PK - Iziko South African Museum, Cape Town, South Africa

ZAR – Zarzaitine Collection, Muséum National d'Histoire Naturelle, Paris, France

Acknowledgements

Christian Klug allowed for permission to scan PIMUZ T 2790 and access to comparative material from the PIMUZ collections. Additionally, we are grateful for collection access by the following curators: Bernhard Zipfel, Sifelani Jirah, and Jonah Choiniere (BP), Oliver Rauhut (BSPG), Li Chun (IVPP), Cristiano Dal Sasso (MSNM), Cornelia Kurz (NMK), Claire Browning and Roger Smith (SAM-PK), Rainer Schoch (SMNS), and Nour-Eddine Jalil (ZAR). Dylan Bastiaans kindly helped in rendering the images for Figures 28 and 29 in Mimics Research v19.0. We would like to thank our colleagues Dylan Bastiaans, Feiko Miedema, Christian Klug, Roger Benson, Jonah Choiniere, Roland Sookias, Richard Butler, Fabio Dalla Vecchia, Oliver Rauhut, and Gabriela Sobral for discussions on the morphology of *Tanystropheus*. We are grateful to the European Synchrotron Radiation Facility (ESRF), Grenoble, France, for synchrotron radiation beamtime at beamline BM05.

References

Babonis LS, and Brischoux F. 2012. Perspectives on the convergent evolution of tetrapod salt glands. *Integrative and comparative biology* 52:245-256. 10.1093/icb/ics073

Beardmore SR, and Furrer H. 2017. Land or water: using taphonomic models to determine the lifestyle of the Triassic protorosaur *Tanystropheus* (Diapsida, Archosauromorpha). *Palaeobiodiversity and Palaeoenvironments* 98. 10.1007/s12549-017-0299-7

Brown EE, Butler RJ, Ezcurra MD, Bhullar BAS, and Lautenschlager S. 2019. Endocranial anatomy and life habits of the Early Triassic archosauriform *Proterosuchus fergusi*. *Palaeontology*. doi: 10.1111/pala.12454

Butler RJ, Ezcurra MD, Montefeltro FC, Samathi A, and Sobral G. 2015. A new species of basal rhynchosaur (Diapsida: Archosauromorpha) from the early Middle Triassic of South Africa, and the early evolution of Rhynchosauria. *Zoological Journal of the Linnean Society* 174:571-588.

Cidade GM, Solórzano A, Rincón AD, Riff D, and Hsiou AS. 2017. A new *Mourasuchus* (Alligatoroidea, Caimaninae) from the late Miocene of Venezuela, the phylogeny of Caimaninae and considerations on the feeding habits of *Mourasuchus*. *PeerJ* 5:e3056. 10.7717/peerj.3056

Clark JM, Welman J, Gauthier JA, and Parrish JM. 1993. The laterosphenoid bone of early archosauriforms. *Journal of Vertebrate Paleontology* 13:48-57.

De Oliveira TM, Oliveira D, Schultz CL, Kerber L, and Pinheiro FL. 2018. Tanystropheid archosauromorphs in the Lower Triassic of Gondwana. *Acta Palaeontologica Polonica*. 10.4202/app.00489.2018

De Oliveira TM, Pinheiro FL, Stock Da Rosa ÁA, Dias Da Silva S, and Kerber L. 2020. A new archosauromorph from South America provides insights on the early diversification of tanystropheids. *PloS one* 15:e0230890. 10.1371/journal.pone.0230890

Dilkes DW. 1995. The rhynchosaur *Howesia browni* from the Lower Triassic of South Africa. *Palaeontology* 38:665-686.

Dilkes DW. 1998. The Early Triassic rhynchosaur *Mesosuchus browni* and the interrelationships of basal archosauromorph reptiles. *Philosophical Transactions of the Royal Society of London B: Biological Sciences* 353:501-541. 10.1098/rstb.1998.0225

Edinger T. 1924. Rückenmark im Wirbelkörper! *Anatomischer Anzeiger* 57:515-519.

Evans SE. 1986. The braincase of *Prolacerta broomi* (Reptilia, Triassic). *Neues Jahrbuch für Geologie und Paläontologie Abhandlungen* 173:181-200.

Evans SE. 1987. The braincase of *Youngina capensis* (Reptilia: Diapsida; Permian). *Neues Jahrbuch für Geologie und Paläontologie Monatshefte* 1987:193-203.

Evers SW, Neenan JM, Ferreira GS, Werneburg I, Barrett PM, and Benson RB. 2019. Neurovascular anatomy of the protostegid turtle *Rhinochelys pulchriceps* and comparisons of membranous and endosseous labyrinth shape in an extant turtle. *Zoological Journal of the Linnean Society* 187:800-828. 10.1093/zoolinnean/zlz063

Ezcurra MD. 2016. The phylogenetic relationships of basal archosauromorphs, with an emphasis on the systematics of proterosuchian archosauriforms. *PeerJ* 4:e1778. 10.7717/peerj.1778

Ezcurra MD, and Butler RJ. 2015. Taxonomy of the proterosuchid archosauriforms (Diapsida: Archosauromorpha) from the earliest Triassic of South Africa, and implications for the early archosauriform radiation. *Journal of Anatomy* 58:141–170.

Ezcurra MD, Scheyer TM, and Butler RJ. 2014. The origin and early evolution of Sauria: reassessing the Permian saurian fossil record and the timing of the crocodile-lizard divergence. *PLoS ONE* 9:e89165.

Ferreira-Cardoso S, Araújo R, Martins NE, Martins GG, Walsh S, Martins RMS, Kardjilov N, Manke I, Hilger A, and Castanhinha R. 2017. Floccular fossa size is not a reliable proxy of ecology and behaviour in vertebrates. *Scientific reports* 7:2005. 10.1038/s41598-017-01981-0

Flynn JJ, Nesbitt SJ, Michael Parrish J, Ranivoharimanana L, and Wyss AR. 2010. A new species of *Azendohsaurus* (Diapsida: Archosauromorpha) from the Triassic Isalo Group of southwestern Madagascar: cranium and mandible. *Palaeontology* 53:669-688.

Ford DP, and Benson RB. 2018. A redescription of *Orovenator mayorum* (Sauropsida, Diapsida) using high-resolution µ CT, and the consequences for early amniote phylogeny. *Papers in Palaeontology*.

Formoso KK, Nesbitt SJ, Pritchard AC, Stocker MR, and Parker WG. 2019. A long-necked tanystropheid from the Middle Triassic Moenkopi Formation (Anisian) provides insights into the ecology and biogeography of tanystropheids. *Palaeontologia Electronica* 22:1-15. 10.26879/988

Foth C, Ezcurra MD, Sookias RB, Brusatte SL, and Butler RJ. 2016. Unappreciated diversification of stem archosaurs during the Middle Triassic predated the dominance of dinosaurs. *BMC evolutionary biology* 16:188. 10.1186/s12862-016-0761-6

Fraser NC, and Rieppel O. 2006. A New Protorosaur (Diapsida) from the Upper Buntsandstein of the Black Forest, Germany. *Journal of Vertebrate Paleontology* 26:866-871. 10.1671/0272-4634(2006)26[866:anpdft]2.0.co;2

Fraser NC, and Shelton CG. 1988. Studies of tooth implantation in fossil tetrapods using high-resolution X-radiography. *Geological Magazine* 125:117-122.

Gardner NM, Holiday CM, and O'Keefe FR. 2010. The Braincase of *Youngina capensis* (Reptilia, Dipsida): New Insights from High-Resolution CT Scanning of the Holotype. *Palaeontologica Electronica* 13.

Gottmann-Quesada A, and Sander PM. 2009. A redescription of the early archosauromorph *Protorosaurus speneri* Meyer, 1832, and its phylogenetic relationships. *Palaeontographica Abteilung A*:123-220.

Gower DJ. 1997. The braincase of the early archosaurian reptile *Erythrosuchus africanus*. *Journal of Zoology* 242:557-576.

Gower DJ, and Sennikov AG. 1996. Morphology and phylogenetic informativeness of early archosaur braincases. *Palaeontology* 39:883-906.

Hullar TE. 2006. Semicircular canal geometry, afferent sensitivity, and animal behavior. *The Anatomical Record Part A* 288:466-472. 10.1002/ar.a.20304

Jalil N-E. 1997. A new prolacertiform diapsid from the Triassic of North Africa and the interrelationships of the Prolacertiformes. *Journal of Vertebrate Paleontology* 17:506-525. 10.1080/02724634.1997.10010998

Jaquier VP, Fraser NC, Furrer H, and Scheyer TM. 2017. Osteology of a New Specimen of *Macrocnemus* aff. *M. fuyuanensis* (Archosauromorpha, Protorosauria) from the Middle Triassic of Europe: Potential Implications for Species Recognition and Paleogeography of Tanystropheid Protorosaurs. *Frontiers in Earth Science* 5. 10.3389/feart.2017.00091

Jaquier VP, and Scheyer TM. 2017. Bone Histology of the Middle Triassic Long-Necked Reptiles *Tanystropheus* and *Macrocnemus* (Archosauromorpha, Protorosauria). *Journal of Vertebrate Paleontology*. 10.1080/02724634.2017.1296456

Jiang D-Y, Rieppel O, Fraser NC, Motani R, Hao W-C, Tintori A, Sun Y-L, and Sun Z-Y. 2011. New information on the protorosaurian reptile *Macrocnemus fuyuanensis* Li et al., 2007, from the Middle/Upper Triassic of Yunnan, China. *Journal of Vertebrate Paleontology* 31:1230-1237. 10.1080/02724634.2011.610853

Li C, Fraser NC, Rieppel O, Zhao L-J, and Wang L-T. 2017. A new diapsid from the Middle Triassic of southern China. *Journal of Paleontology*:1-7. 10.1017/jpa.2017.12

Lingham-Soliar T. 1995. Anatomy and functional morphology of the largest marine reptile known, *Mosasaurus hoffmanni* (Mosasauridae, Reptilia) from the Upper Cretaceous, Upper Maastrichtian of the Netherlands. *Philosophical Transactions of the Royal Society of London Series B: Biological Sciences* 347:155-180. 10.1098/rstb.1995.0019

Liu J, Organ CL, Benton MJ, Brandley MC, and Aitchison JC. 2017. Live birth in an archosauromorph reptile. *Nature communications* 8:14445. 10.1038/ncomms14445

Marugán-Lobón J, Chiappe LM, and Farke AA. 2013. The variability of inner ear orientation in saurischian dinosaurs: testing the use of semicircular canals as a reference system for comparative anatomy. *PeerJ* 1:e124. 10.7717/peerj.124

Massare JA. 1988. Swimming capabilities of Mesozoic marine reptiles: implications for method of predation. *Paleobiology* 14:187-205.

Metzger K. 2002. Cranial kinesis in lepidosaurs: skulls in motion. *Topics in functional and ecological vertebrate morphology*:15-46.

Miedema F, Spiekman SNF, Fernandez V, Reumer JWF, and Scheyer TM. in press. Cranial morphology of the tanystropheid *Macrocnemus bassanii* unveiled using synchrotron microtomography. *Scientific Reports*.

Modesto SP, and Sues H-D. 2004. The skull of the Early Triassic archosauromorph reptile *Prolacerta broomi* and its phylogenetic significance. *Zoological Journal of the Linnean Society* 140:335-351.

Motani R, Ji C, Tomita T, Kelley N, Maxwell E, Jiang D-y, and Sander PM. 2013. Absence of suction feeding ichthyosaurs and its implications for Triassic mesopelagic paleoecology. *PLoS One* 8. 10.1371/journal.pone.0066075

Neenan JM, Reich T, Evers SW, Druckenmiller PS, Voeten DF, Choiniere JN, Barrett PM, Pierce SE, and Benson RB. 2017. Evolution of the sauropterygian labyrinth with increasingly pelagic lifestyles. *Current Biology* 27:3852-3858. e3853. 10.1016/j.cub.2017.10.069

Neenan JM, and Scheyer TM. 2012. The braincase and inner ear of *Placodus gigas* (Sauropterygia, Placodontia)—a new reconstruction based on micro-computed tomographic data. *Journal of Vertebrate Paleontology* 32:1350-1357. 10.1080/02724634.2012.695241

Nesbitt SJ. 2011. The early evolution of archosaurs: relationships and the origin of major clades. *Bulletin of the American Museum of Natural History* 352:292 p. 10.1206/352.1

Nesbitt SJ, Flynn JJ, Pritchard AC, Parrish JM, Ranivoharimanana L, and Wyss AR. 2015. Postcranial anatomy and relationships of *Azendohsaurus madagaskarensis*. *Bulletin of the American Museum of Natural History* 398:1-126. 10.1206/amnb-899-00-1-126.1

Nosotti S. 2007. *Tanystropheus longobardicus* (Reptilia, Protorosauria): Re-interpretations of the anatomy based on new specimens from the Middle Triassic of Besano (Lombardy, northern

Italy). *Memorie della Società Italiana di Scienze Naturali e del Museo Civico di Storia Naturale di Milano* 35:1-88.

Olsen PE. 1979. A new aquatic eosuchian from the Newark Supergroup (Late Triassic-Early Jurassic) of North Carolina and Virginia. *Postilla* 176:1-14.

Pierce SE, Williams M, and Benson RB. 2017. Virtual reconstruction of the endocranial anatomy of the early Jurassic marine crocodylomorph *Pelagosaurus typus* (Thalattosuchia). *PeerJ* 5:e3225. 10.7717/peerj.3225

Pinheiro FL, Simão-Oliveira DD, and Butler RJ. 2019. Osteology of the archosauromorph *Teyujagua paradoxa* and the early evolution of the archosauriform skull. *Zoological Journal of the Linnean Society* XX:1-40. 10.1093/zoolinnean/zlz093

Pritchard AC, Gauthier JA, Hanson M, Bever GS, and Bhullar B-AS. 2018. A tiny Triassic saurian from Connecticut and the early evolution of the diapsid feeding apparatus. *Nature communications* 9:1213.

Pritchard AC, Turner AH, Nesbitt SJ, Irmis RB, and Smith ND. 2015. Late Triassic tanystropheids (Reptilia, Archosauromorpha) from Northern New Mexico (Petrified Forest Member, Chinle Formation) and the biogeography, functional morphology, and evolution of Tanystropheidae. *Journal of Vertebrate Paleontology*:e911186. 10.1080/02724634.2014.911186

Renesto S. 2005. A new specimen of *Tanystropheus* (Reptilia Protorosauria) from the Middle Triassic of Switzerland and the ecology of the genus. *Rivista Italiana di Paleontologia e Stratigrafia* 111:377-394.

Renesto S, and Dalla Vecchia FM. 2000. The unusual dentition and feeding habits of the prolacertiform reptile *Langobardisaurus* (Late Triassic, Northern Italy). *Journal of Vertebrate Paleontology* 20:622-627. 10.1671/0272-4634(2000)020[0622:tudafh]2.0.co;2

Rieppel O. 1978. Streptostyly and muscle function in lizards. *Cellular and Molecular Life Sciences* 34:776-777.

Rieppel O. 2002. Feeding mechanics in Triassic stem-group sauropterygians: the anatomy of a successful invasion of Mesozoic seas. *Zoological Journal of the Linnean Society* 135:33-63.

Rieppel O, Li C, and Fraser NC. 2008. The skeletal anatomy of the Triassic protorosaur *Dinocephalosaurus orientalis*, from the Middle Triassic of Guizhou Province, southern China. *Journal of Vertebrate Paleontology* 28:95-110. 10.1671/0272-4634(2008)28[95:tsaott]2.0.co;2

Schoch RR. 1999. Comparative Osteology of *Mastodonsaurus giganteus* (Jaeger, 1828) from the Middle Triassic (Lettenkeuper: Longobardian) of Germany (Baden-Württemberg, Bayern, Thüringen). Staatliches Museum für Naturkunde.

Schwab JA, Young MT, Neenan JM, Walsh SA, Witmer LM, Herrera Y, Allain R, Brochu CA, Choiniere JN, and Clark JM. 2020. Inner ear sensory system changes as extinct crocodylomorphs transitioned from land to water. *Proceedings of the National Academy of Sciences*. 10.1073/pnas.2002146117

Sen K. 2003. *Pamelaria dolichotrachela*, a new prolacertid reptile from the Middle Triassic of India. *Journal of Asian Earth Sciences* 21:663-681.

Sennikov AG. 2011. New tanystropheids (Reptilia: Archosauromorpha) from the Triassic of Europe. *Paleontological Journal* 45:90-104. 10.1134/s0031030111010151

Smith KK. 1980. Mechanical significance of streptostyly in lizards. *Nature* 283:778-779. 10.1038/283778a0

Sobral G, Hipsley CA, and Müller J. 2012. Braincase redescription of *Dysalotosaurus lettowvorbecki* (Dinosauria, Ornithopoda) based on computed tomography. *Journal of Vertebrate Paleontology* 32:1090-1102. 10.1080/02724634.2012.693554

Sobral G, and Müller J. 2016. Archosaurs and their kin: The ruling reptiles. In: Clack JA, Fay RR, and Popper AN, eds. *Evolution of the Vertebrate Ear - Evidence from the Fossil Record* 59 ed: Springer, 285-326.

Sobral G, and Müller J. 2019. The braincase of *Mesosuchus browni* (Reptilia, Archosauromorpha) with information on the inner ear and description of a pneumatic sinus. *PeerJ* 7:e6798.

Sobral G, Sookias RB, Bhullar B-AS, Smith RMH, Butler RJ, and Müller J. 2016. New information on the braincase and inner ear of *Euparkeria capensis* Broom: implications for diapsid and archosaur evolution. *Royal Society Open Science* 3.

Spiekman SNF. 2018. A new specimen of *Prolacerta broomi* from the lower Fremouw Formation (Early Triassic) of Antarctica, its biogeographical implications and a taxonomic revision. *Scientific reports* 8:17996. 10.1038/s41598-018-36499-6

Spiekman SNF, Neenan JM, Fraser NC, Fernandez V, Rieppel O, Nosotti S, and Scheyer TM. in press. Aquatic habits and niche partitioning in the extraordinarily long-necked Triassic reptile *Tanystropheus Current Biology*.

Spiekman SNF, and Scheyer TM. 2019. A taxonomic revision of the genus *Tanystropheus* (Archosauromorpha, Tanystropheidae). *Palaeontologia Electronica* 22:1-46. 10.26879/1038

Spielmann JA, Lucas SG, Rinehart LF, and Heckert AB. 2008. The Late Triassic archosauromorph *Trilophosaurus*. *New Mexico Museum Naturall History and Science Bulletin* 43:1-177.

Stockar R. 2010. Facies, depositional environment, and palaeoecology of the Middle Triassic Cassina beds (Meride Limestone, Monte San Giorgio, Switzerland). *Swiss Journal of Geosciences* 103:101-119. 10.1007/s00015-010-0008-2

Sues H-D. 2003. An unusual new archosauromorph reptile from the Upper Triassic Wolfville Formation of Nova Scotia. *Canadian Journal of Earth Sciences* 40:635-649. 10.1139/E02-048

Troelsen PV, Wilkinson DM, Seddighi M, Allanson DR, and Falkingham PL. 2019. Functional morphology and hydrodynamics of plesiosaur necks: Does size matter? *Journal of Vertebrate Paleontology* 39:e1594850. 10.1080/02724634.2019.1594850

Voeten DF, Reich T, Araújo R, and Scheyer TM. 2018. Synchrotron microtomography of a *Nothosaurus marchicus* skull informs on nothosaurian physiology and neurosensory adaptations in early Sauropterygia. *PloS one* 13:e0188509.

Voogd J, and Wylie DR. 2004. Functional and anatomical organization of floccular zones: a preserved feature in vertebrates. *Journal of Comparative Neurology* 470:107-112. 10.1002/cne.11022

Walsh SA, Barrett PM, Milner AC, Manley G, and Witmer LM. 2009. Inner ear anatomy is a proxy for deducing auditory capability and behaviour in reptiles and birds. *Proceedings of the Royal Society B: Biological Sciences* 276:1355-1360. 10.1098/rspb.2008.1390

Wild R. 1973. Die Triasfauna der Tessiner Kalkalpen XXII. *Tanystropheus longobardicus* (Bassani) (Neue Ergebnisse). *Schweizerische Paläontologische Abhandlungen* 95:1-182.

Figure 1

The holotype of *Tanystropheus hydroides* PIMUZ T 2790.

(A) The complete specimen. (B) Close-up of the skull in dorsal view. (C) Close-up of the skull in oblique right lateral view.

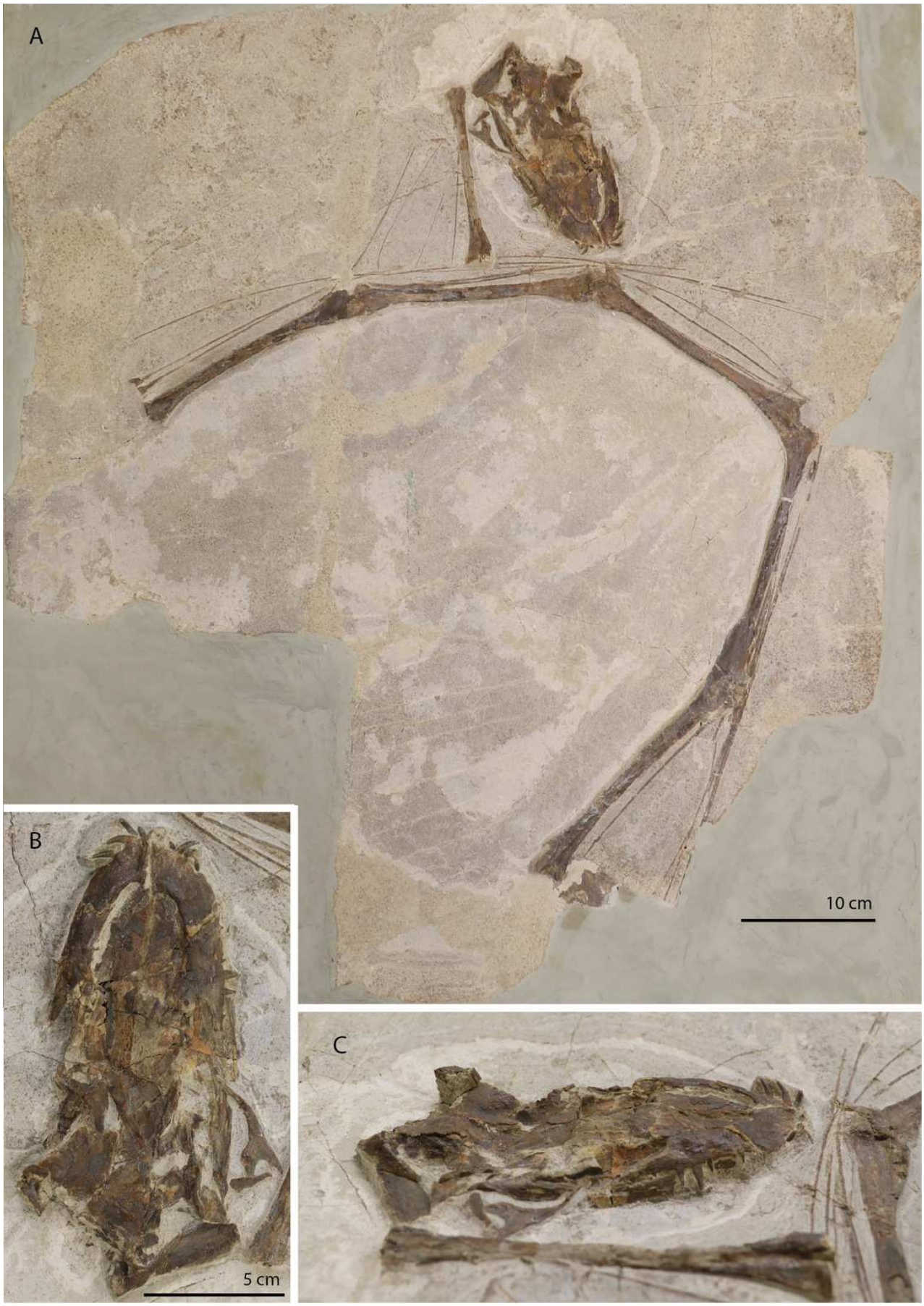
A
10 cm
B
5 cm
C

Figure 2

Digital reconstruction of the skull and proximal cervical vertebrae of PIMUZ T 2790.

(A) Dorsal view. (B) Ventral view.

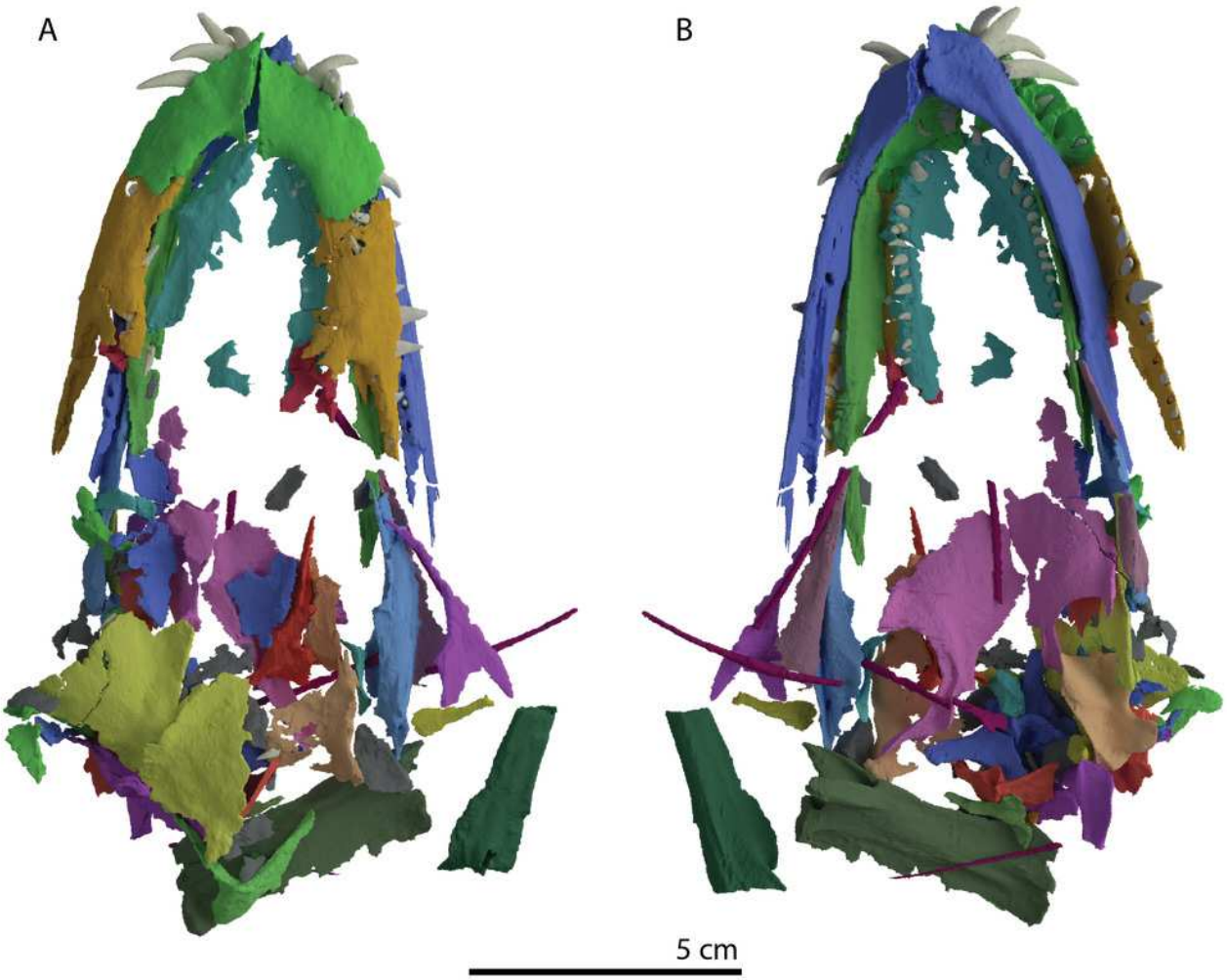

Figure 3

‘Re-assembled’ digital reconstruction of the skull and proximal cervical vertebrae of PIMUZ T 2790.

(A) Right lateral view. (B) Left lateral view. (C) Dorsal view. (D) Ventral view. Abbreviations: an, angular; ana, atlas neural arch; ar, articular; ax, axis; axi, axis intercentrum; bo, basioccipital; br, braincase; cv3, cervical vertebra 3; de, dentary; ect, ectopterygoid; fr, frontal; j, jugal; la, lacrimal; mx, maxilla; na, nasal; pa, parietal; pal, palatine; pbs, parabasisphenoid; pmx, premaxilla; po, postorbital; pra, prearticular; prf, prefrontal; pt, pterygoid; q, quadrate; qj, quadratojugal; sa, surangular; sq, squamosal; vo, vomer.

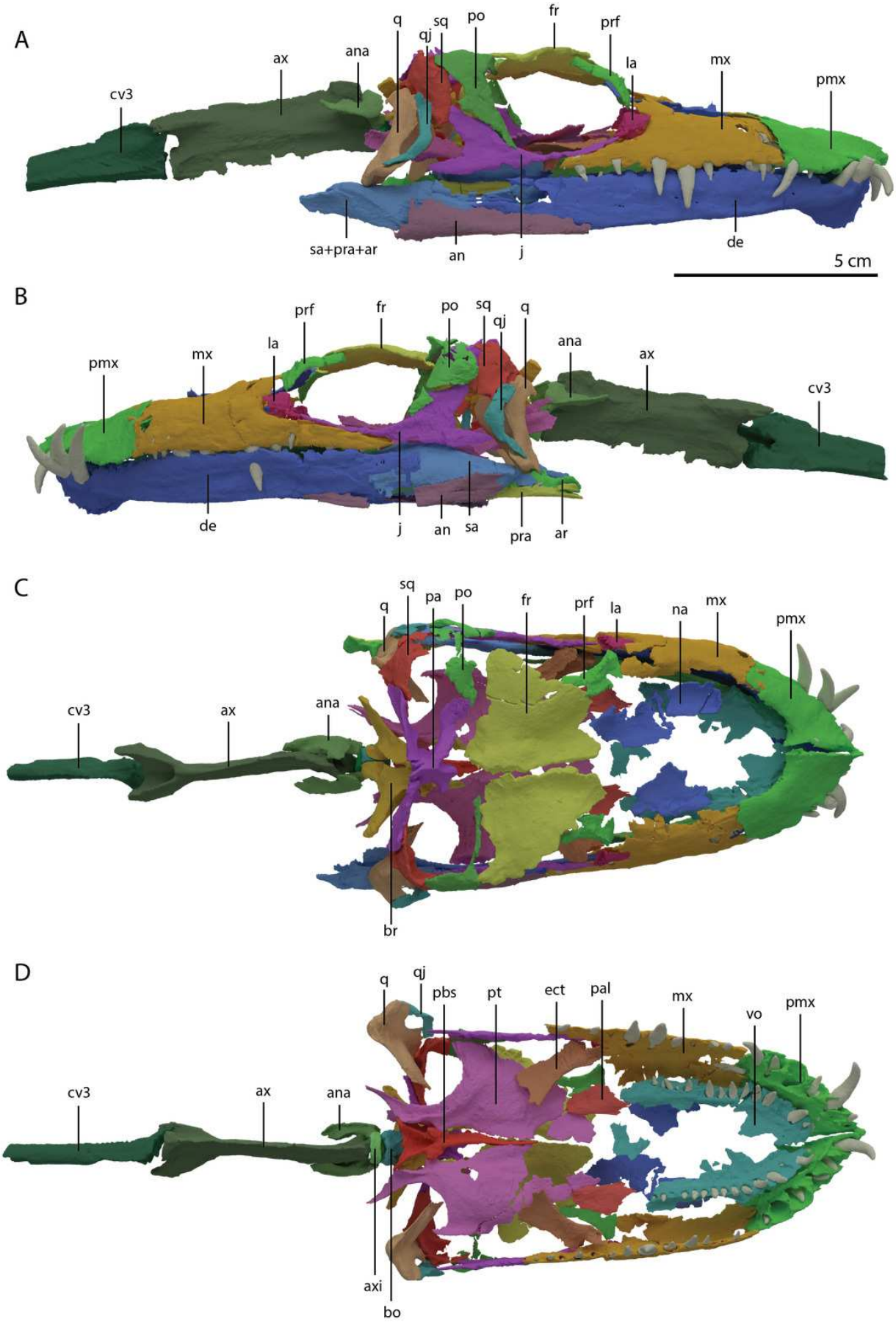
A
cv3
ax
ana
q
qj
sq
po
fr
prf
la
mx
pmx
sa+pra+ar
an
j
de
5 cm
B
pmx
mx
la
prf
fr
po
sq
qj
q
ana
ax
cv3
de
j
an
sa
pra
ar
C
cv3
ax
ana
q
sq
pa
po
fr
prf
la
na
mx
pmx
br
D
cv3
ax
ana
q
qj
pbs
pt
ect
pal
mx
vo
pmx
axi
bo

Figure 4

Reconstruction drawing of the skull of *Tanystropheus hydroides* largely based on PIMUZ T 2790.

(A) Left lateral view. (B) Dorsal view. (C) Ventral view. Abbreviations: an, angular; ar, articular; bo, basioccipital; de, dentary; ect, ectopterygoid; fr, frontal; j, jugal; la, lacrimal; mx, maxilla; na, nasal; pa, parietal; pal, palatine; pbs, parabasisphenoid; pmx, premaxilla; po, postorbital; pof, postfrontal; pra, prearticular; prf, prefrontal; pt, pterygoid; q, quadrate; qj, quadratojugal; sq, squamosal; vo, vomer.

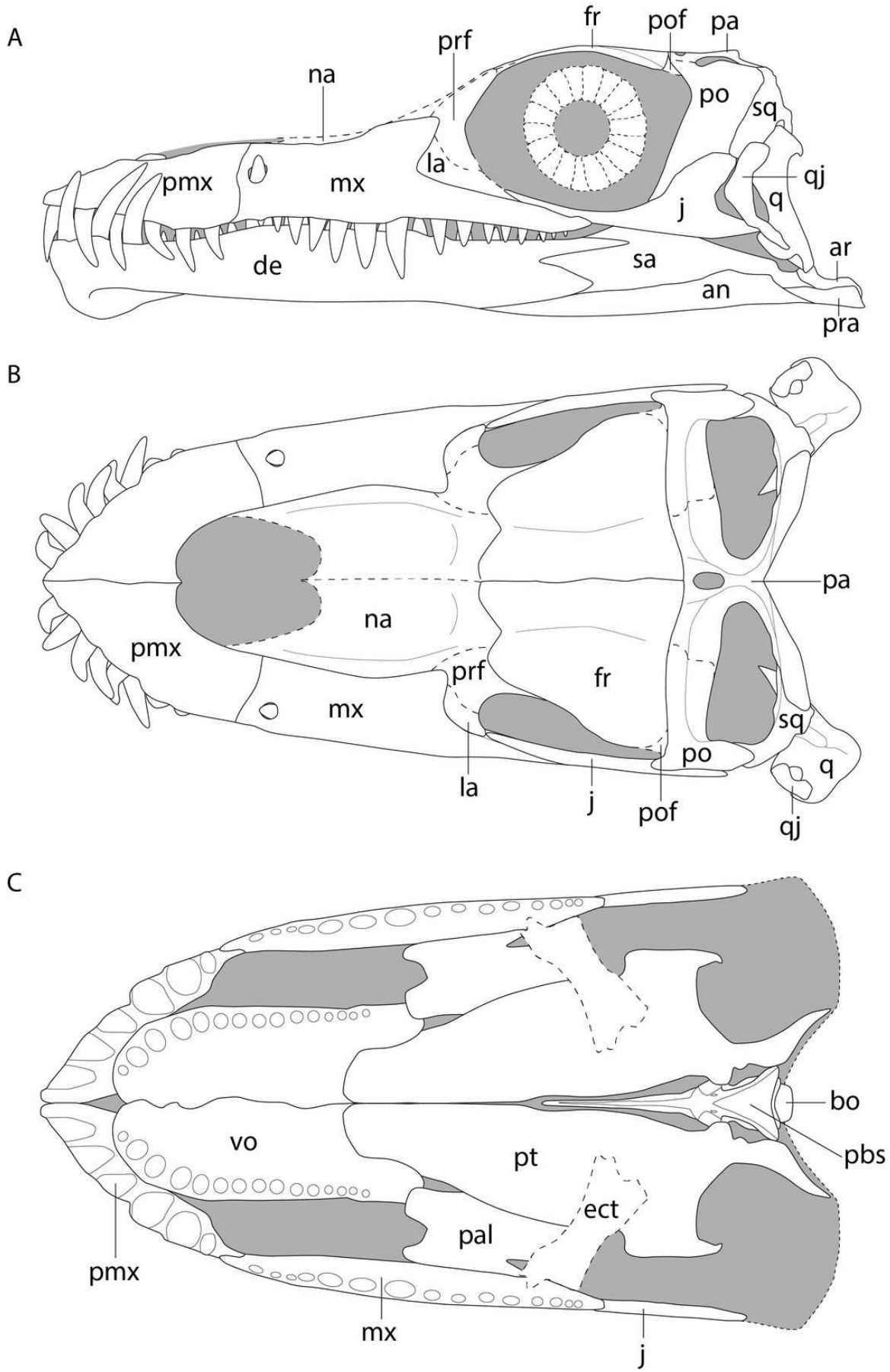
A
fr
pof
pa
prf
na
po
sq
la
qj
pmx
mx
q
j
ar
de
sa
an
pra
B
pa
na
pmx
prf
fr
mx
sq
po
q
la
j
pof
qj
C
bo
vo
pt
pbs
ect
pal
pmx
mx
j

Figure 5

Articulated digital reconstruction of the left premaxilla and maxilla of PIMUZ T 2790.

(A) Lateral or labial view. (B) Medial or lingual view. (C) Dorsal view. (D) Ventral view. Abbreviations: al, alveolus; apm, ascending process maxilla; ipp, incipient prenarial process; jas, jugal facet; mx, maxilla; odt, opening for dental tooth; palf, palatine facet; pmx, premaxilla; ppm, posterior process maxilla.

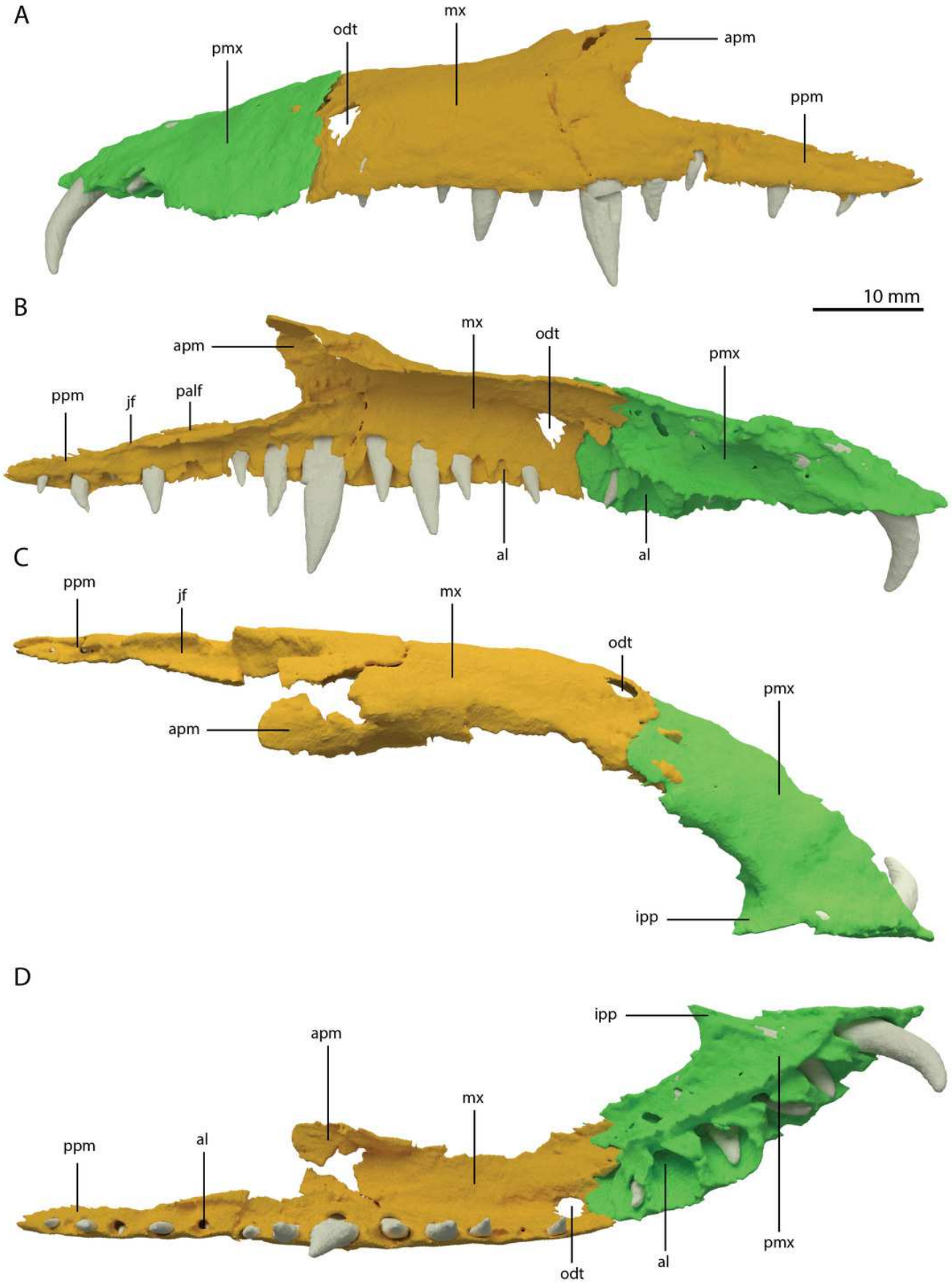
A
pmx
odt
mx
apm
ppm
10 mm
B
apm
mx
odt
pmx
ppm
jf
palf
al
al
C
ppm
jf
mx
odt
pmx
apm
ipp
D
ipp
apm
mx
ppm
al
odt
al
pmx

Figure 6

Digital reconstruction of the left lacrimal and left prefrontal of PIMUZ T 2790.

(A) Left lacrimal in lateral view. (B) Left lacrimal in posterior view. (C) Left prefrontal in lateral view. (D) Left prefrontal in medial view. Abbreviations: nld, nasolacrimal duct; or, orbital rim.

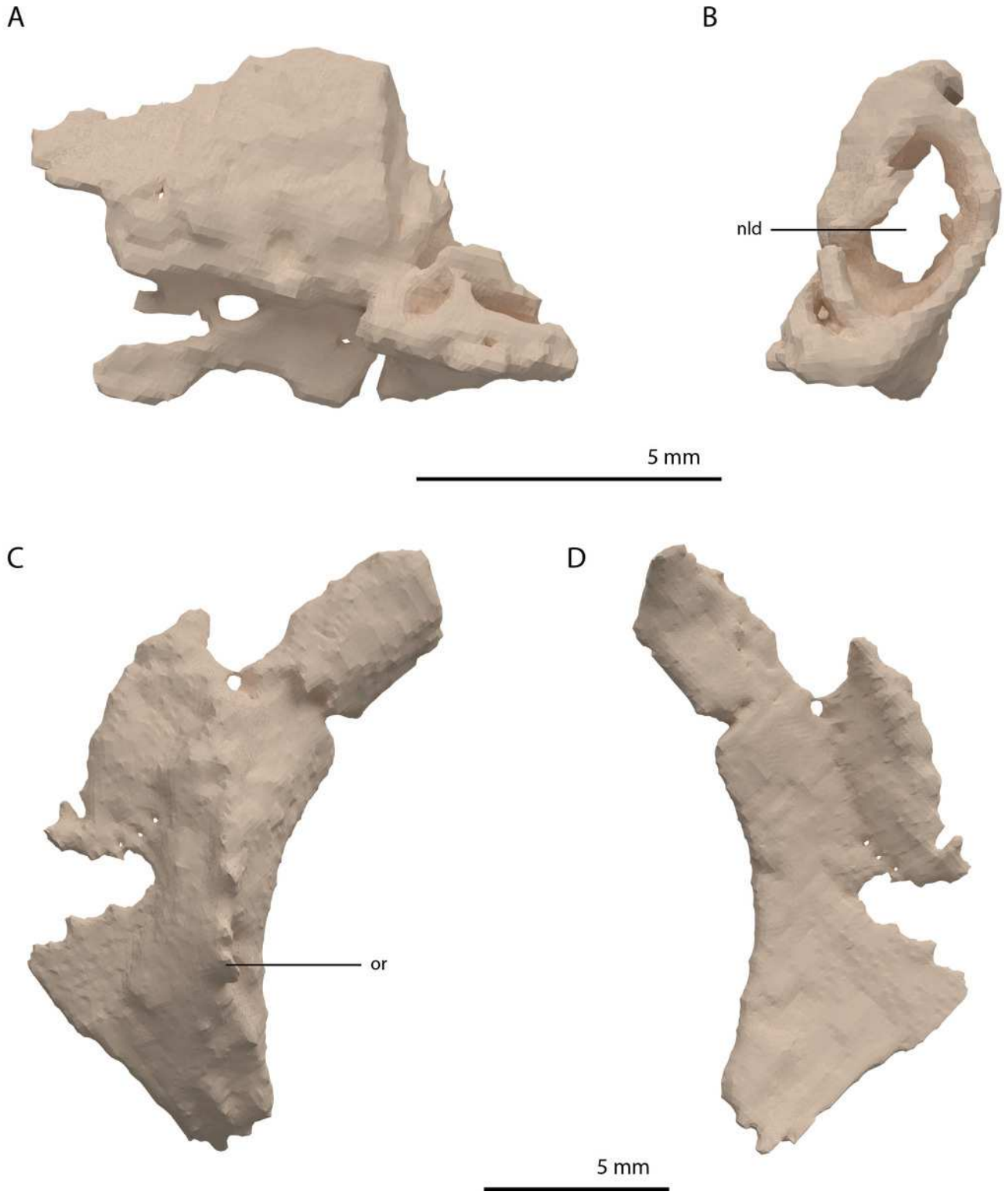
A
B
nld
5 mm
C
D
or
5 mm

Figure 7

Digital reconstruction of the frontals of PIMUZ T 2790.

(A) Dorsal view. (B) Ventral view. (C) Oblique left anterolateral view. Abbreviations: md, medial depression; mls, midline suture; nf, nasal facet; olt, olfactory tract; or, orbital rim.

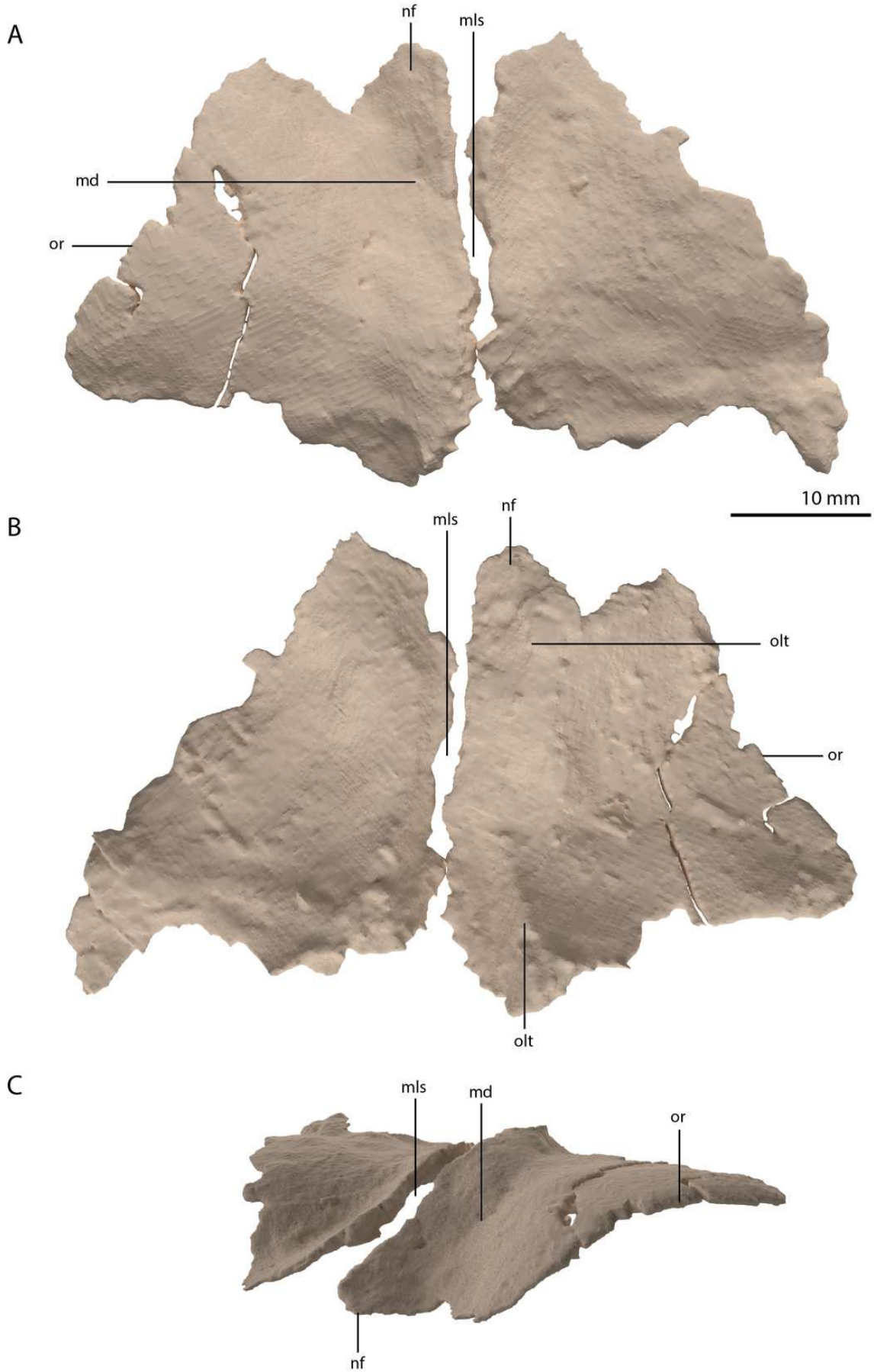
A
nf
mls
md
or
10 mm
B
mls
nf
olt
or
olt
C
mls
md
or
nf

Figure 8

Digital reconstruction of the parietal of PIMUZ T 2790.

(A) Dorsal view. (B) Posterior or occipital view. (C) Ventral view. (D) Right lateral view. (D) Left lateral view. Abbreviations: alp, anterolateral process; pf, pineal foramen; plp, posterolateral process; sc, sagittal crest; sqf, squamosal facet; stf, supratemporal fossa.

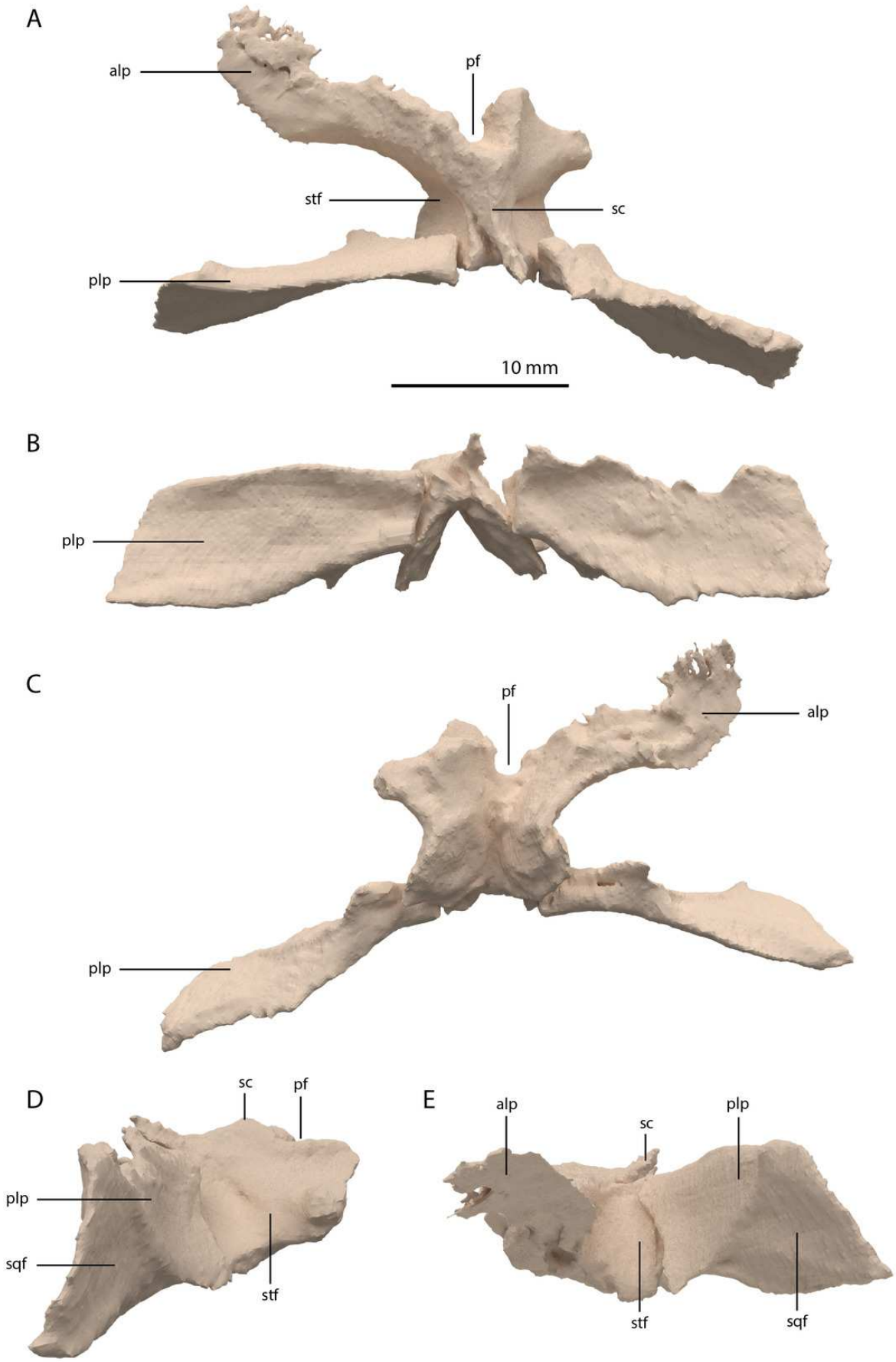
A
alp
pf
stf
sc
plp
10 mm
B
plp
C
pf
alp
plp
D
sc
pf
plp
sqf
stf
E
alp
sc
plp
stf
sqf

Figure 9

Digital reconstruction of the right postorbital of PIMUZ T 2790.

(A) Lateral view. (B) Medial view. (C) Anterior view. (D) Posterior view. (E) Dorsal view. (F) Ventral view. Abbreviations: ff, frontal facet; jf, jugal facet; mp, medial process; or, orbital rim; pp, posterior process; sqf, squamosal facet; vp, ventral process.

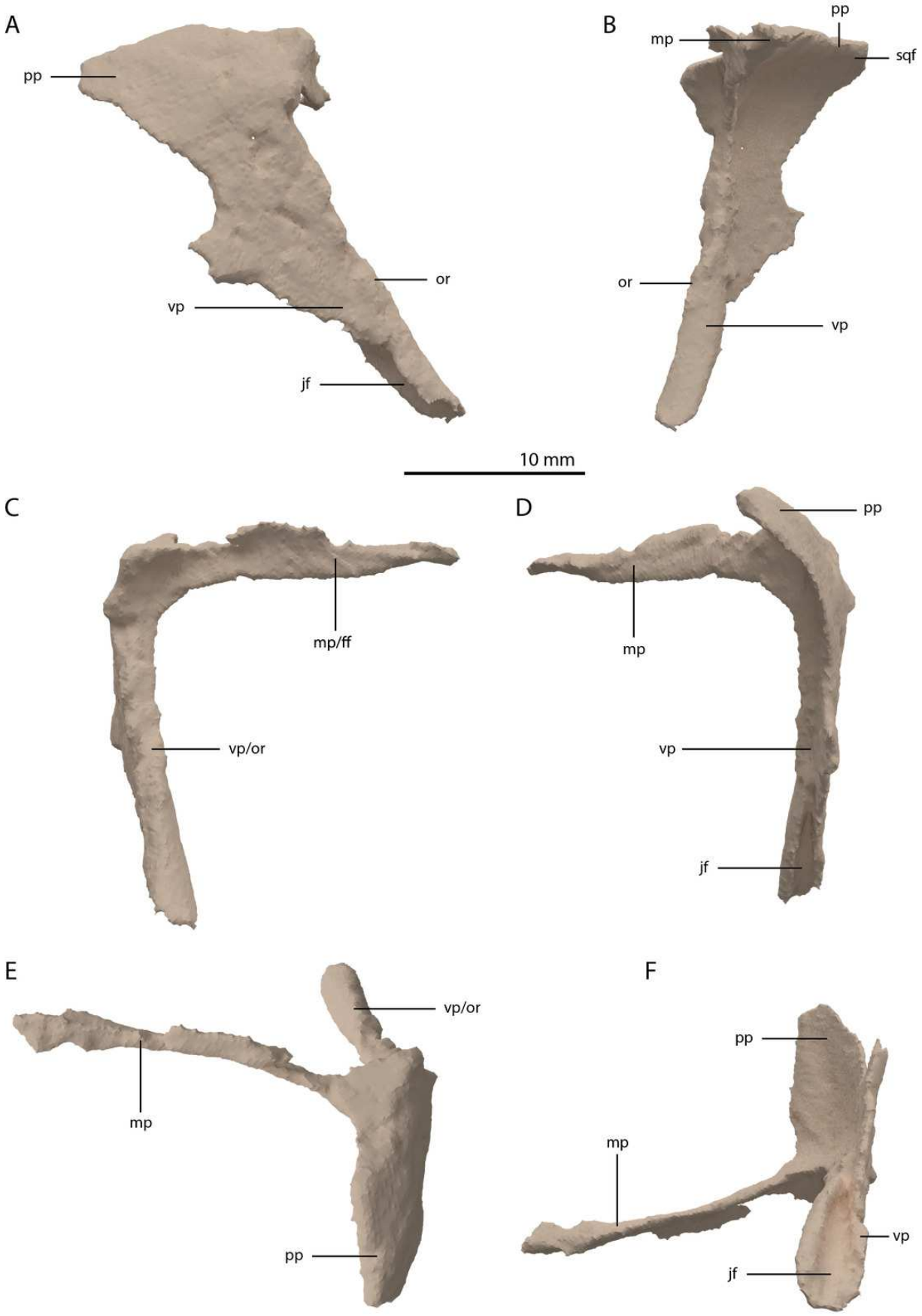
A
pp
or
vp
jf
B
pp
mp
sqf
or
vp
10 mm
C
mp/ff
vp/or
D
pp
mp
vp
jf
E
vp/or
mp
pp
F
pp
mp
vp
jf

Figure 10

Digital reconstruction of the right jugal of PIMUZ T 2790.

(A) Incomplete jugal as visible in the SRµCT data in lateral view. (B) Incomplete jugal as visible in the SRµCT data in medial view. (C) Jugal with missing portions reconstructed in lateral view. (D) Jugal with missing portions reconstructed in medial view. The stippled line indicates the dorsal margin of the ascending process as inferred from the well-preserved jugal of the *Tanystropheus hydroides* specimen PIMUZ T 2819. Abbreviations: ap, anterior process; ascp, ascending process; pp, posterior process.

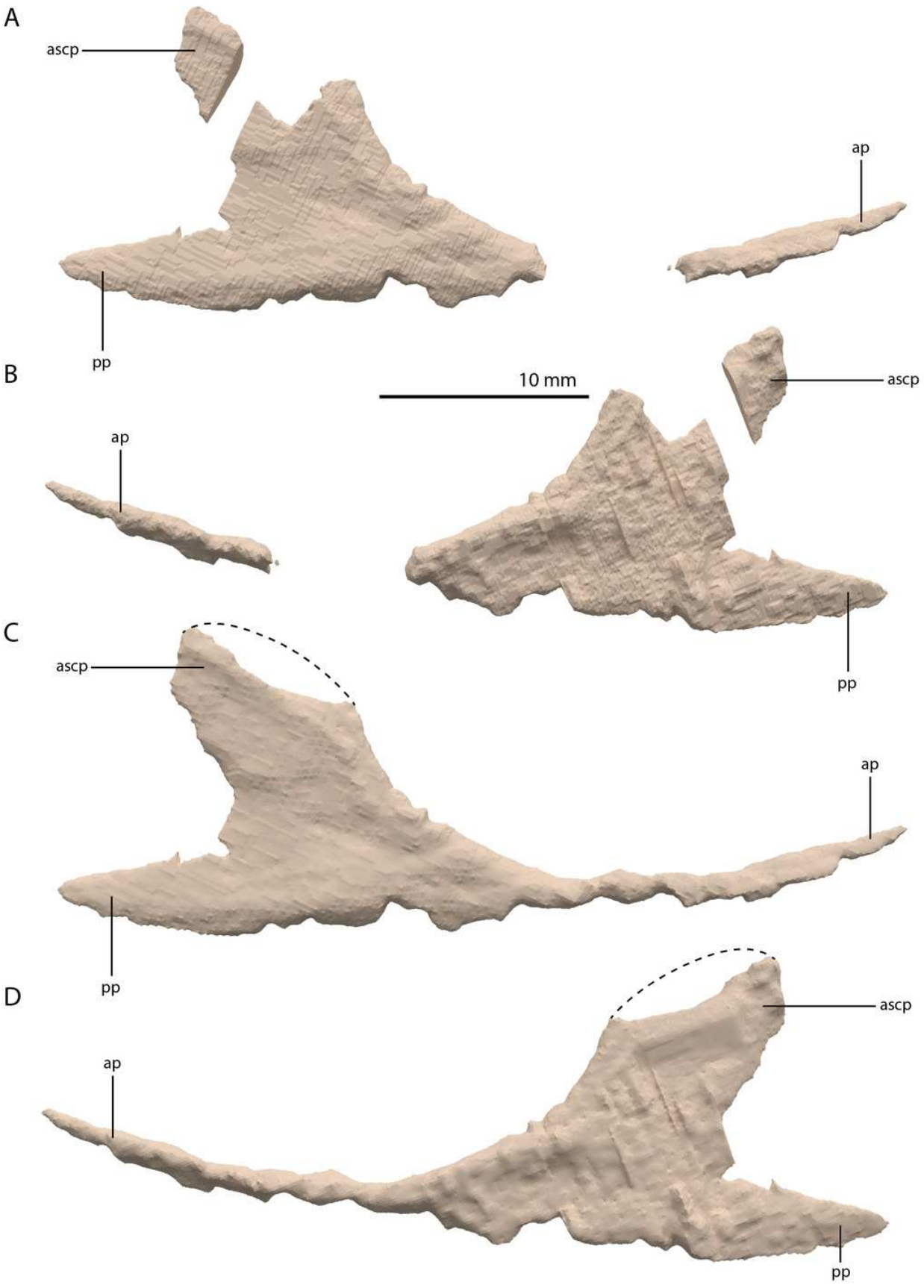
A
ascp
ap
pp
B
10 mm
ascp
ap
pp
C
ascp
ap
pp
D
ascp
ap
pp

Figure 11

Digital reconstruction of the right squamosal of PIMUZ T 2790.

(A) Lateral view. (B) Medial view. (C) Posterior view. (D) Posterior or occipital view. (E) Dorsal view. (F) Ventral view. Abbreviations: ap, anterior process; mp, medial process; paf, parietal facet; pof, postorbital facet; ppf, paroccipital process facet; qf, quadrate facet.

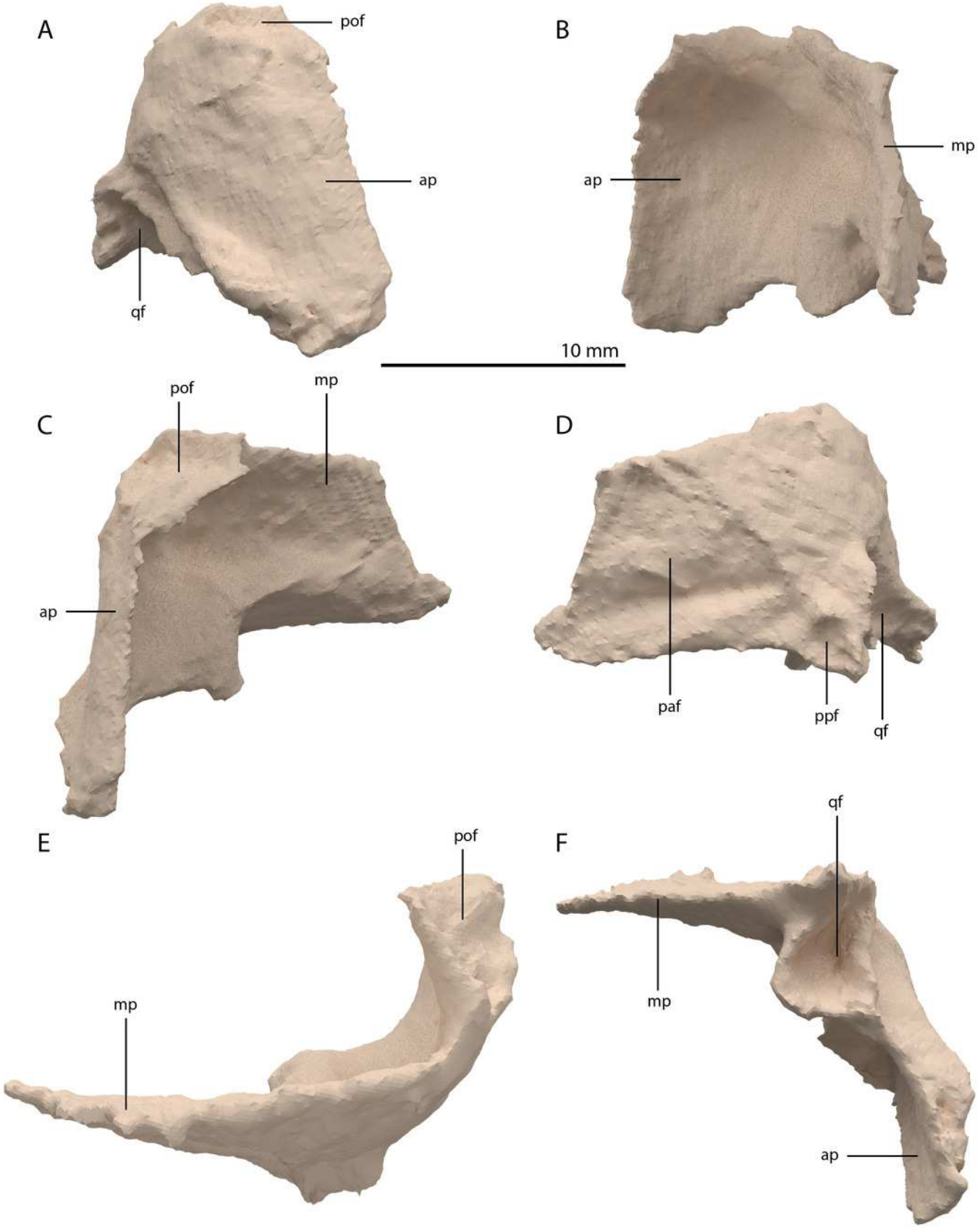
A
pof
ap
qf
B
mp
ap
10 mm
C
pof
mp
ap
D
paf
ppf
qf
E
pof
mp
F
qf
mp
ap

Figure 12

Digital reconstruction of the right quadrate of PIMUZ T 2790.

(A) Lateral view. (B) Medial view. (C) Dorsal view. (D) Ventral view. (E) Anterior view. (F) Posterior view. Abbreviations: dhe, dorsal head; dho, dorsal hook; lc, lateral condyle; mc, medial condyle; ptr, pterygoid ramus; ptrc, pterygoid ramus concavity; qjf, quadratojugal facet; sh, shaft; tc, tympanic crest.

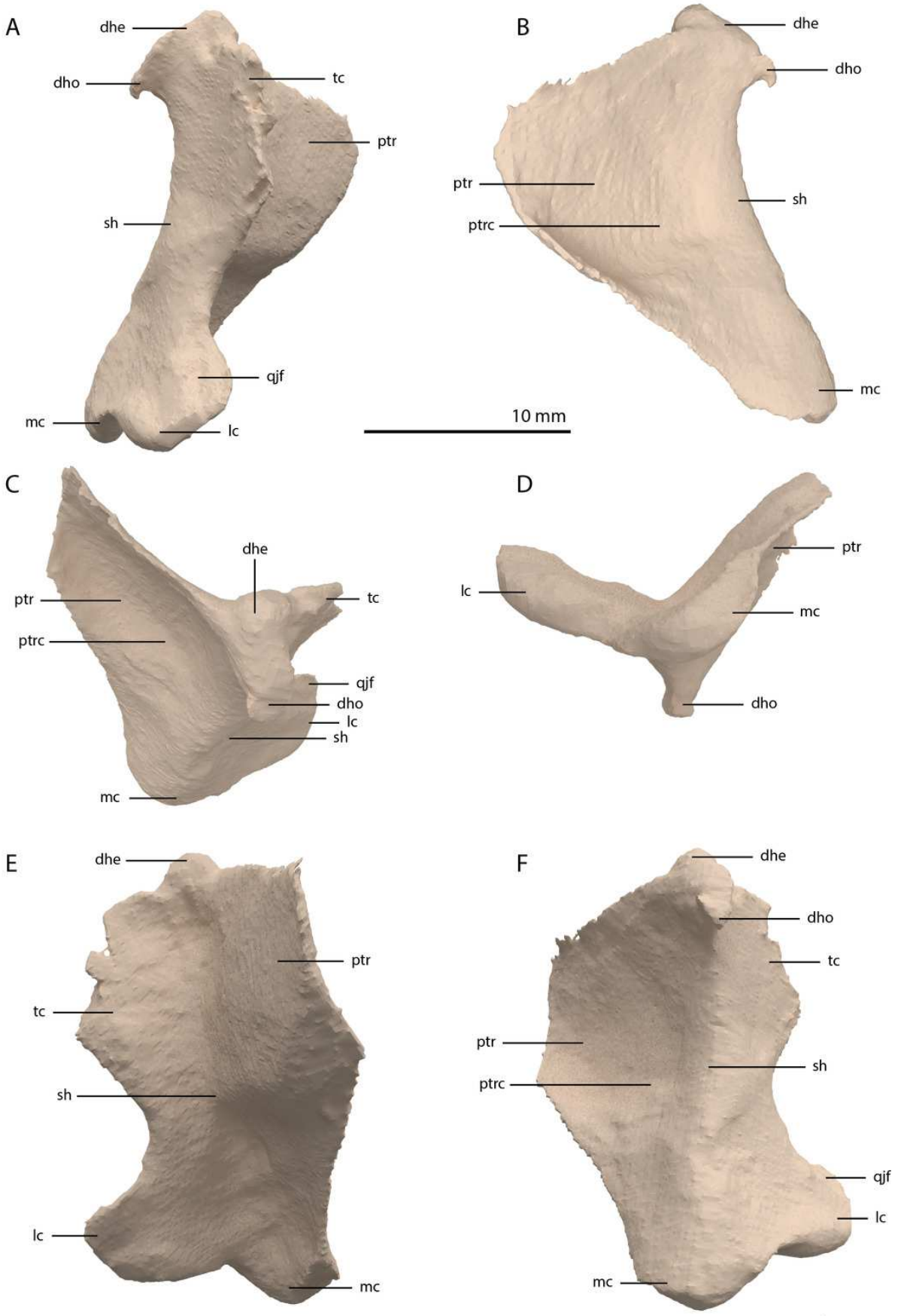
A
dhe
dho
tc
ptr
sh
qjf
mc
lc
B
dhe
dho
ptr
sh
ptrc
mc
10 mm
C
dhe
ptr
tc
ptrc
qjf
dho
lc
sh
mc
D
ptr
lc
mc
dho
E
dhe
ptr
tc
sh
lc
mc
F
dhe
dho
tc
ptr
sh
ptrc
qjf
lc
mc

Figure 13

The right quadrate of *Tanystropheus longobardicus* specimen PIMUZ T 2484 in lateral view, revealing a morphology similar to that of *Tanystropheus hydroides*.

Abbreviations: dhe, dorsal head; ptr, pterygoid ramus; sh, shaft; tc, tympanic crest; vc, ventral condyle.


dhe
ptr
tc
sh
vc
5 mm

Figure 14

Articulated digital reconstruction of the right quadrate and quadratojugal of PIMUZ T 2790.

(A) Lateral view. (B) Medial view. Abbreviations: q, quadrate; qj, quadratojugal.

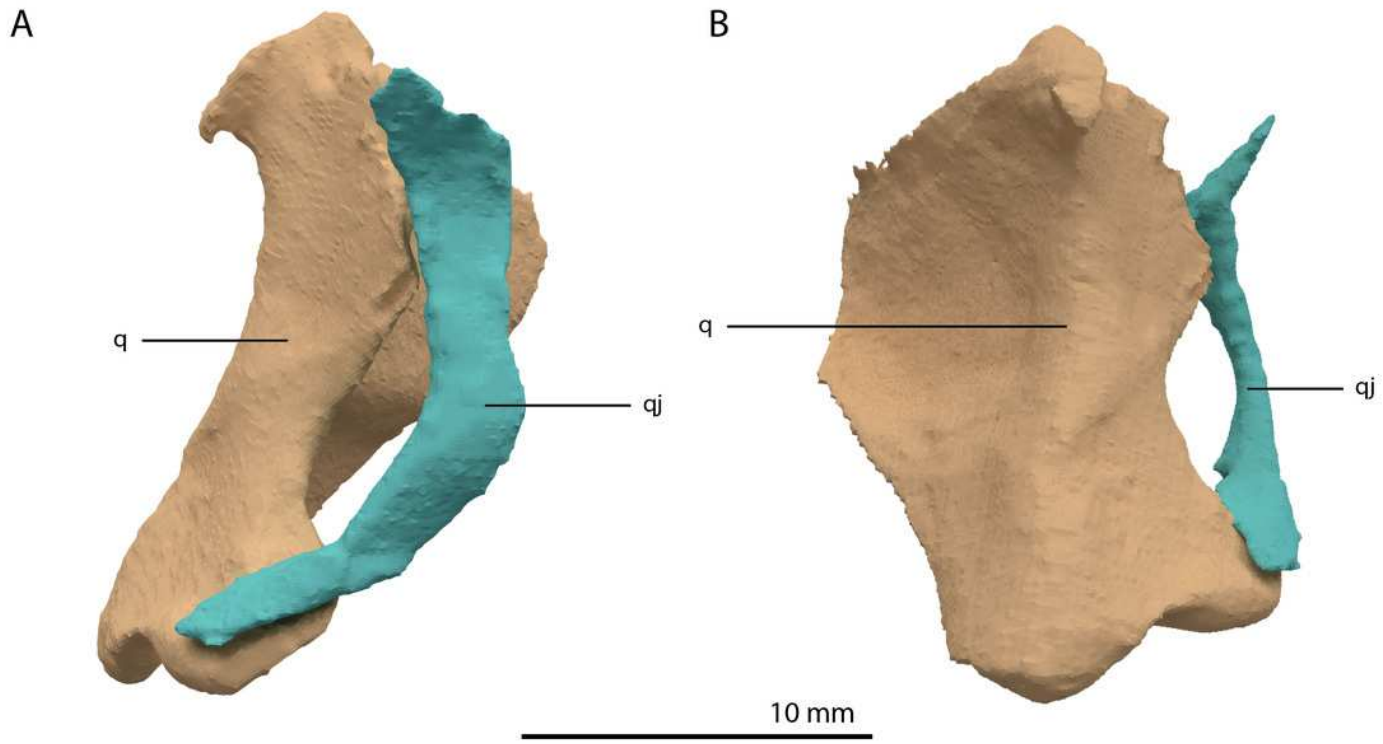

Figure 15

Digital reconstruction of the vomers of PIMUZ T 2790.

(A) Dorsal view. (B) Ventral view. Abbreviations: al, alveolus; lv, left vomer; rv, right vomer.

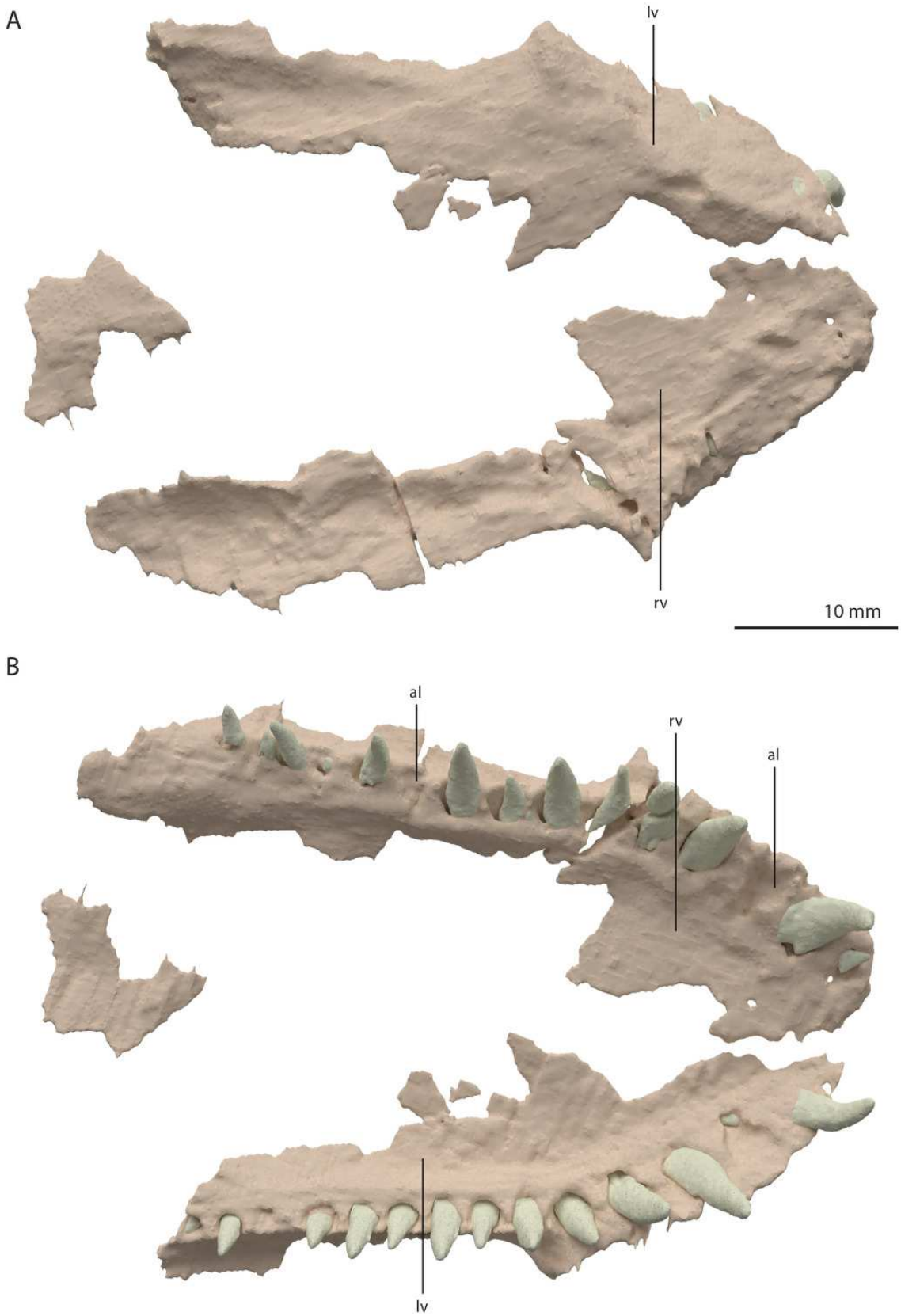
A
lv
rv
10 mm
B
al
rv
al
lv

Figure 16

Digital reconstruction of the element tentatively interpreted as the right ectopterygoid of PIMUZ T 2790.

(A) Dorsal view. (B) Ventral view. (C) Anterior view. (D) Posterior view. (E) Lateral view. (F) Medial view. Abbreviations: mf, maxilla facet; ptf, pterygoid facet; sh, shaft; tc, triangular concavity; vdp, ventrally deflected process.

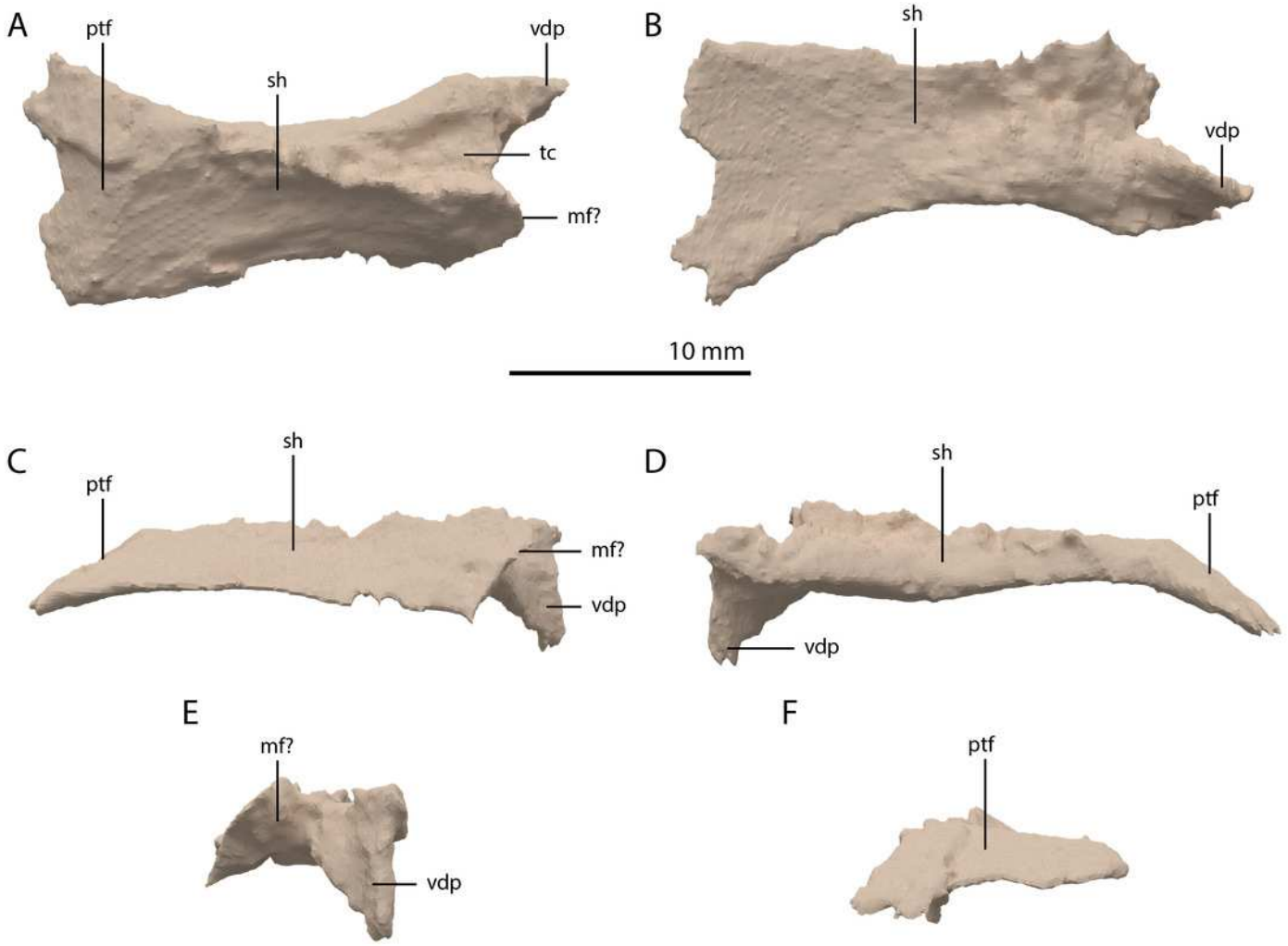

Figure 17

Digital reconstruction of the right pterygoid of PIMUZ T 2790.

(A) Dorsal view. (B) Ventral view. (C) Lateral view. (D) Medial view. (E) Anterior view. (F) Posterior view. Abbreviations: af, arcuate flange; bptf; basipterygoid facet; df, dorsal flange; epif, epipterygoid facet; par, palatal ramus; qr, quadrate ramus; tf, transverse flange.

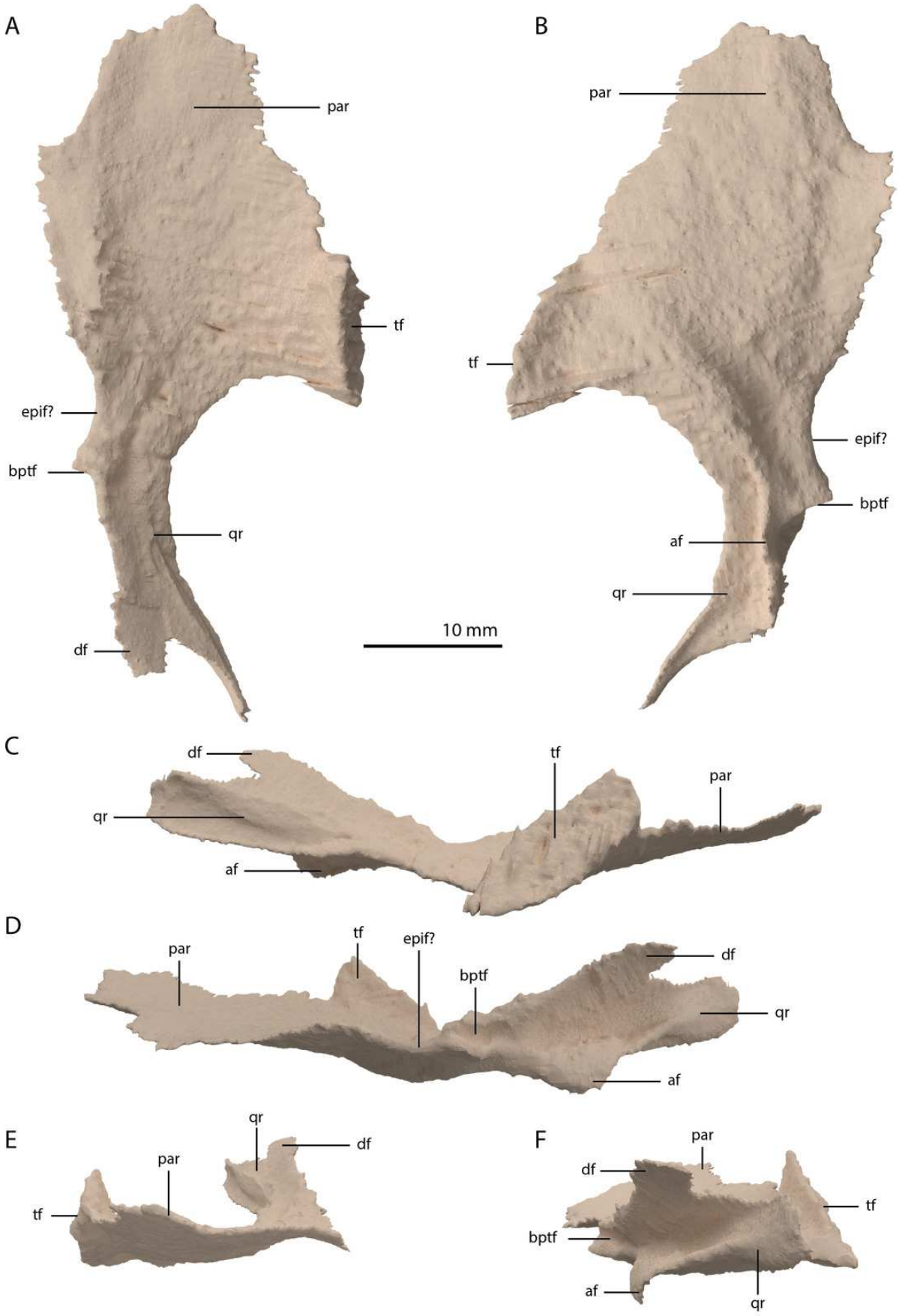
A
par
tf
epif?
bptf
qr
df
B
par
tf
epif?
bptf
af
qr
10 mm
C
df
tf
par
qr
af
D
par
tf
epif?
bptf
df
qr
af
E
qr
df
par
tf
F
par
df
tf
bptf
af
qr

Figure 18

Digital reconstruction of the right epipterygoid of PIMUZ T 2790.

(A) Lateral view. (B) Medial view. Abbreviations: ptf, pterygoid facet; sh, shaft.

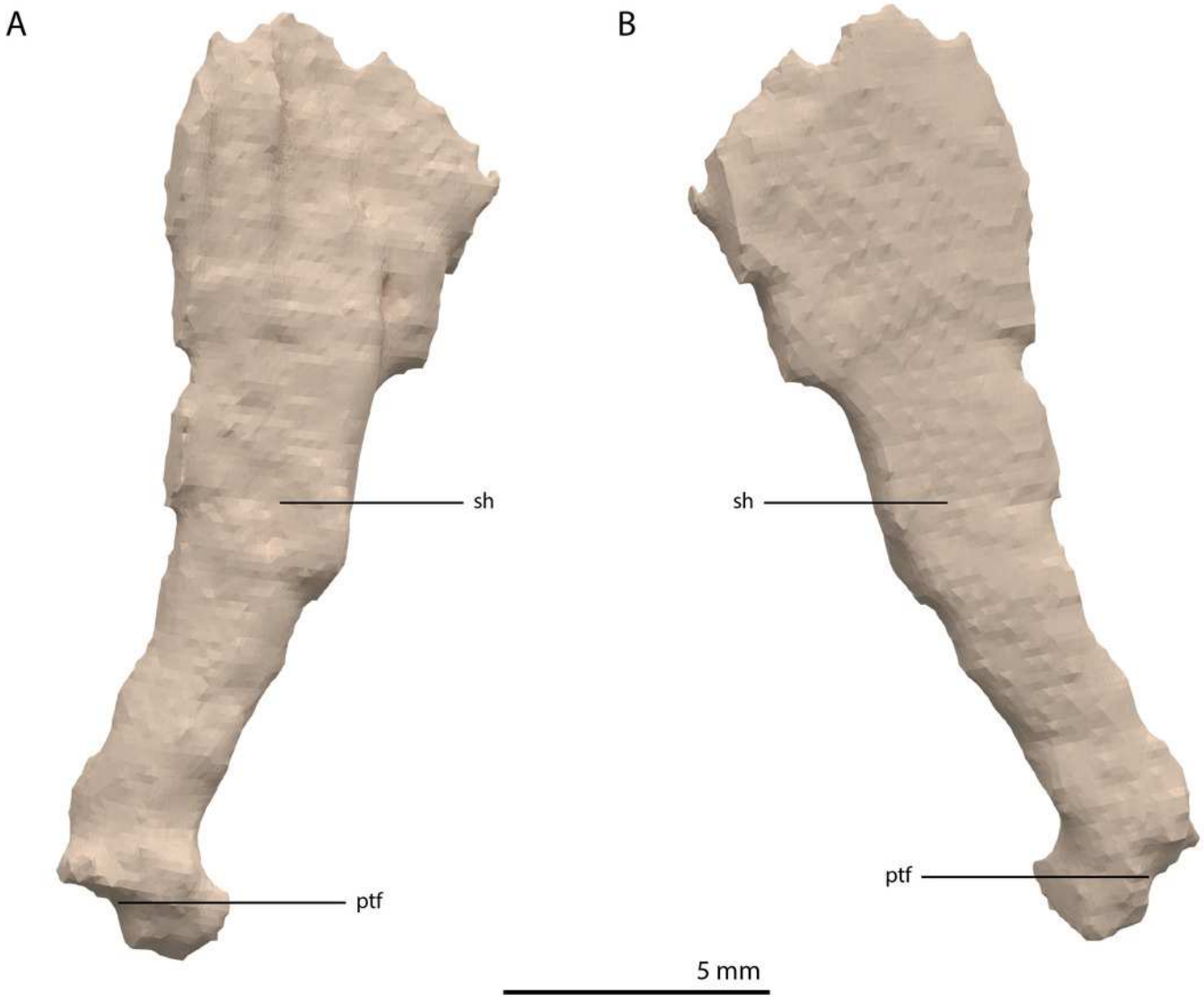

Figure 19

Articulated digital reconstruction of the braincase of PIMUZ T 2790.

(A) Right lateral view. (B) Left lateral view. (C) Dorsal view. (D) Ventral view. (E) Posterior or occipital view. (F) Anterior view. Abbreviations: aip, anterior inferior process; bo, basioccipital; bptp, basipterygoid process; btbo, basal tuber basioccipital; btpbs, basal tuber parabasisphenoid; CN, cranial nerve; cp, cultriform process; eo, exoccipital; fm, foramen magnum; ls, laterosphenoid; mpr, median pharyngeal recess; ocbo, basioccipital contribution occiput; oceo, exoccipital contribution occiput; op, opisthotic; pbs, parabasisphenoid; pop, paroccipital process; pro, prootic; so, supraoccipital; tr, trough.

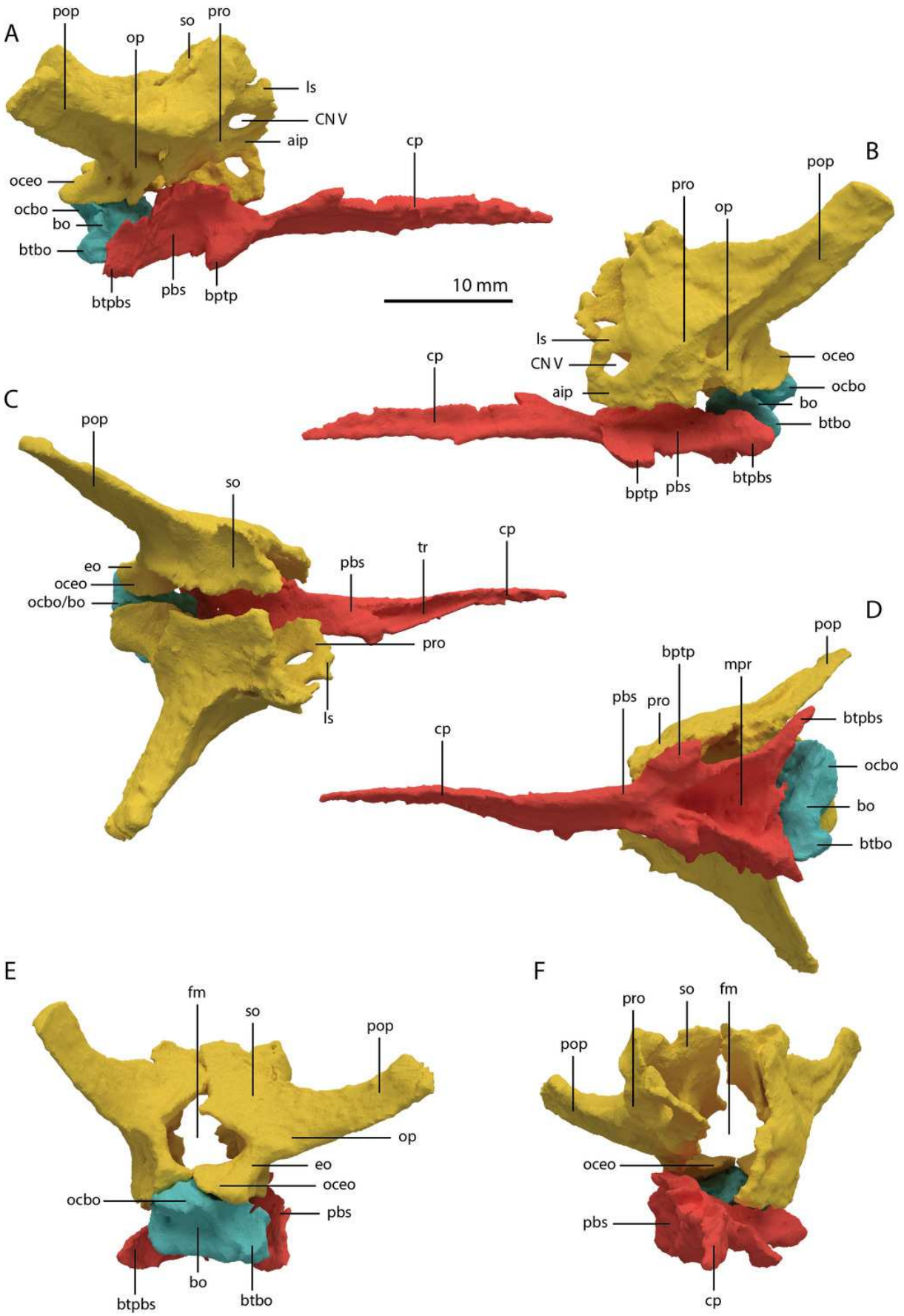
A
pop
so
pro
op
ls
CN V
aip
cp
oceo
ocbo
bo
btbo
btpbs
pbs
bptp
10 mm
B
pop
pro
op
ls
CN V
aip
cp
oceo
ocbo
bo
btbo
bptp
pbs
btpbs
C
pop
so
cp
tr
pbs
eo
oceo
ocbo/bo
pro
ls
D
pop
bptp
mpr
pbs
pro
btpbs
cp
ocbo
bo
btbo
E
fm
so
pop
op
eo
oceo
ocbo
pbs
bo
btpbs
btbo
F
pro
so
fm
pop
oceo
pbs
cp

Figure 20

Digital reconstruction of the basioccipital of PIMUZ T 2790.

(A) Posterior or occipital view. (B) Anterior view. (C) Dorsal view. (D) Ventral view. (E) Left lateral view. (F) Right lateral view. Abbreviations: bt, basal tuber; eof, exoccipital facet; ind, indentation; ocbo, basioccipital contribution occipital condyle; ri, ridge.

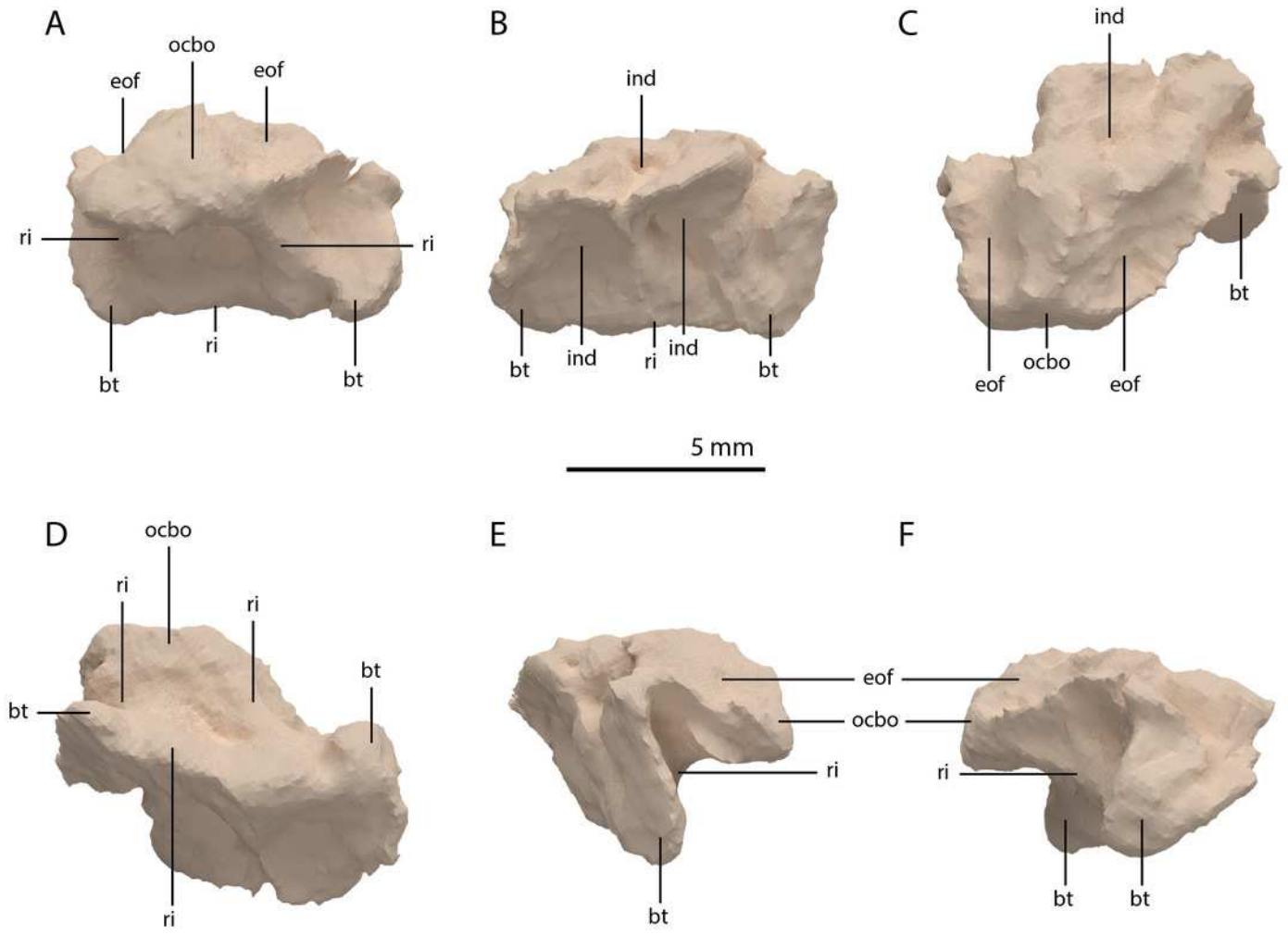

Figure 21

Digital reconstruction of the parabasisphenoid of PIMUZ T 2790.

(A) Ventral view. (B) Dorsal view. (C) Right lateral view. (D) Left lateral view. (E) Posterior view. (F) Anterior view. Abbreviations: bof, basioccipital facet; bptp, basipterygoid process; bt, basal tuber; clp, clinoid process; cup, cultriform process; ds, dosum sella; mpr, median pharyngeal recess; pf, pituitary fossa; pobt, posterior opening basal tubera; prf, prootic facet; psc, parasphenoid crest; tr, trough.

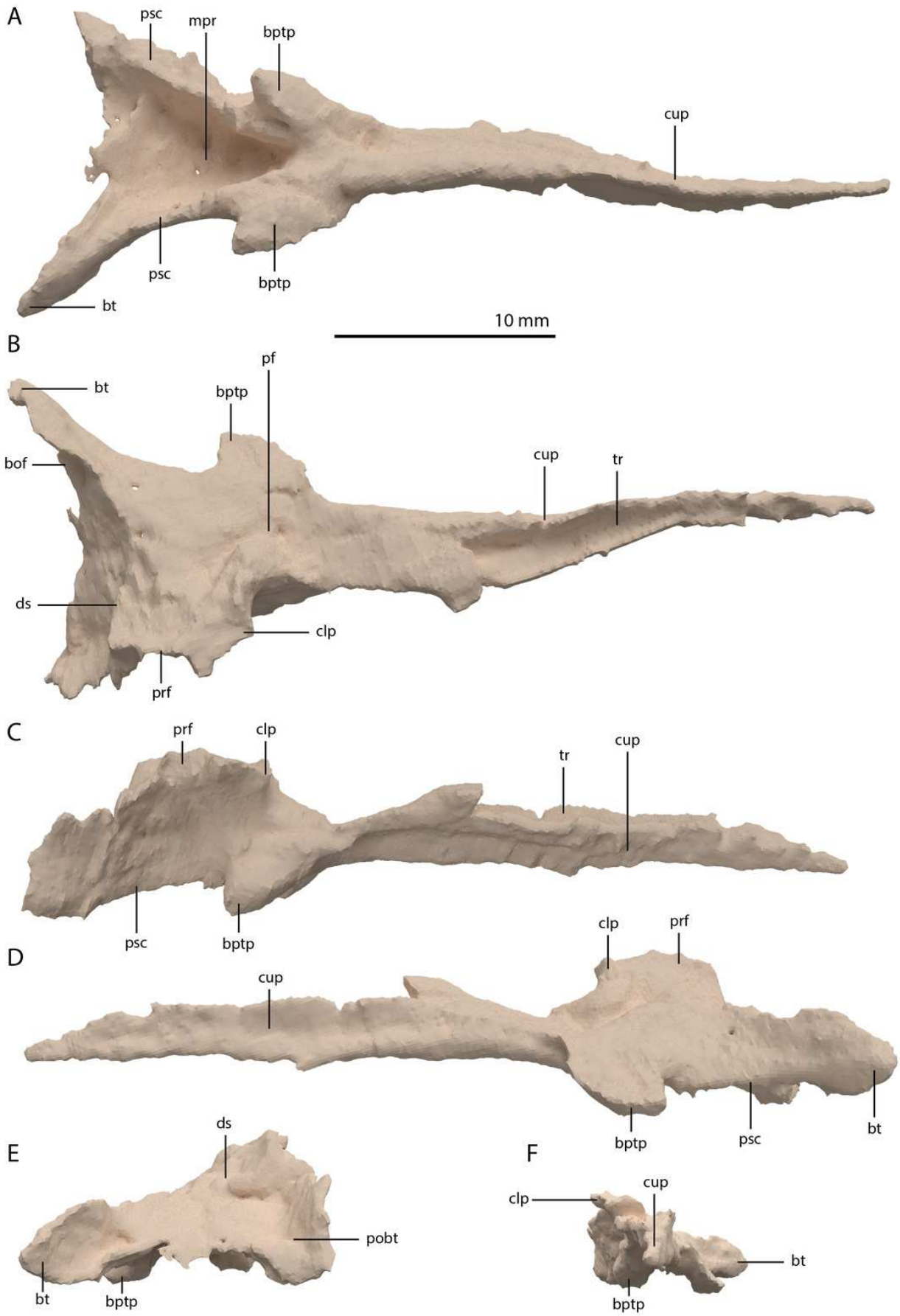
A
psc
mpr
bptp
cup
psc
bptp
bt
10 mm
B
bt
bptp
pf
bof
cup
tr
ds
clp
prf
C
prf
clp
tr
cup
psc
bptp
D
clp
prf
cup
bptp
psc
bt
E
ds
pobt
bt
bptp
F
cup
clp
bt
bptp

Figure 22

Digital reconstruction of the right fused braincase element of PIMUZ T 2790, consisting of part of the supraoccipital, the right exoccipital, the right opisthotic, the right prootic, and the right laterosphenoid.

(A) Posterior or occipital view. (B) Anterior view. (C) Dorsal view. (D) Ventral view. (E) Lateral view. (F) Medial view. Abbreviations: aip, anterior inferior process; bof, basioccipital facet; CN, cranial nerve; cr al, crista alaris; fm, foramen magnum; floci, flocculus indentation; fov, fenestra ovalis; eo, exoccipital; ls, laterosphenoid; no, notch; ocf, occipital foot; op, opisthotic; pop, paroccipital process; pro, prootic; pro pop, prootic contribution paroccipital process; sci, semi-circular canal indentation; so, supraoccipital; stg, stapedial groove; vr, ventral ramus.

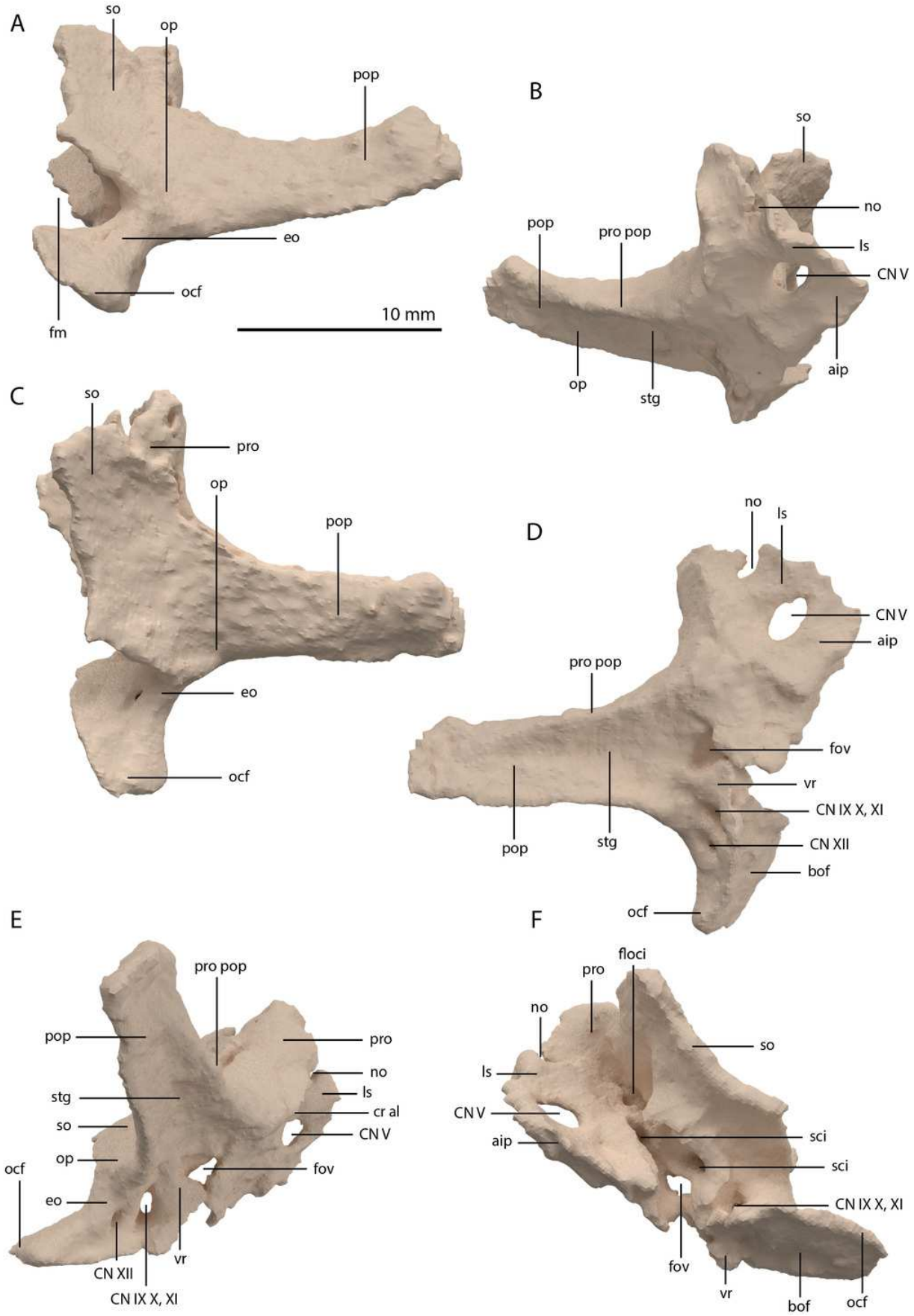
A
so
op
pop
eo
ocf
fm
10 mm
B
so
no
pop
pro pop
ls
CN V
op
stg
aip
C
so
pro
op
pop
eo
ocf
D
no
ls
CN V
aip
pro pop
fov
vr
CN IX X, XI
pop
stg
CN XII
bof
ocf
E
pro pop
pop
pro
no
ls
stg
cr al
so
CN V
op
fov
ocf
eo
vr
CN XII
CN IX X, XI
F
floci
pro
no
so
ls
CN V
sci
aip
sci
CN IX X, XI
fov
vr
bof
ocf

Figure 23

Digital reconstruction of the element tentatively identified as the left stapes of PIMUZ T 2790.

(A) Anterior or posterior view. (B) Opposite view of (A). (C) The element in reconstructed articulation with the braincase. The fused braincase element is indicated in yellow. The endocast is indicated in blue. The endosseous labyrinth is indicated in red. The braincase, endocast, and endosseous labyrinth were mirrored for this reconstruction. Abbreviations: sf, stapedial foramen; pop, paroccipital process; pro pop, prootic contribution paroccipital process; sh, shaft; st, stapes.

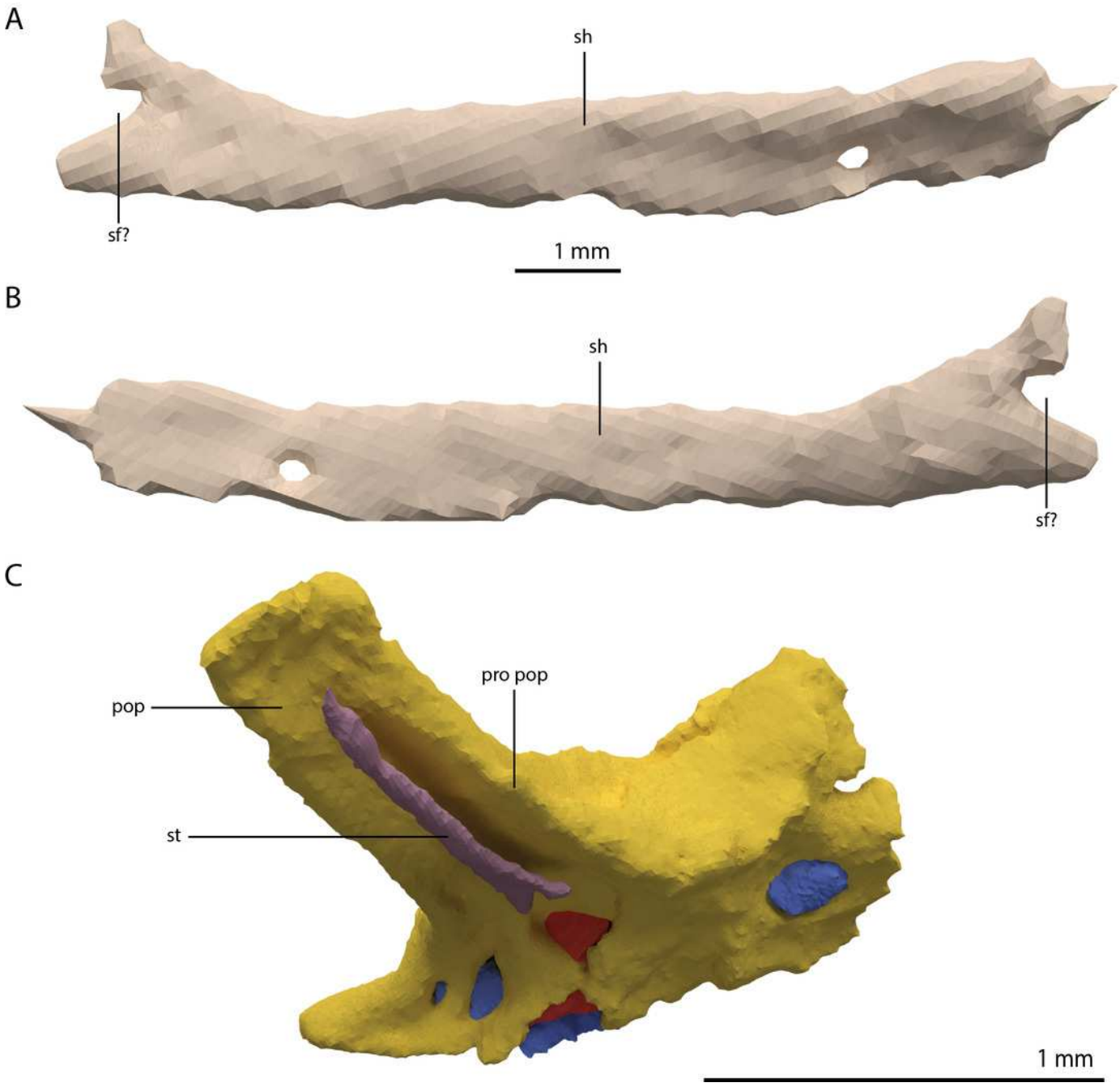
A
sh
sf?
1 mm
B
sh
sf?
C
pro pop
pop
st
1 mm

Figure 24

Digitally reconstructed endocast and endosseous labyrinth of the right fused braincase element of PIMUZ T 2790 in lateral view.

The endocast is indicated in blue, the endosseous labyrinth in red, and the cranial nerves in yellow. Abbreviations: ASC, anterior semicircular canal; cb, cerebellum; cc, common crus; ecd, endosseous cochlear duct; CN, cranial nerve; flo, flocculus; fv, fenestra vestibuli; LSC, lateral semicircular canal; medulla oblongata; PSC, posterior semicircular canal.

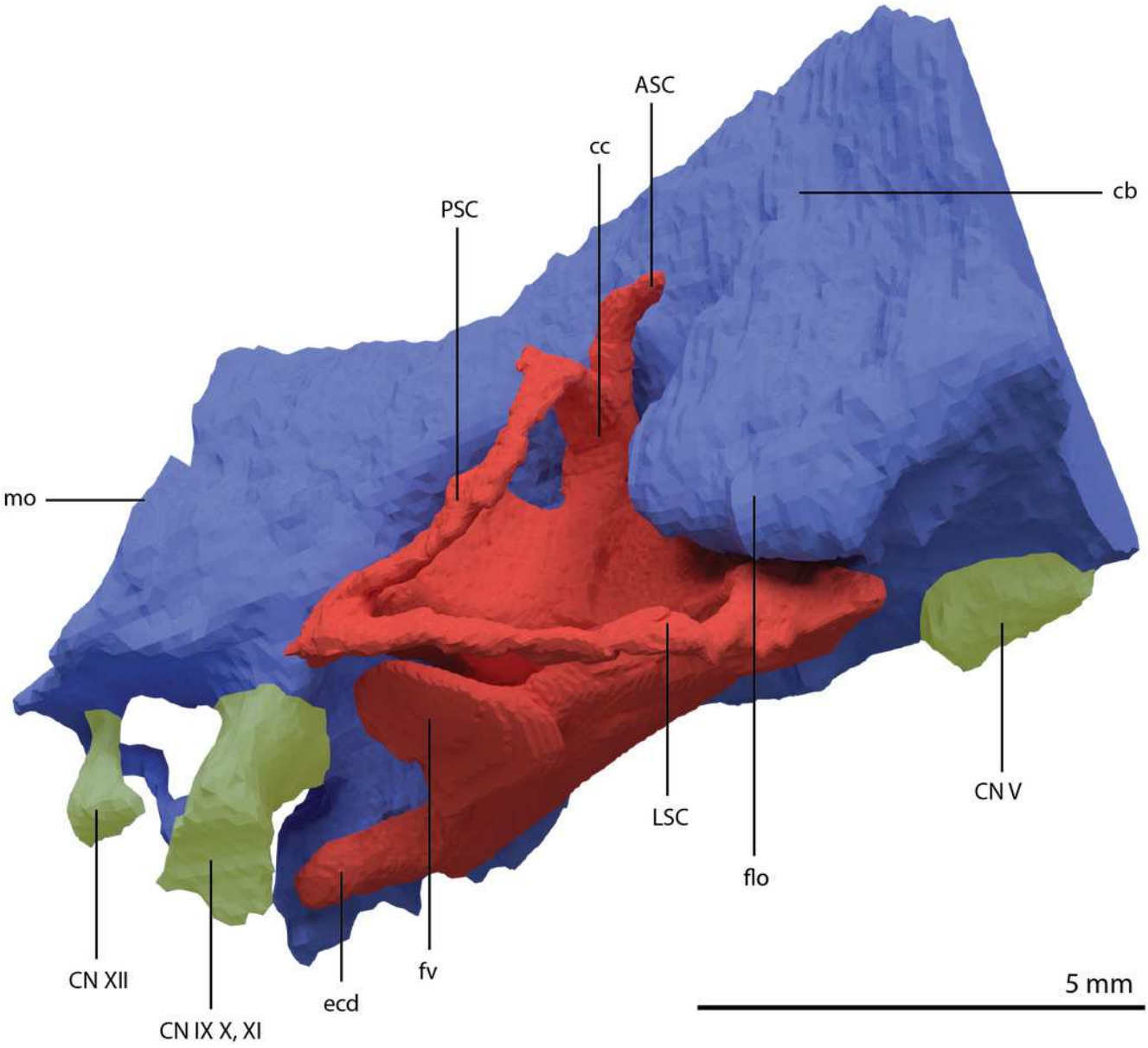
ASC
cc
cb
PSC
mo
LSC
flo
CN V
CN XII
CN IX X, XI
ecd
fv
5 mm

Figure 25

Digital reconstruction of the left mandible of PIMUZ T 2790.

(A) Lateral view. (B) Medial view including splenial. (C) Medial view excluding splenial. (D) Dorsal view. (E) Ventral view. (F) Close-up of the posterior part of the mandible, including the glenoid fossa and retroarticular process, in posterolateral view. (G) Close-up of the posterior part of the mandible in dorsal view. Abbreviations: adf, adductor fossa; al, alveoli; an, angular; ar, articular; cp, coronoid process; de, dentary; glf, glenoid fossa; Mg, Meckelian groove; pdp, posterodorsal process; pra, prearticular; psaf, posterior surangular foramen; pvp, posteroventral process; r, ridge; rap, retroarticular process; sa, surangular; spl, splenial; sy, symphysis; vk, ventral keel.

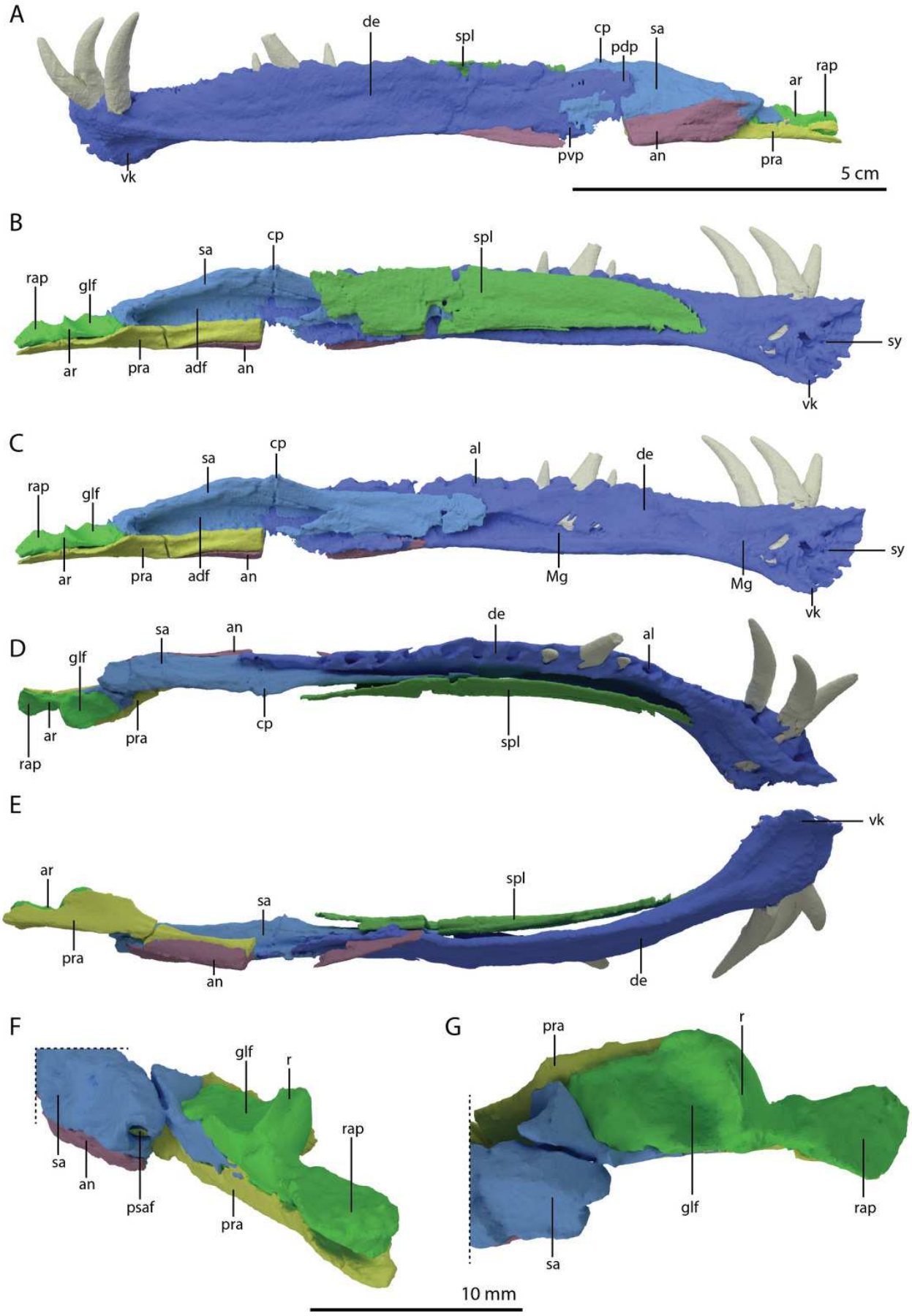
A
de
spl
cp
sa
pdp
rap
ar
pvp
an
pra
vk
5 cm
B
cp
spl
sa
rap
glf
sy
ar
pra
adf
an
vk
C
cp
al
de
sa
rap
glf
sy
ar
pra
adf
an
Mg
Mg
vk
D
de
sa
an
al
glf
ar
pra
cp
spl
rap
E
vk
ar
spl
sa
pra
an
de
F
glf
r
rap
sa
an
psaf
pra
G
pra
r
glf
rap
sa
10 mm

Figure 26

Digital reconstruction of the tooth bearing elements of PIMUZ T 2790.

The dentaries (in blue) are shown in dorsal view. The premaxillae (green), maxillae (orange), and vomers (turquoise) are shown in ventral view. The numbers indicate the position of each alveolus for each element counted from anterior to posterior.

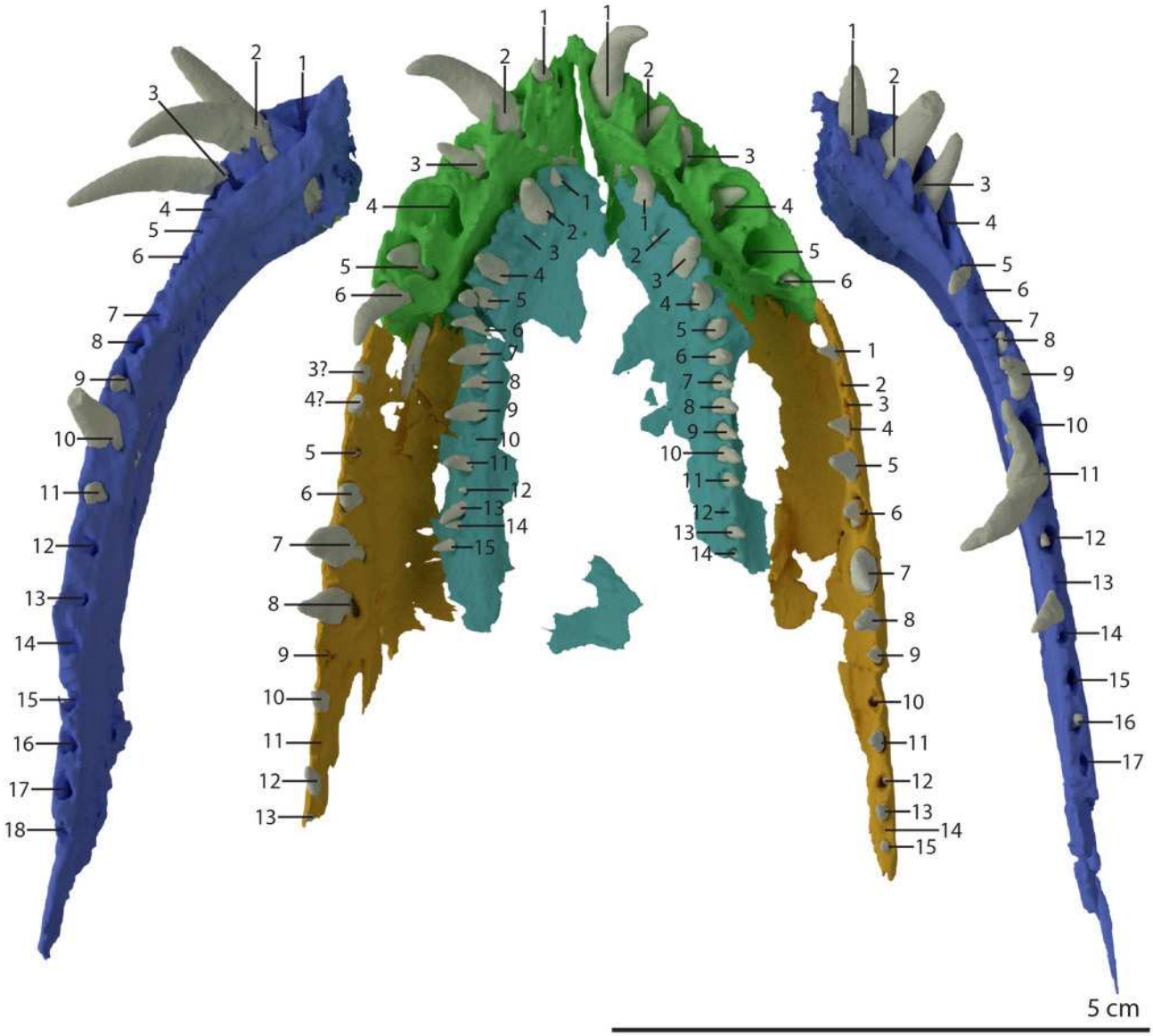

Figure 27

‘Re-assembled’ digital reconstruction of the atlas-axis complex of PIMUZ T 2790.

(A) Oblique right anterolateral view. (B) Right lateral view. (C) Disarticulated oblique left anterolateral view. (D) Anterior view. (E) Oblique left anterolateral view of the atlas-axis complex in articulation with the basioccipital and the right fused braincase element. Abbreviations: atic, atlas intercentrum; atna, atlas neural arch; atpl, atlas pleurocentrum; ax, axis; axic, axis intercentrum; axna, axis neural arch; axplc, axis pleurocentrum; bo, basioccipital; bt, basal tuber; cv, cervical vertebra; dmp, dorsomedial process; nc, neural canal; ns, neural spine; ocbo, basioccipital contribution occiput; oceo, exoccipital contribution occiput; poz, postzygapophysis; pp, posterior process; prz, prezygapophysis; rbc, right braincase; vk, ventral keel; vmp, ventromedial process.

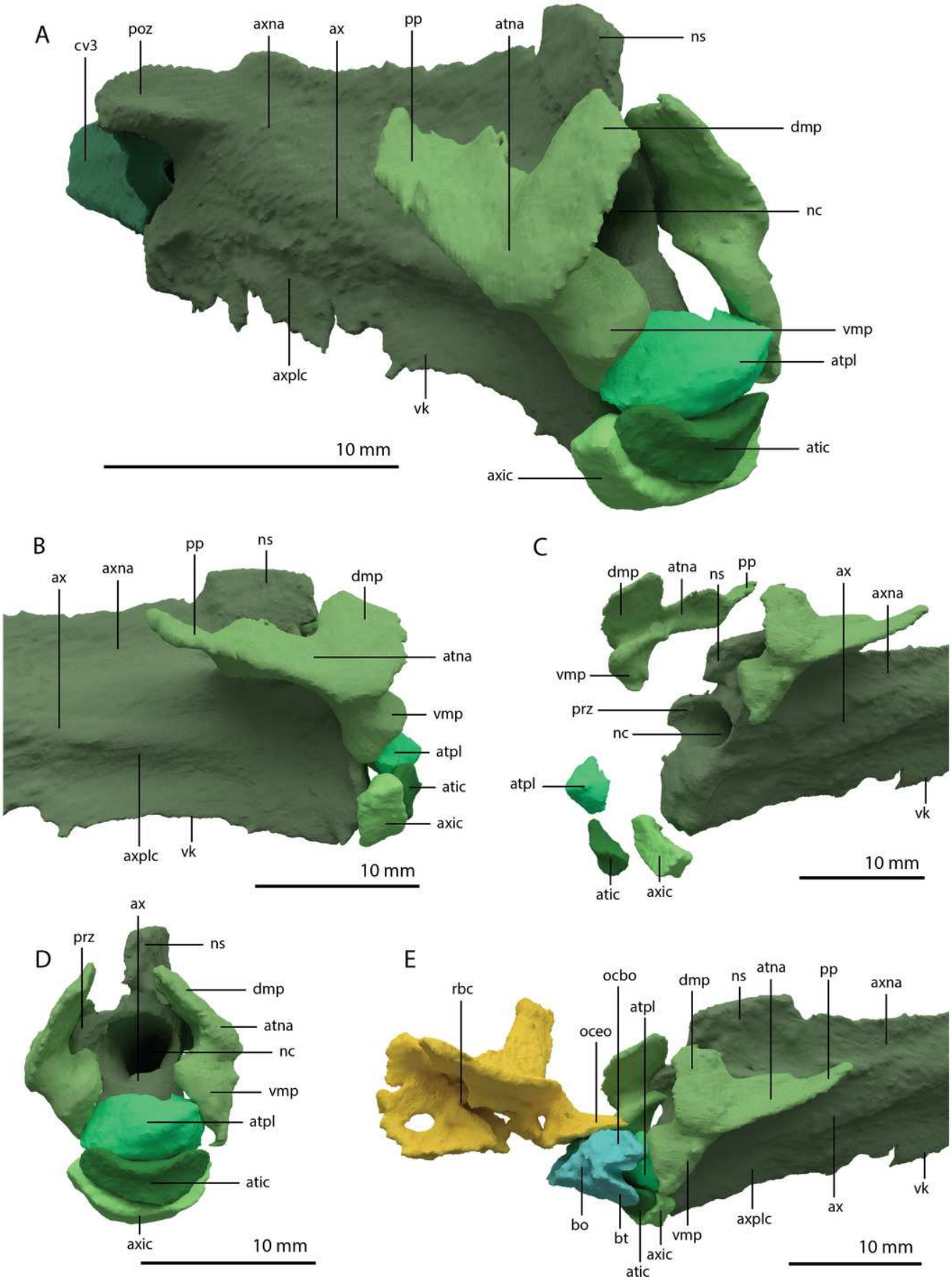
A
cv3
poz
axna
ax
pp
atna
ns
dmp
nc
vmp
atpl
atic
axic
axplc
vk
10 mm
B
ax
axna
pp
ns
dmp
atna
vmp
atpl
atic
axic
axplc
vk
10 mm
C
dmp
atna
ns
pp
ax
axna
vmp
prz
nc
atpl
vk
atic
axic
10 mm
D
ax
prz
ns
dmp
atna
nc
vmp
atpl
atic
axic
10 mm
E
rbc
ocbo
oceo
atpl
dmp
ns
atna
pp
axna
bo
bt
axic
atic
vmp
axplc
ax
vk
10 mm

Figure 28

Inner anatomy of the axis of PIMUZ T 2790.

(A) Transparent digital rendering of the axis, with the neural canal indicated in purple, in right lateral view. (B) Digital sagittal cross-section of the axis in right lateral view. The numbers above the stippled lines correspond to the numbers of the SRµCT slices in axial view.

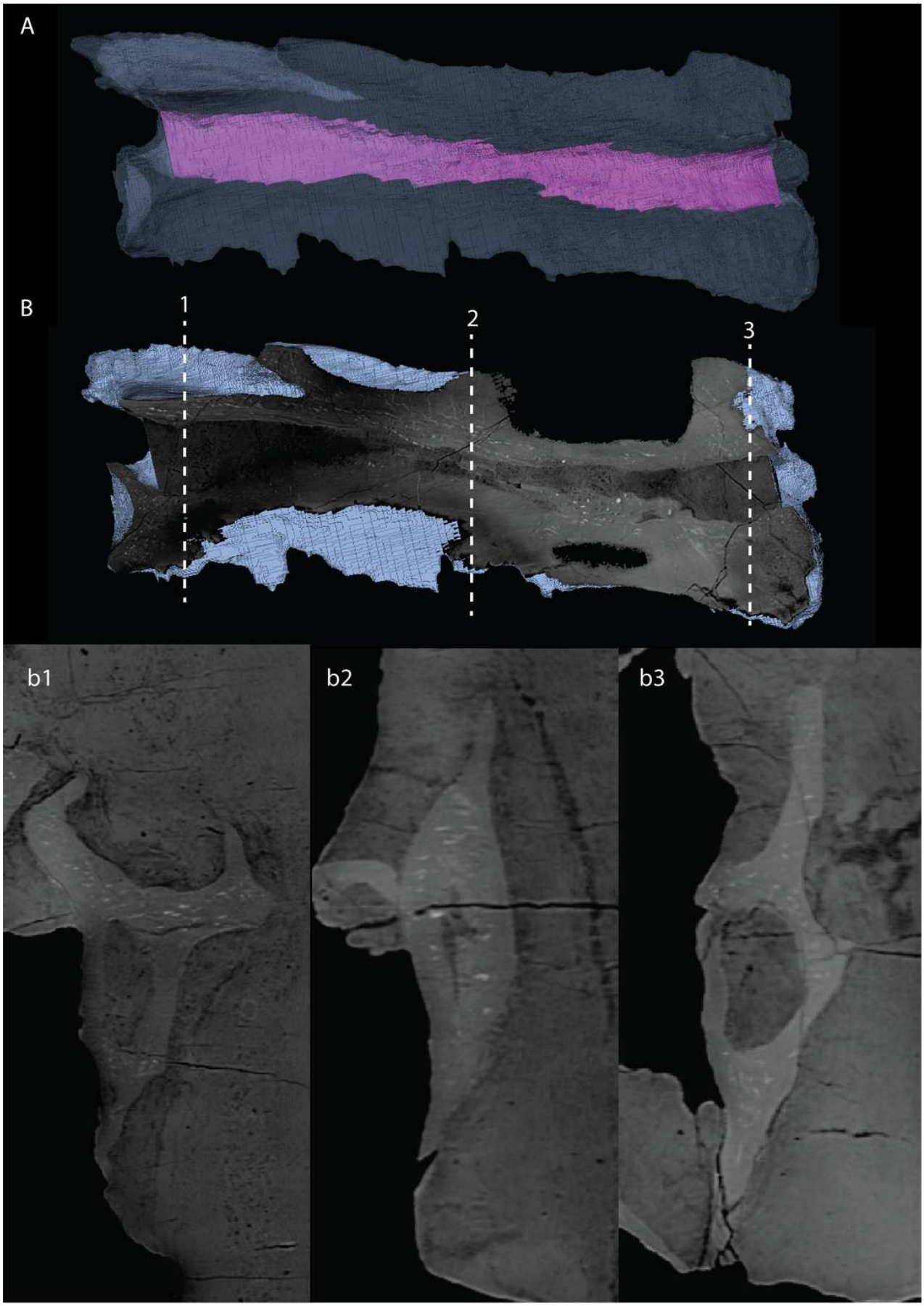
A
B
1
2
3
b1
b2
b3

Figure 29

Inner anatomy of the anterior part of the third cervical vertebra of PIMUZ T 2790.

(A) Transparent digital rendering of the third cervical, with the neural canal indicated in purple, in right lateral view. (B) Digital sagittal cross-section of the third cervical in right lateral view. The numbers above the stippled lines correspond to the numbers of the SRµCT slices in axial view.

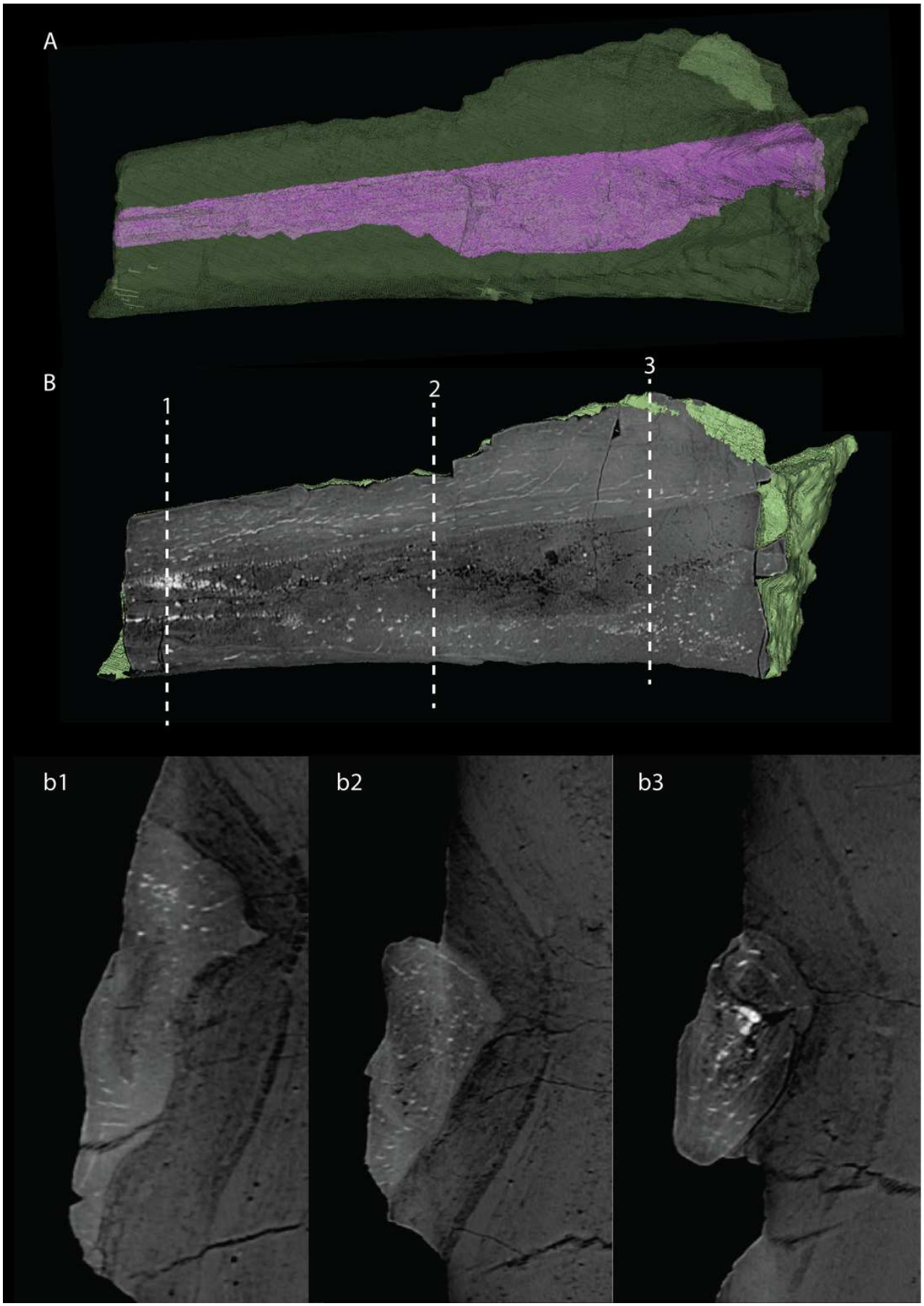
A
B
1
2
3
b1
b2
b3